UNIVERSITY OF
BIRMINGHAM

THE COMPATIBILITY OF SEMI-SYNTHETIC ENGINE OIL WITH CONVENTIONAL DIESEL AND BIODIESEL FUELS

by

JOSHUA ARIEH SHENKER

A thesis submitted to
The University of Birmingham
for the degree of

DOCTOR OF PHILOSOPHY

School of Mechanical Engineering
The University of Birmingham
June 2014

ABSTRACT

Recent trends to downsize diesel engines have increased the stress on lubricants. Engine oils naturally degrade during operation, undergoing continual reactions, changing both chemically and physically, detracting in performance from its initial specifications.

This thesis investigates the role of fuel in the ageing of diesel engine oils, specifically Ultra Low Sulphur Diesel (ULSD) and Rapeseed Methyl Ester (RME – a common European biodiesel). Oil ageing is assessed distinctly with fuel dilution; the entrainment of exhaust gases; and the effects of soot loading.

Results show fuel dilution has the greatest influence on oil performance. Effects are seen with an instant blending of properties, with the resultant fluid performing as an amalgam of the oil and fuel. This can be both positive and negative, depending on the property being measured, with the entrainment of biodiesel generally being beneficial. The entrainment of exhaust gases in the oil leads to increased unburnt hydrocarbons and fuel content, with similar dilution effects.

Soot loaded oil performance is heavily dependent on the respective fuel content. RME contamination has a positive influence which far outweighs its negligible soot production, whereas ULSD detracts from oil performance, and also produces more soot. During an equivalent timeframe, the influence of RME is seen to be less detrimental than ULSD on overall engine oil performance.

ACKNOWLEDGEMENTS

I would like to take this opportunity to thank all those that have helped me to achieve this thesis. Firstly, my supervisors; Drs. Karl Dearn and Athanasios Tsolakis, without your guidance and support none of this would have been possible. I gratefully thank The University of Birmingham for the provision of a PhD scholarship and maintenance grant for the duration of my study.

To the many members of the University's technical staff who helped me at different stages with testing and training, specifically from the schools of Mechanical Engineering, Chemical Engineering, Chemistry, and Metallurgy and Materials.

A special thanks goes to those I have gotten to know as both colleagues and friends from the Future Power System Group. Post Docs Drs. Jose Martin Herreros, Jakub Piaszyk, and Dale Turner. My contemporaries whom graduated before me, Drs. Ekarong Sukjit, Simaranjit Gill, Hendry Tira and Chia Lau. To those whom are soon to graduate with or after me; Tom Hoskins, Wentao Wang, Isaline Lefort, Danny Fennell and David Eckold. And lastly, to one whom shall sadly never get to graduate, Umar Musbahu, may his memory and work live on.

Lastly and most importantly, I would like to thank my family and long term girlfriend Ilana, whose support, encouragement, patience and motivation got me through till the end of my PhD. Without you, I doubt I could have achieved it, Thank you.

Joshua Arieh Shenker

June 2014

TABLE OF CONTENTS

LIST OF FIGURES

LIST OF TABLES

LIST OF NOTATIONS

Symbols	Definition
η	*dynamic viscosity (mPa.s or cP)*
μ	*coefficient of friction*
ρ	*density (kg/m^3)*
t	*time (Hours)*
T	*Temperature (°C)*

Measurement	Definition
B100	100% Biodiesel Blend
cP	Centipoise = 0.001 Pa.s
CAD	Crank Angel Degree
ppm	parts per million
TAN	Total Acid Number, mg KOH/g
TIC	Total Ion Current
w/w	weight per weight

Chemicals	Definition
C_2H_2	Acetylene
CO	Carbon Monoxide
CO_2	Carbon Dioxide
H_2O	Water
HO_2	Hydroperoxyl
H_2SO_3	Sulphurous acid
H_2SO_4	Sulphuric acid
KOH	Potassium Hydroxide
NO	Nitric Oxide
NO_2	Nitrogen Dioxide
NOx	Nitrogen Oxides
SO_2	Sulphur Dioxide
SO_x	Sulphur Oxides
ZDDP	Zinc Dialkyl Dithiophosphate

LIST OF ABBREVIATIONS

ACEA	European Automobile Manufacturers Association (Association des Constructeurs Européens d'Automotobiles)
AFM	Atomic Force Microscope
ASTM	American society for testing and material
AWSD	Average Wear Scar Diameter
BN	Base Number
CI	Compression Ignition
CLD	Chemiluminescence Detection
COF	Coefficient of Friction
CPC	Condensation Particle Counter
DES	Department of Education and Science
DI	Direct Injection
DMA	Differential Mobility Analyser
DOC	Diesel Oxidation Catalyst
DPF	Diesel Particulate Filters
ECR	Electrical Contact Resistance
EELS	Electron Energy-Loss Spectroscopy
EGR	Exhaust Gas Recirculation
EHD	Elastohydrodynamic
FAME	Fatty Acid Methyl Ester
FID	Flame Ionization Detection
GC	Gas Chromatography
HC	Hydrocarbons
HFRR	High Frequency Reciprocating Rig
HTHS	High Temperature High Shear
IC	Internal Combustion
IMEP	Indicated Mean Effective Pressure
LSD	Low Sulphur Diesel
LTLS	Low Temperature Low Shear
MPD	Magneto-Pneumatic Detection
MS	Mass Spectrometry
NAC	NOx Adsorber Catalyst
NDIR	Non-Dispersive Infrared
NOx	Nitrogen Oxides
PAH	Polycyclic Aromatic Hydrocarbon
PM	Particulate Matter
RME	Rapeseed Methyl Ester
SAE	Society of Automotive Engineers
SCR	Selective Catalytic Reduction
SME	Soybean Methyl Ester
SMPS	Scanning Mobility Particle Sizer

SOF	Soluble Organic Fraction
TAN	Total Acid Number
TDC	Top Dead Centre
TEM	Transmission Electron Microscope
THC	Total Hydrocarbons
TIC	Total Ion Current
UHC	Unburnt Hydrocarbons
ULSD	Ultra Low Sulphur Diesel
USV	Ultra Shear Viscometer
VI	Viscosity Index
ZDDP	Zinc Dialkyl Dithiophosphate

CHAPTER 1 - INTRODUCTION

1.1 - Background of Tribology

Tribology is the science of interacting surfaces, embracing the fields of physics, chemistry, engineering and metallurgy (Jost 1990). The word tribology is derived from the Greek word *'τρίβω' or* '*tribos'*, meaning rubbing, a more in-depth definition given as:

> *"The science and technology of interacting surfaces in relative motion - and of associated subjects and practices"*
>
> Jost (1966)

Although the word is a fairly recent invention, the subject has existed in some entity since early civilisation, with examples scattered through history dating as far back as the Egyptians and Mesopotamians. Some of the earliest pioneers who conceived many fundamental tribological principals include Leonardo da Vinci (1452-1519); Robert Hooke (1635-1703); Sir Isaac Newton (1642-1727) and Guillaume Amontons (1663-1705).

Tribology only came into public awareness in 1966 when a committee of the British Department of Education and Science (DES), headed by Dr. Peter Jost published *'The Jost Report'.* This report described the potential savings to the UK economy if greater attention were paid to tribological design (Jost 1966). By making equipment more efficient or less prone to wear, long-term financial savings could be made in almost every industry by reducing maintenance costs and increasing productivity.

1.1.1 - Automotive Tribology

The growth of the automotive industry has had a global impact, helping to advance economies and improve the lives of people living in developing and developed countries alike. But for all their wonders, automobiles are not simple machines and consist of many hundreds of thousands of components which rely on tribological principles in their everyday function.

Friction is something all vehicle components must deal with, either by utilising, overcoming or reducing its effects. One consequence of friction is wear, requiring the replacement of worn or damaged components. To minimise the effects of friction, lubrication is a key factor, but if poorly designed, it can be the chief culprit in many mechanical failures (Stachowiak & Batchelor 2005). Quantifying the influence of friction as a whole on the efficiency of a vehicle, as shown in Figure 1.1, demonstrates the importance of tribology on vehicle and engine design.

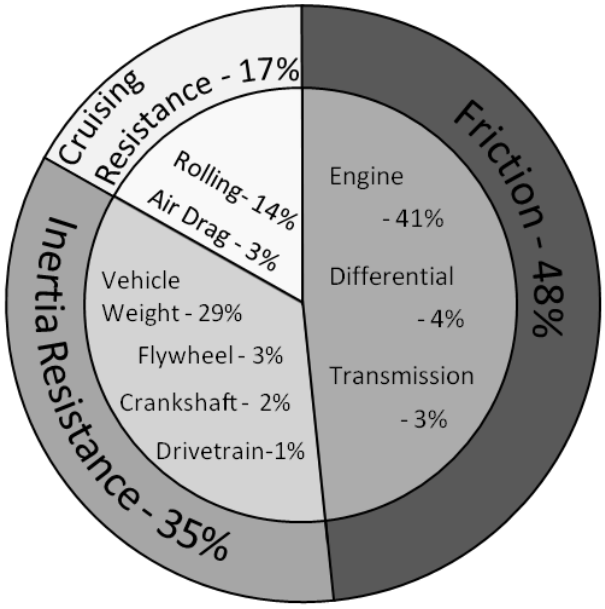

Figure 1.1 - Vehicle Energy Consumption, adapted from Nakasa (1995)

1.1.2 - Internal Combustion Engines

Internal Combustion (IC) engines are the prime movers for motored vehicles, with their popularity stemming from their multi-functionality. There is however a downside to IC engines, which is their poor thermal and mechanical efficiencies as well as being a significant contributor to atmospheric pollutants and greenhouse gases (Kapoor et al. 2001). IC engines emit high quantities of Carbon Dioxide (CO_2), Nitrogen Oxides (NO_x), Particulate Matter (PM) and other Hydrocarbons (HC) as a by-product of combustion which must be reduced and eventually eliminated. It is approximated that more than 20% of net CO_2 emissions originate from the combustion of fuels used for all forms of transportation (Inderwildi & King 2009). However, with few alternatives available having similar power densities and range, IC engines are thought to be the dominant power source for road going vehicles for the foreseeable future (Kapoor et al. 2001).

Figure 1.1 shows the poor efficiency associated with vehicles when converting the energy stored in fuels into useful mechanical power. The highest associated losses are from friction, specifically from the engine causing higher fuel consumption rates which in turn increases exhaust emissions. By reducing total engine friction; small savings in fuel economy and emission levels can be made per vehicle. This may seem negligible, but considering the number of vehicles globally, these slight improvements can have a global impact on air quality and the environment (Taylor 1998).

Figure 1.2 illustrates typical frictional losses experienced by in-engine components, which are predominantly lubricated by the sump oil. Reducing engine friction remains a huge

challenge as the oil must maintain a suitable lubrication regime across a broad and dynamic range of operating conditions.

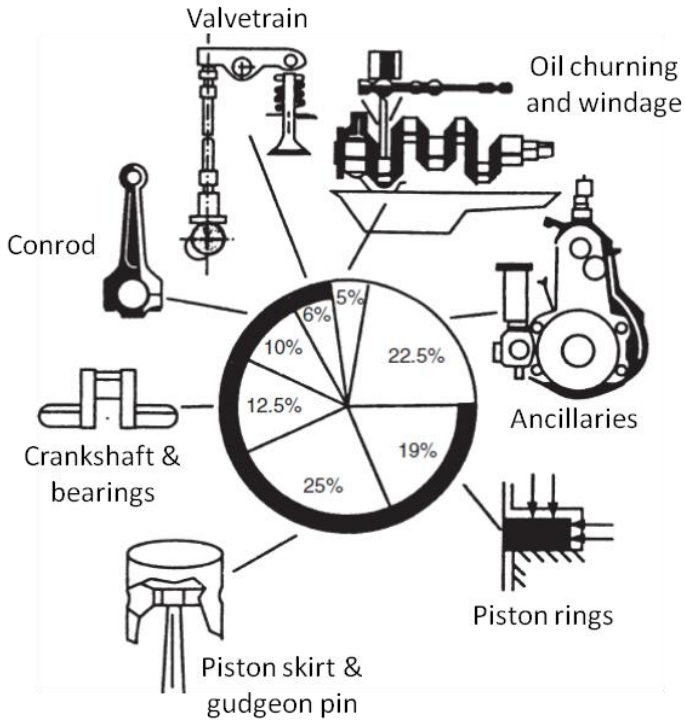

Figure 1.2 - Distribution of friction losses in an IC Engine (Martyr & Plint 2007)

1.1.3 - Engine Oils

The primary function of the oil within an IC engine is to provide lubrication between components in relative motion. The oil provides a continuous film between mated surfaces, minimising contact, friction and wear. Oils naturally degrade with age, undergoing continual chemical reactions within the engine, changing both physically and chemically over a prolonged period of time. This will in turn alter the oil's functional performance from its initial specifications and hence require replacing. However, the recent trend to downsize engines has amplified the level of stress experienced by the oil, accelerating its degradation.

This has led to shorter and more frequent drainage intervals, and the requirement for more expensive formulated engine oils.

The causes and mechanisms as to how engine oils age are well understood, however the physical and chemical stresses experienced by the oil are exacerbated by engine conditions during combustion. Physical factors include thermal loading and high mechanical stresses as the oil functions as both a coolant and a load carrier within the engine. Chemical degradation occurs as a consequence of fuel combustion, with the entrainment of contaminants including unburnt fuel and exhaust by-products. Oil ageing will therefore be affected differently by several factors which all must be balanced to maintain performance.

1.1.4 - Engine Fuelling Developments

With an increase in global fuel demands and diminishing oil reserves, there is a need for alternative fuel sources. This has been met with an increasing trend towards cleaner and more sustainable fuels to meet stricter governmental emission regulations. This area of research has led to many advances in fuel formulation, additive production and aftertreatment devices. However, more research is being focussed on bio- and synthetic diesels which have the potential to be both sustainable and renewable. The intention is to slowly phase these fuels into common use, initially as blends with conventional diesel, and eventually as neat unblended fuels, performing similarly but with more favourable combustion characteristics.

The development of such fuels poses new questions of what role the fuel plays with the degradation of sump oil. With many inherent changes to the fuel's physical and chemical properties, the manner with which the fuel interacts with engine oil, and the rate at which it does will also differ. This can either be directly through fuel dilution, or indirectly as the fuel is combusted forming by-products.

1.2 - Research Aims and Objectives

This thesis describes a study of the degradation of modern diesel engine oils and the influence of fuelling by conventional petroleum diesel and biodiesel. The overall aims for this research are:

1) To understand which is the most influential factor on oil ageing within a Compression Ignition engine?

2) To assess how these factors differ when fuelled with biodiesel?

This includes answering the following questions:

i. How influential is fuel dilution upon the thermo-oxidative degradation of oil?
ii. What effects do combustion blowby gases have on oil functionality and age?
iii. What are the true effects of Particulate Matter entrainment on oil performance?

This was achieved by evaluating changes in oil properties whilst artificially ageing the oil using a bespoke test rig and a Compression Ignition (CI) engine. The test rig enabled the degradation of the engine oil to be accelerated, and allowed for contributing factors to be examined in isolation.

1.3 - Thesis Outline

This thesis is structured to assess the effects of oil ageing within a CI engine during regular operation. An experimental programme has been devised such that the contributing factors of oil ageing are isolated and individually assessed before being recombined again to replicate actual engine conditions. Each factor is shown to alter the oil's properties in some way, with the most influential detailed. Chapter 4 studies the ageing effects from thermo-oxidation, and includes the influence of fuel dilution. Chapter 5 looks at the entrainment of gaseous emissions formed from the by-products of combustion only. Chapter 6 describes the analysis of all emissions with the emphasis on the entrainment of Particulate Matter (PM). This is achieved by artificially ageing the oil using a bespoke test rig and a single cylinder Compression Ignition (CI) engine, evaluating oil properties using a range of analytical equipment, all described in chapter 3.

CHAPTER 2 - LITERATURE REVIEW

This chapter outlines the key areas underlying this research and the following analytical chapters, including properties and performance of the chosen fuels and engine oil. The literature then goes on to detail the effects on engine oil performance from fuel dilution; fuel combustion; and finally the entrainment of Particulate Matter.

2.1 - Modern Diesel Fuels

This section describes key differences between the two fuel types used within this research, a conventional diesel and a biodiesel, highlighting properties which could be influential to the overall degradation of sump oil.

2.1.1 - Ultra Low Sulphur Diesel

ULSD was introduced as a replacement fuel for Low Sulphur Diesel (LSD) used in light duty vehicles. This change was intended to reduce the amount of sulphur present in diesel fuels which was relatively high for a low sulphur fuel (<500ppm), but new legislation reduced this further to <15ppm for ULSD. Sulphur has been shown to increase the level of Particulate Matter (PM) generated during combustion, thought to be as a response to the formation of sulphur dioxide (SO_2) and sulphate particulates (Thornton et al. 2006; Tan et al. 2009).

The move to low sulphur fuels greatly increased the efficiency and operational life of many advanced aftertreatment systems which are susceptible to sulphur poisoning (Fritz & Pitchon 1997; Thornton et al. 2006). However, it was only later discovered that sulphur also

contributed to the natural lubricity of the fuel. By moving to low and ultra low sulphur fuels, the failure rates of engine parts reliant upon the fuel as the lubricant, such as fuel injectors and pumps was greatly increased (Alleman & Mccormick 2003; Knothe & Steidley 2005). The solution was the addition of commercial additives to the fuel, which subsequently returned the lubricity of the fuel back to regulatory levels.

Commercial diesel fuels contain many additives; some enhance fuel performance such as cetane number, emissions and even aftertreatment activity. Other additives may be incorporated to improve fuel stability and handling, enhancing anti-corrosion, antifoaming and anti-oxidising performance for example.

2.1.2 - Biodiesel

The term 'Biodiesel' is often incorrectly associated with biologically sourced fuels used in diesel engines. However the American Society for Testing of Materials (ASTM) defines a biodiesel as: *'a fuel comprised of mono-alkyl esters of long chain fatty acids derived from the* ***transesterification*** *of vegetable oils or animal fats'*. This definition restricts the use of unprocessed oils and fats wrongly associated with being a biodiesel (Sappok & Wong 2008; Monyem & Van Gerpen 2001).

The main aim of transesterification is to produce a fuel that has better long-term stability and enhanced combustion performance than its non-refined form. The process of transesterification involves the conversion of a triacyl-glyceride to a series of mono-esters and glycerol by the addition of alcohol and a catalyst (Graboski & McCormick 1998).

Figure 2.1 shows the transesterification of a triglyceride, from either an oil or fat, with the addition of methanol in the presence of sodium hydroxide used as the catalyst. This produces glycerol as a by-product, and Fatty Acid Methyl Esters (FAMEs) as the biodiesel. Post reaction, the biodiesel will contain unused reactants such as methanol and sodium hydroxide which **must** be removed from the fuel to meet commercial specifications such as ASTM D6751 in the US, and EN 14214 in the EU (Sappok & Wong 2008).

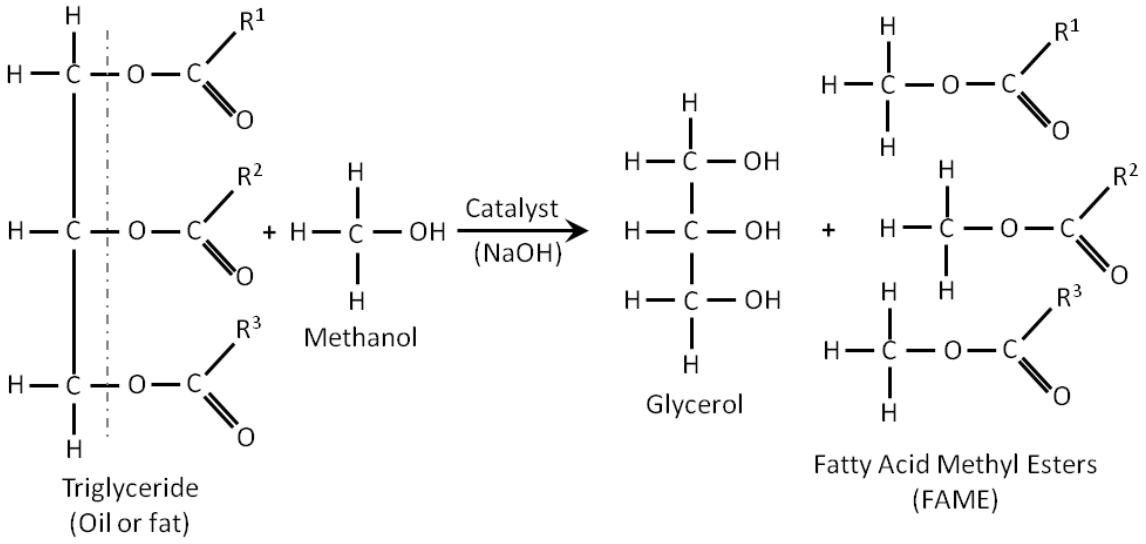

Figure 2.1 - The Transesterification Process of Triglycerides into Esters, adapted from Kim et al. (2004); Graboski & McCormick (1998) and Singh & Singh (2010)

Biodiesels can therefore be produced from various oils, mainly from crops such as corn, sesame, sunflower, peanut, palm, cottonseed, linseed, rapeseed and soybean. Even animal fats such as pork lard, beef tallow, fish oil and poultry fat, and several non-edible oils such as Jatropha, Mahua, Babassu and karanja have been converted into biodiesels, with varying degrees of success (Shahid & Jamal 2008; Agarwal 2007; Parsons 2007). Triglycerides which are currently used in the production of commercial biodiesel are rapeseed in the EU, and soybean in the US, which when reacted with methanol produce Rapeseed Methyl Ester

(RME) Soybean Methyl Ester (SME). In general, the biodiesel produced will have a lower viscosity; lower boiling and flash point; better cetane number; higher oxygen content; and enhanced cold flow properties than its non-refined triglyceride form.

2.1.3 - Fuel Comparisons

Table 2.1 compares some of the most relevant fuel properties for ULSD and RME, the two fuels used within this research. Structurally the two fuel types differ greatly, where biodiesels will consist of large methyl esters with little to no aromatics, diesels consist of straight chained hydrocarbons with aromatics. Because of this, biodiesels tend to be more stable under heating, and have higher and more distinct boiling and flash temperatures (Sappok & Wong 2008; Agarwal & Das 2001). Biodiesels also have a higher natural lubricity than conventional diesels, which is thought to be due to their higher oxygen content (Knothe & Steidley 2005).

Table 2.1 - Fuel properties, adapted from Sukjit and Dearn (2011)

Properties	ULSD	RME	Method
Cetane number	53.9	54.7	ASTM D613
Density @ 15°C (kg/m^3)	827.1	883.7	ASTM D4052
Viscosity at 40°C (cSt)	2.467	4.478	ASTM D445
50% distillation (°C)	264	335	ASTM D86
90% distillation (°C)	329	342	ASTM D86
Lower Calorific Value (MJ/kg)	42.7	39	
Sulphur (mg/kg)	46	5	ASTM D2622
Aromatics (%w/w)	24.4	<0.1	
C (%w/w)	86.5	77.2	
H (%w/w)	13.5	12	
O (%w/w)	≈0	10.8	
H/C Ratio (Molar)	1.88	1.85	
Surface Tension at 30°C (N/m)*	0.0255	0.0280	

**Taken from Kegl (2006)*

There is still a lot of negative perceptions surrounding biodiesels, which is due in part to the usage of 'poor' quality fuels, either from using non-transesterified fuels, or biodiesels that contain trace quantities of reactants and do not fully meet specifications (Fraer et al. 2005). In general, biodiesels have a lower oxidative stability than regular diesels which reduces its capability for long term storage (Parsons 2007). There are several factors which affect this, which include hydrocarbon chain length; degree of saturation; and the presence of any naturally occurring anti-oxidants. Biodiesels produced from FAMEs will generally be unsaturated, making them less thermally stable and more susceptible to free radical attack (Parsons 2007).

These differences in the two fuel types' physical and chemical properties have a considerable effect on their respective combustion performance. Of most significance, biodiesels will typically produce less overall carbon emissions, making it a more carbon neutral fuel than conventional diesels. Although this is favourable, only some emissions generated from its combustion are reduced, however this is at the expense of increasing other greenhouse gases, as described in more detail within section 2.4.2.

2.2 - Engine Oil Performance

This section looks at the functional performance of engine oils, and how they relate to their physical and chemical properties. This section also discusses the degradation of oils and the need for drainage intervals.

2.2.1 - Properties of Engine Oils

The primary and sometimes assumed only functions of engine oils is to reduce friction and prevent wear, but in reality oil is the lifeblood of the engine as its role fulfils a great deal more. For example, a consequence of friction is the generation of heat, oil behaves as a coolant transferring heat from areas of high temperature such as the piston and combustion chamber, to heat sinks such as the sump and cooling jacket.

The oil also behaves as a corrosion inhibitor by coating parts with a thin film, providing a barrier from oxidation. The oil will also contain and neutralise acid contaminants that may form or collect in the sump. Within the engine, the oil performs a cleaning role, by dispersing contaminants, preventing the build up of deposits and residues which can agglomerate and block oil channels. The oil will also actively remove and transport waste and debris to be filtered, whilst simultaneously transporting additives to sights of importance. The oil also aids in providing the seal for the combustion chamber between the piston, piston rings and the cylinder liner (Haycock & Hillier 2004).

These are all desired functional properties which for most engine oils are a prerequisite. However there also needs to be a compromise with more negative requirements which stipulate that an oil cannot perform in other ways. For example, an engine oil should not have too high a viscosity, as this causes too great a film thickness to form which in turn increases viscous drag. Likewise an engine oil should not have too low a viscosity, as this provides an insufficient film thickness which will increase wear. Therefore the viscosity

requirement will not be defined to a certain degree, but rather between a range of values or to a limit which should not be exceeded.

Other examples of these requirements include not having a low Viscosity Index (VI), i.e. the oil should not thin or thicken too much under heating and cooling respectively. Oils should not have a high volatility, should not be corrosive to the engine, should not produce deposits or residues, and should not be toxic; however they should be resistant to chemical and oxidative attack. Some of these requirements are legislative, others are a minimum requirement between oil drainage intervals. Automotive manufacturers will specify more than 40 properties required of an oil before it is used within their engines (Haycock & Hillier 2004).

A further requirement of engine oils is longevity; that is, it must continue to maintain all of its functional properties for a prolonged period of time, so that a used oil will perform similar to when it was new, right up until it is due for a scheduled change (Naylor et al. 2001). However, this requirement becomes a more complex process when combustion is involved, as the peak temperatures and conditions the oil must operate within fluctuate, placing immense stress upon the oil, accelerating its degradation.

2.2.2 - Lubrication

Referring back to the primary function of engine oils, which is to lubricate, reduce friction and prevent wear between moving parts. Engine oils are able to do this by creating and maintaining a lubricant film between sliding and rotating parts. The size and thickness of

the produced film will depend upon the fluid viscosity, the applied load and the relative speed between moving parts. The then formed film thickness ratio is therefore a relationship between size of the newly formed film relative to the combined surface roughness of the two contact surfaces (Haycock & Hillier 2004; Kapoor et al. 2001).

The relationship defining fluid friction was originally derived from experimental measurements using journal bearings by Professor Stribeck over 100 years ago. His work plotted the deviation of two non-dimensional groupings, the coefficient of friction 'μ', and a controlling parameter group 'ηU/W', which includes the dynamic viscosity, relative speed and load. The type of curve shown in Figure 2.2 is often called a Stribeck curve, which shows for all but very small sliding speeds, friction is proportional to the controlling parameter (Priest & Taylor 2000; Stachowiak & Batchelor 2005). Figure 2.2 also highlights regions on the Stribeck curve of different lubrication regimes, as well as visual examples, namely boundary, mixed and hydrodynamic. However, the boundaries between lubricating regimes will typically not be so clearly defined, and will depend on specific design features and dimensions.

Under hydrodynamic lubrication, there is a full fluid film between surfaces whereby even the largest asperities are separated. To achieve full hydrodynamic lubrication, a sustained pressure within the fluid film is required to carry the load. From Figure 2.2 it is clear that within the hydrodynamic regime, the fluid frictional forces will increase with viscosity, and that viscous drag will also increase with bearing speed. Therefore, for any given system there will be an optimum viscosity whereby the internal friction will be at a minimum, making the

dynamic viscosity one of the prime characteristics in hydrodynamic lubrication (Stachowiak & Batchelor 2005; Haycock & Hillier 2004; Taylor 1998).

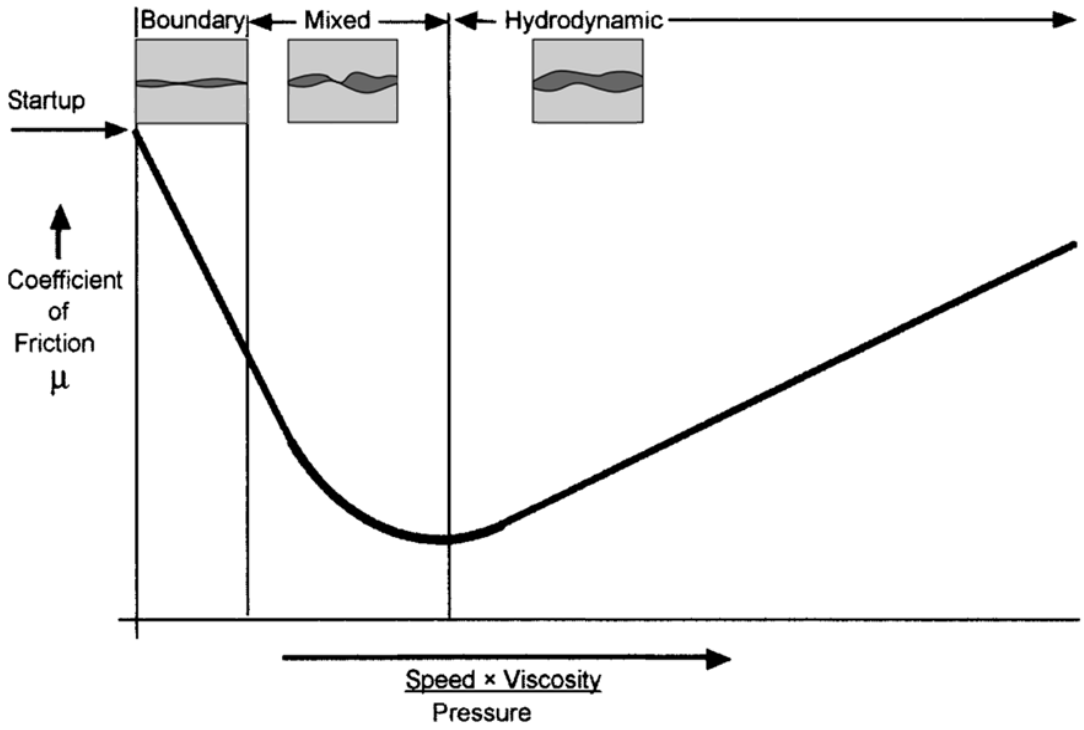

Figure 2.2 - Stribeck curve, adapted from Haycock & Hillier (2004) and Kapoor et al. (2001)

In the case of boundary lubrication, these relationships are inverted, by reducing the viscosity and/or speed, or by increasing the load will lead to greater contact between surface asperities, causing a sharp rise in friction, and in turn wear. Under these conditions, the frictional performance will be defined more by the chemical and physical actions of the molecularly thin lubricant films formed on the component surfaces. There is also a common noise phenomenon associated with components experiencing boundary lubrication known as 'stick-slip', caused by continual start-stop motion. Here, the additive package will have a more significant role to smooth the transitions between rest and relative motion (Haycock & Hillier 2004; Kapoor et al. 2001; Priest & Taylor 2000).

Between fully hydrodynamic and boundary lubrication regimes lies two further regimes. The first is mixed lubrication whereby the hydrodynamic film still supports most of the load, but cannot prevent some asperity contact between opposing surfaces. The second type is Elastohydrodynamic (EHD) lubrication in which surfaces are separated, but involves very thin films and includes other phenomena such as the effect of pressure on viscosity, and the elastic distortion of surfaces (Stachowiak & Batchelor 2005; Taylor 1998).

Different engine components will rely upon the various lubricating regimes to perform adequately, with oil conditions dependant on which component it is adsorbed to. Some components will experience more than one regime during a single cycle, for example many reciprocating components will experience both boundary and mixed lubrication due to the rapid changes in speed and reversals of motion (Priest & Taylor 2000; Haycock & Hillier 2004). Bearings on the other hand are designed to operate only within the hydrodynamic regime, whereby metal-to-metal contact will only occur at very low speeds such as during engine startup. In addition, each component's individual lubrication regimes may change with use, as surface asperities are flattened or reduced through wear, and as lubricants degrade over time (Kapoor et al. 2001).

2.2.3 - Engine Oil Formulating

Engine oils are formulated to fulfil desired performance characteristics as a result of its physical and chemical properties. When formulating an oil, there are several key steps which will determine its functionality, the first being the selection of an appropriate base stock. The base oil is the foundation with which the overall formulation's properties are built

upon, as well as being the last line of defence once the additives become depleted. Base oils are conventionally formulated from refined crude stocks and will typically contain paraffinic (straight or branched), naphthenic (cycloparaffins) and some aromatic hydrocarbons as shown in Figure 2.3. Base oils derived predominantly through refining processes are typically known as “mineral” oils (Kapoor et al. 2001).

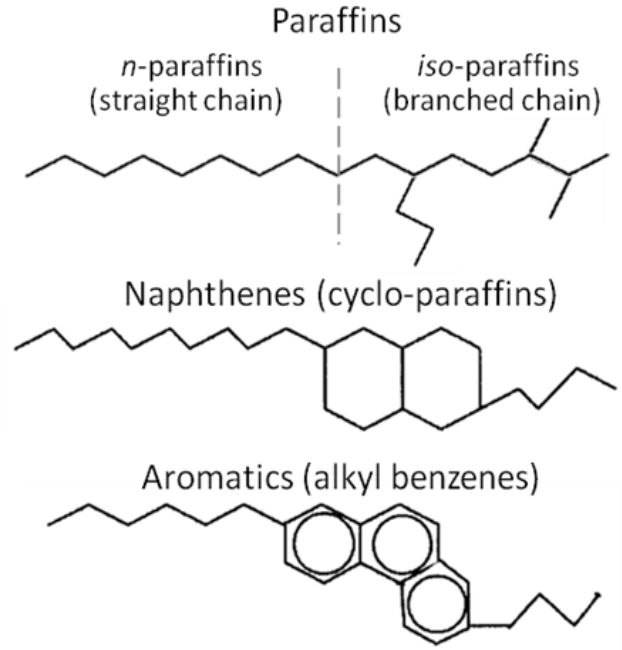

Figure 2.3 - Basic hydrocarbon structures of engine oils (Haycock & Hillier 2004)

Commercial engine oils are therefore an amalgam of refined hydrocarbon molecules of varying lengths and weights, typically containing 20 to 40 carbon atoms each. The base oil composition will be a mix of hydrocarbons that consist of straight, branched or cyclic chains all bonded together, and may not be purely paraffinic or naphthenic in nature. Therefore within a single oil sample, the number of possible variations of oil molecules could be in the millions (Haycock & Hillier 2004; Stachowiak & Batchelor 2005).

The next step is to formulate an oil with the best cost-performance trade-off. The stability of the oil will depend on the level of refinement of its base, but at the same time this adds to the overall cost (Barnes 2004). Here lies the trade-off in cost and performance, as refining is required to remove the inherent impurities within many mineral oils, which will in turn increase the resilience and operational life of the oil (Adhvaryu et al. 2002).

Refining is required for several reasons, such as the removal of aromatics and unsaturates which make the oil susceptible to thermal and oxidative attack. Likewise the removal or cracking of high molecular weight hydrocarbons is required to prevent the oil from solidifying and forming waxes at low temperatures, which will in turn lower the overall pour-point of the formulation. The removal of sulphur and nitrogen compounds is also important as they are thought to contribute to the corrosion of worn surfaces, resulting in accelerated wear (Stachowiak & Batchelor 2005).

Synthetic oils are more resilient to thermal and oxidative attack than mineral oils and will typically provide an overall superior performance, although at a slightly greater cost. Synthetic base oils were originally produced in countries lacking in a reliable source of mineral oil. Synthetic oils are ‘manufactured’ through the polymerisation of low molecular weight hydrocarbons derived from the ‘cracking’ of larger petroleum products. Cracking is required to reduce the range and variation of molecules present in the oil, creating an oil with carefully controlled performance characteristics (Stachowiak & Batchelor 2005).

Partial and semi-synthetic engine oils are formulations that have had their base stocks enhanced in some manner, typically by blending mineral and synthetic oils together. Semi-synthetic oils are intended to have many of the benefits of purely synthetic oils, but at a lower cost due to the synthetic portion contributing to less than 30%. Other forms of semi-synthetic oils contain synthetic esters, added to improve the solubility and compatibility of certain additives (Kapoor et al. 2001).

The final step in formulating an engine oil is the addition of organometallic additives, aimed at enhancing certain elements of the oil's performance. Although the base oil forms the bulk weight, the contribution from additives and additivised solutions can be as much as 20% for a fully formulated oil (Perez 2000). There are several purposes of additives, aimed to improve different elements of the oil's functional performance. This includes friction modifiers and anti-wear additives, used to lower the coefficient of friction between surfaces and alter the lubricant boundary layers, to provide sufficient anti-wear performance. This is also achieved by altering their adsorption characteristics, and to encourage Extreme Pressure (EP) lubrication.

Viscosity modifiers or Viscosity Index (VI) improvers are required to reduce excessive thinning of the lubricant or lowering of the viscosity at high temperatures. They operate by being more soluble in the base stock at high temperatures than at low temperatures, increasing the overall viscosity as the oil itself naturally thins. An additive type with an opposing function is pour point depressants, which lowers the temperature at which the oil begins to solidify and congeal.

The cleaning performance is controlled by Detergents and Emulsifiers, which control the contamination from reaction products, wear particles, water and debris, preventing them from collecting and agglomerating. Several additives also behave as Anti-Oxidants, others inhibit and control rust and corrosion, whereas a final type prevent the sump oil from foaming when air is introduced into the oil (Haycock & Hillier 2004; Stachowiak & Batchelor 2005).

2.2.4 - Mechanisms of Oil Degradation and Ageing

The degradation of engine oils can be measured by the decline of certain properties from their initial specifications established during formulation. This will be as a result of some physical or chemical change occurring during operation. Figure 2.4 summarises the main forms of oil degradation which are evaporation, thermal degradation, oxidation, polymerisation, and deposit formation (Gatto et al. 2008).

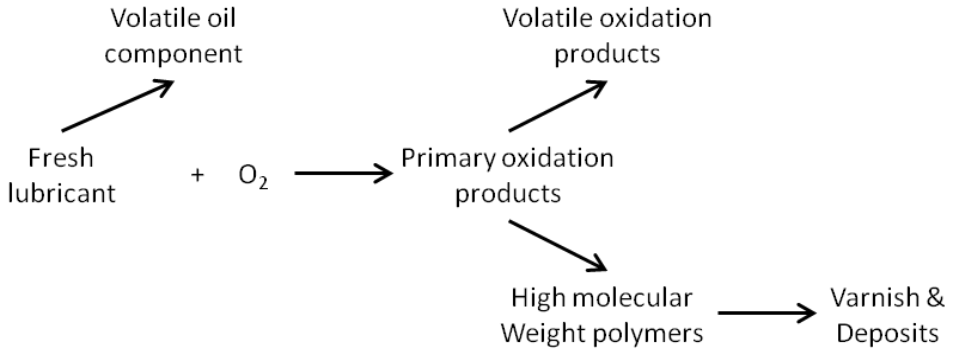

Figure 2.4 - Kinetic model of lubricant degradation (Gatto et al. 2008)

Evaporation occurs as the removal of the most volatile fraction, and the removal of volatile by-products formed through oxidation and ageing (Chen & Hsu 2003). As the base oil contains hydrocarbons of varying weights, volatility does not increase linearly with

temperature, but in proportion to hydrocarbon mass composition (Barman 2002). Under regular engine conditions, only the most volatile mass fractions evaporate, however this fraction increases rapidly with temperature as longer chained molecules begin to boil-off.

Oxidation is the dominant stage of oil degradation within most diesel engines and occurs predominantly within the crankcase and sump. The rate at which oil oxidises is primarily influenced by temperature and increases exponentially, which for a mineral oil can double with each 10°C rise above 75°C (Stachowiak & Batchelor 2005). Synthetic oils tend to be preferred for high temperature applications due to their greater level of refinement which makes them less susceptible to oxidation. Other factors that determine the rate of oxidation include the level of oxygen/air dissolved in the oil, and the presence of catalysts.

Oxidation is an autocatalytic free radical reaction that involves four steps: initiation, propagation, branching, and termination, with each step resulting in the addition of oxygen to the base oil (Barman 2002; Barnes 2004). In the following sets of equations, R and RH represent different hydrocarbon alkyl groups, $R^{\bullet}$ is a free radical, $H^{\bullet}$ is a hydrogen ion, $ROO^{\bullet}$ is a peroxide radical and ROOH is an organic acid (Chen & Hsu 2003; Stachowiak & Batchelor 2005).

1. **Initiation**

$$RH \xrightarrow[Heat/catalyst]{} R^{\bullet} + H^{\bullet}$$

Initiation commences the entire oxidation process and is dependent on environmental conditions, and the age and state of the oil. Initiation is the formation of free radicals which

is a thermally activated process governed by the dissociation energy required to separate the carbon and hydrogen atoms.

2. Propagation

$$R^{\bullet} + O_2 \longrightarrow ROO^{\bullet}$$
$$ROO^{\bullet} + RH \longrightarrow ROOH + R^{\bullet}$$

Propagation follows and is a two stage process, starting with the previously formed free radicals reacting with oxygen to form peroxide radicals. The peroxide radicals, being more reactive than the free radicals, become the catalyst for the whole reaction governing the overall rate of oxidation (Chen & Hsu 2003).

During the second stage of propagation, the peroxide radicals react with other hydrocarbons present in the oil, forming carboxylic acids and additional free radicals. Oxidation then becomes an autocatalytic reaction, as the product of one reaction cycle feeds the next, continuously producing more free radicals, thus creating a self perpetuating cycle that accelerates the rate of oxidation (Stachowiak & Batchelor 2005).

3. Branching

$$ROOH \longrightarrow RO^{\bullet} + HO^{\bullet}$$
$$RO^{\bullet} + RH \longrightarrow ROH + R^{\bullet}$$
$$HO^{\bullet} + RH \longrightarrow H_2O + R^{\bullet}$$

Branching involves the secondary oxidation action of already formed oxidised products, further promoting propagation. As an overall process, oxidation begins as a trace quantity within the sump, but accelerates up until a critical point is reached, when a larger fraction of oil is being oxidised at any one time. Engine oils will contain anti-oxidant additives which

attempt to delay the onset of rapid oxidation. They operate either by scrubbing radicals from the oil, inhibiting propagation, or by neutralising the acid which controls the branching.

4. Termination

$$\left.\begin{array}{c} R^{\bullet} + R^{\bullet} \\ R^{\bullet} + OOR^{\bullet} \\ OOR^{\bullet} + OOR^{\bullet} \\ RO^{\bullet} + R^{\bullet} \end{array}\right] \longrightarrow \begin{array}{c} alcohol \\ aldehydes \\ ketones \\ acids \end{array}$$

Oxidation ends with the termination of the chain reaction, with the formed free radical hydrocarbons able to follow multiple pathways. This produces a complex assortment of unsaturated and oxygenated products such as alcohols, aldehydes, ketones or acids, which condense and remain in the sump. These contribute to the latter stages of oil degradation, through the polymerisation of oxidised compounds to high-molecular-weight products (Chen & Hsu 2003). The combined effects of this results in the formation of sludges (oxidised polymeric substances), resins, varnishes and deposits which eventually thicken and increase the oil's overall viscosity (Diaby et al. 2009). Polymerisation is sensitive to oil age and condition, as well as any entrained contaminants such as fuel, acids and soot (Lee et al. 2006).

A commonly seen effect is the formation of deposits which involves the 'baking' of polymerised and oxygenated species to the piston assembly. Typically, the partially oxidised oil will circulate to the piston, forming thin-films and experiencing high temperatures due to its close proximity to the combustion chamber. Deposits reduce engine performance, can block oil pathways, and cause serious mechanical failures (Gatto et al. 2008; Stachowiak & Batchelor 2005).

2.2.5 - Reactors

Degradation occurs throughout the oil's life at various stages, and across many areas of the engine. However, each stage requires different conditions to accommodate the reactions; oil therefore won't fully degrade if it is static, and so it must move around the engine to experience different conditions. For example, in the sump the oil is held at an elevated temperature, but not high enough to sufficiently thermally degrade for it to require changing. However, oil in the piston ring pack **will** thermally degrade, and upon returning to the sump will contain free radicals and exhaust contaminants which can slowly change the properties of the bulk of the oil. The rate of degradation will be determined by the residence time and volume of oil in both the piston ring pack and the sump, and the flow rate between the two (Lee et al. 2006).

The engine can therefore be viewed as a series of reactors with oil flowing between. Each reactor has its own conditions and residence time which causes the oil to degrade and chemically alter in different ways. Lee et al (2006) proposed that a typical engine has two reactors; the sump, and the pistons. However Chen & Hsu (2003) proposed a three reactor model with the pistons split into two sub-reactors as shown in Figure 2.5. The top ring groove and the volume above the top piston ring as the first reactor; the volume enclosed between the piston rings and the cylinder liner wall as the second reactor; and the sump as the third.

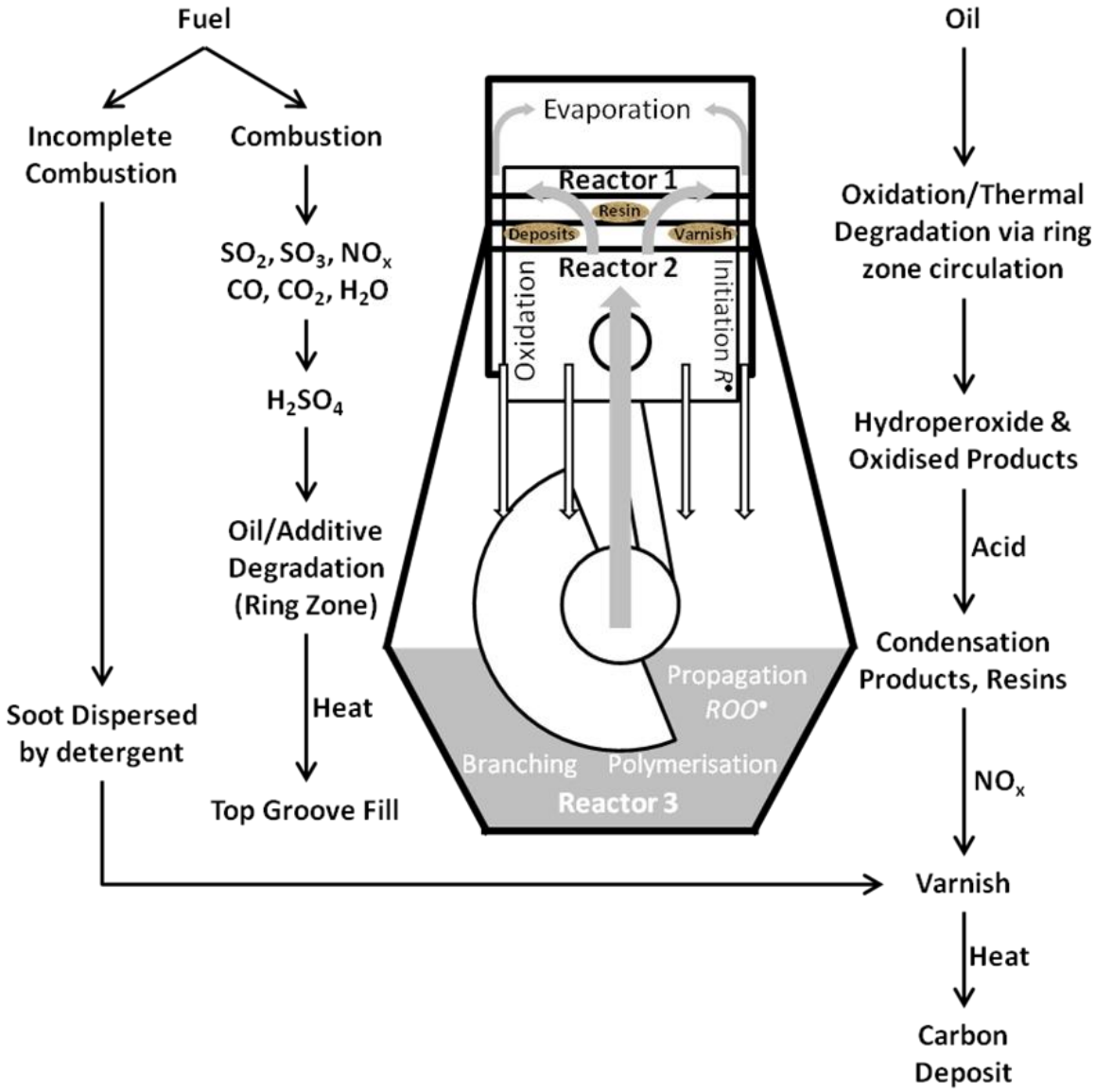

Figure 2.5 - Engine schematic representing a three reactors model in series with mechanisms of deposit formation, adapted from Chen and Hsu (2003)

The oil flow path between reactors can be viewed as two loops. Oil is siphoned from the sump (3) via an auxiliary mechanical pump, to the piston ring pack (2). Here the oil can reside for several minutes around the piston skirt and rings whilst circulating between reactors 1 and 2 by the reciprocating movement of the piston. Oil can easily travel from the top ring landing (1) to the piston ring pack (2), but not directly to the sump (3). Oil conditions in each reactor are summarised in Table 2.2.

Table 2.2 - Typical oil conditions around engine components

#	Reactor	Temperature	Residence time	Primary Degradation
1	Top ring and piston landing	250-300°C	Seconds	Evaporation, Thermal
2	Piston rings and cylinder liner	150-250°C	Minutes	Thermal, Oxidation, Polymerisation, Deposit
3	Sump	<150°C	≈40Hours/litre	Evaporation (volatiles only), Oxidation, Polymerisation

References: (Lee et al. 2006; Stark et al. 2005; Chen & Hsu 2003)

Whilst in reactor 1, the average temperature per stroke experienced is very high (250-300°C), but the interaction with oxygen is low due to combustion, adding to evaporation. In reactor 2, the temperature decreases but the residence time is longer. With sufficient oxygen able to diffuse into the oil film, oxidation becomes the primary degradation mechanism. Any oil lingering around the combustion chamber and piston will collect combustion by-products, thermally degrading with free radical initiation and deposit formation likely (Chen & Hsu 2003).

Oil leaves reactor 2 either by scraping from the liner wall, blow-by gases or gravity and returns to the sump (reactor 3) (Lee et al. 2005). Temperatures are too low for initiation to occur, however free radicals generated in reactor 2 will now be present in the sump through contamination. Evaporation will at first dominate, but only of the most volatile fraction, typically when fresh oil is introduced to the sump (Chen & Hsu 2003). Other sump contaminants likely to be present which are prone to evaporation include volatile by-products of degradation, unburnt fuel and potentially water. For short periods when the engine is warming and cooling, these contaminants may react with the oil and each other. During longer residence times and at elevated temperatures, oxidation and polymerisation

can occur due to the presence of free radical contaminants, leading to oil thickening and sludge formation (Lee et al. 2006).

Figure 2.5 also shows the mechanism of deposit formation which can be caused by the accumulation of insoluble and oxidised products suspended in the oil (Chen & Hsu 2003). Under high temperatures, these deposits are formed by further oxidation reactions which cause poor lubrication and engine wear. However, these oxidised products require high temperatures which are found around the piston where the oil itself has the highest surface area to volume ratio (Sinha & Agarwal 2008).

2.3 - Fuel dilution

2.3.1 - Mechanisms

Diesel fuels and engine oil come into contact in and around the combustion chamber when the cylinder walls are wetted by uncombusted fuel. The amount of fuel that is able to reach the cylinder walls will depend on factors such as fuel vaporisation, in-cylinder temperatures, fuel charge density, charge motion and injection strategy (Heywood 1988). This is a natural process that occurs during the combustion cycle and can also be affected by external factors such as cold engine start-ups, low engine loads and short stroke lengths (Andreae et al. 2007; Froelund & Ross 2005; Haycock & Hillier 2004). Engine age can also increase dilution levels as an older engine will be expected to have greater levels of wear, reducing the sealing capability from the combustion chamber, which will in turn increase the levels of blowby able to reach the sump (Gatto et al. 2008).

The introduction of high pressure fuel injectors in small and midsized diesel engines has also increased the interaction of fuels with sump oil. Fuels are injected further and faster into the combustion chamber, increasing the likelihood of the fuel impingement against the cylinder walls (Bijwe et al. 2004). In small diesel engines, the fuel would normally be dissolved into the oil film if it failed to vaporise. However, in some circumstances, the fuel spray may even be enough to 'wash' away the oil film (Froelund & Ross 2005). Exposed cylinder surfaces become wetted with unburnt fuel (and oil), which is then transported to the sump by the scraping and reciprocating action of the piston rings (Agarwal et al. 2003).

Sump dilution levels have also been seen to rise in conjunction with increasing aftertreatment devices that require regeneration (He et al. 2011). Modern fuel injectors are able to change injection strategy mid-stroke, enabling late in-cylinder injections required for the active regeneration of certain aftertreatment devices (Fang et al. 2006). These include Diesel Particulate Filters (DPF), Diesel Oxidation Catalysts (DOC), NOx Adsorber Catalysts (NAC) and Selective Catalytic Reduction (SCR).

A delayed injection strategy can be used to increase the exhaust temperature, or alternatively increase the level of Unburnt Hydrocarbons (UHC) in the exhaust stream, required for aftertreatment regeneration (Andreae et al. 2007). Typically, a rich fuel/air mixture is injected into the combustion chamber post-injection, i.e. after the actual fuel combustion injection occurs. This happens at a delayed crank angle after the piston is at Top Dead Centre (TDC), when the exposed surface area of the cylinder wall is greater (Fang et al. 2007). The piston also undergoes an expansion stroke, reducing the in-cylinder temperature

and density, which also increases the likelihood of cylinder wall wetting and oil contamination (Thornton et al. 2009).

For most diesel engines, sump oil dilution is deemed critical above 5% w/w (Froelund & Ross 2005; Sappok & Wong 2008; Andreae et al. 2007). However, fuel dilution does not solely rely on the rate of fuel entering the sump oil, but also the rate at which it leaves. During base mode operation, the rate at which fuel enters the sump is considered constant but limited, contributing to 1-2% dilution (Cracknell & Stark 2007). However, during regeneration mode the rate at which fuel enters the sump is greatly increased. But as regeneration is intermittent, and occurs as a fraction of the total engine operating time, the additional gain in fuel contamination is not as detrimental as was once thought (Andreae et al. 2007).

Evaporation from the sump on the other hand is considered constant throughout, however sump temperatures rarely reach a maximum of 150°C, languishing between 90-110°C under normal operation (Waynick 2005). This may not be high enough to remove all of the fuel collected in the sump, but is enough to remove the most volatile fractions through evaporation. When the fuel begins to evaporate, it is the lighter paraffinic compounds which are first removed, leaving behind the heavier aromatic compounds. Therefore after a prolonged period of time, the fuel content remaining in the sump will have an entirely different composition than the fuel that initially entered. This begins to alter our understanding of how the oil and fuel interact, as previous work has focussed on conventional fuels interacting with sump oil. This would suggest that the fuel found within

the sump is compositionally different, and perhaps interacts differently with the oil than previously expected.

2.3.2 - Effects of fuel dilution

The common effect of fuel dilution is a change in oil viscosity. It is thought that the heavier aromatic fuel compounds that remain post evaporation become a substrate for oil oxidation, which increases viscosity (Gatto et al. 2008; Andreae et al. 2007). However, if fuel dilution is more dominant than oxidation, this can lead to a significant lowering of the sump oil's overall viscosity. This will in turn lower the its load bearing capability, leading to increased levels of friction and scuffing (Agarwal 2007; Andreae et al. 2007).

The effects of fuel dilution have also been seen to behave either as an anti-oxidant, scrubbing free radicals, or an oxidiser if hydrogen abstraction is readily available (Cracknell & Stark 2007). This depends on the age and state of the fuel before it enters the sump, as its stability will also dictate its behaviour. Other effects of excessive fuel dilution include the reduced effectiveness of additives which can preferentially react with the fuel as a sump contaminant (Thornton et al. 2009).

2.3.3 - Effects of Biodiesel dilution

Differences in the effects and dilution levels for biodiesel are caused by variations in fuel properties as summarised in Table 2.1 for ULSD and RME. Chemically and structurally the two fuels are very different, RME consists of large methyl esters with high oxygen content and almost no aromatic compounds. Whereas ULSD consists primarily of straight

chained hydrocarbons with some aromatics, higher sulphur content and no oxygen. RME's structure causes it to have a high but very distinct boiling range whereas ULSD has a lower and broader boiling range making it more volatile.

The polar nature of RME has been seen to enhance the overall lubricity of fuel blends due to its interaction with other hydrocarbons (Knothe & Steidley 2005). RME has greater intermolecular bonding which can increase surface tension, but also make the fuel more stable under heating with an increased boiling temperature and reduced vaporisation (Sappok & Wong 2008; Agarwal & Das 2001). As a result, RME during injection has a greater degree of impingement against in-cylinder surfaces, and enters the sump at a faster rate than conventional diesel (Fang et al. 2007). Due to RME's lower volatility, it also remains in the sump for longer, resulting in an overall higher dilution rate than ULSD (Andreae et al. 2007; He et al. 2011).

As previously stated, the level of diesel fuel dilution will typically increase in conjunction with the number of aftertreatment devices requiring regeneration. Several researchers have shown that RME fuelled engines require less frequent and shorter DPF regeneration phases than ULSD fuelled engines.

As an actual sump diluent, RME is hydroscopic unlike ULSD, and is likely to form organic acids. These acids are believed to be responsible for compatibility issues with certain metals, elastomers and seals, which in the past have been associated with biodiesel fuelled engines (Parsons 2007; Parker et al. 2009; Terry 2006). Once in the sump, biodiesel dilution has been

shown to accelerate the oxidation of base oils, increasing viscosity and acid content in the process (Sinha & Agarwal 2008; Parsons 2007). However some of these effects may not be relevant until fuel dilution levels reach a critical limit, as some research has shown little difference between ULSD and B100 at dilution levels up to 5% (Sappok & Wong 2008).

The polar nature of biodiesels has also shown the fuel to perform a similar function as antiwear additives, directly competing for available surfaces (Fang et al. 2006). However, excessive dilution with biodiesel facilitates the direct interaction with other oil additives, either causing them to drop out of the oil, or form complex compounds with partially oxidised fuel fractions (Fang et al. 2007; Sinha & Agarwal 2008).

ZDDP (Zinc-Dialkyldithiolphosphate), a popular commercial antiwear additive has been observed to decrease in functionality with increasing biodiesel content (Sappok & Wong 2008). It has been proposed that ZDDP forms complex molecules with the oxidised esters of biodiesel, increasing in severity with the level of fuel oxidation. This suggests that aged biodiesel products interact to a greater extent with ZDDP, reducing the additive's ability to protect the engine against wear (Fang et al. 2007).

There is evidence that biodiesels can have a positive influence on sump oils, with biofuelled engines exhibiting less wear and lower metallic content found within the sump oil (Bijwe et al. 2004). The reduced level of wear of in-cylinder components improves sealing between moving parts; reducing blowby; oil consumption and contamination; and power losses (Sinha & Agarwal 2008). There is a suggestion that the improved lubrication achieved solely from

biodiesel could eventually reduce overall engine maintenance and operating costs (Parker et al. 2009).

There is much confusion amongst researchers as to whether biodiesel dilution actually helps or hinders the oil lubricity as both have been reported as being true. The lowering of the antiwear additives functionality competes with the increased lubricating capability of biodiesel, but eventually one must dominate over the other. One conclusion that can be agreed upon is that the influence that fuel dilution has on oil degradation is determined by both the age and condition of each fluid (Sappok & Wong 2008).

2.4 - Combustion Blowby Gases

IC engines gain their mechanical power from the conversion of chemical energy stored within the fuel during combustion. Under idealised conditions, complete combustion produces only Carbon Dioxide (CO_2) and water (H_2O) as by-products. As combustion is never ideal, the emissions which are produced can be both harmful to humans and the environment. These emissions arise due to the incomplete combustion of fuel; or the combustion of lubricating oil, additives and non-hydrocarbon compounds.

Exhaust emissions can vary immensely and are influenced by engine design, fuel quality, combustion strategy and the air/fuel ratio. There are five classes of **pollutant** species found in the exhaust stream, they include partially burned and unburned Hydrocarbons (Total HC/THC), Sulphur Oxides (SO_x), Carbon Monoxide (CO), Nitrogen Oxides

(NO_x=NO+NO_2), and particulates (Bowman 1975). This section looks at the effects of exhaust pollutants on the degradation of engine oil.

2.4.1 - Effects of blowby

Blowby is the leakage of exhaust by-products from the combustion chamber into the crankcase which have circumvented the piston rings in the process. Exhaust blowby has become more of a concern with small mass-produced CI engines due to the lowering tolerances between pistons and cylinder liners. Blowby is influenced predominantly by combustion pressure, engine age and condition, and the ratio of stroke length to conrod length as this imparts lateral loading which impairs ring sealing (Haycock & Hillier 2004). The influence of blowby gases and combustion by-products on engine oil inevitably will vary between exhaust species.

2.4.1.1 - Water

One product of combustion is water, and is produced in large quantities irrelevant of how complete the combustion is. Under normal operating conditions, water remains as a vapour and is exhausted from the engine. However when water vapour does contribute to blowby, it is able to condense within the relatively cooler crankcase. This can lead to several issues including rusting/corrosion, or the formation of sludge if mixed with the oil directly (Haycock & Hillier, 2004).

2.4.1.2 - Hydrocarbons (HC)

Total Hydrocarbon (THC) emissions are formed from the incomplete combustion of fuel producing unburned and partially decomposed HCs in the exhaust stream. THC content increases with low engine loads, low combustion temperatures and an excess air to fuel ratio. These can all suppress flame propagation, allowing fuel to escape the combustion chamber and enter the sump (Haycock & Hillier 2004). Lubricating oil can also contribute to HC emissions when consumed from the cylinder walls, however this contribution is considered to be minimal for an engine in good condition. HC emissions discussed in this context relate to gaseous emissions only, but can also be liquid or solid, referred to as PM. The consequences of HC contamination are similar to that of fuel dilution discussed earlier in section 2.3.

2.4.1.3 - Sulphur Dioxides (SO_x)

The progressive oxidation of residual sulphur in the fuel and the lubricating oil produces sulphate ions that either intermixes with the oil via the cylinder walls; or contributes to the formation of PM. SO_x is also a precursor of acid rain as it can hydrolyse in the presence of water making it a dangerous pollutant as shown in equations 1-4 (Haycock & Hillier 2004).

	$S + O_2 \rightarrow SO_2$		... (1)
	$2SO_2 + O_2 \rightarrow 2SO_3$		... (2)
Then,	$SO_2 + H_2O \rightarrow H_2SO_3$	(Sulphurous acid)	... (3)
	$SO_3 + H_2O \rightarrow H_2SO_4$	(Sulphuric acid)	... (4)

The level of acidity present in the crankcase is known to have a direct effect on wear (Murakami 1995). Any entrained acid can lead to corrosion, but can also act as a catalyst for

oxidation. The polymerisation of unburned fuels with acid forms sticky or lacquer-like deposits (gums) which 'bake' when coming into contact with hot engine components (Haycock & Hillier 2004).

2.4.1.4 - CO/CO_2

Carbon monoxide formation is due to the incomplete combustion of fuel as a result of insufficient oxygen typically from a rich fuel-air mixture. CO is an intermediary in the combustion of hydrocarbons, formed from the progressive combustion of HC radicals depicted in the following schematic reaction as '*R*' (Bowman 1975):

$$RH \rightarrow R \rightarrow RO2 \rightarrow RCHO \rightarrow RCO \rightarrow CO \quad \text{... (5)}$$

Most of the CO produced is formed at the early stage of combustion, but as diesel engines typically run a lean cycle, an abundance of oxygen and time allows the CO to further oxidise to CO_2, lowering total CO emissions, as shown in reaction 6.

$$CO + OH \rightarrow CO_2 + H \quad \text{... (6)}$$

2.4.1.5 - Nitrous Oxides (NO_x)

Of the gaseous exhaust emissions, Nitrogen Oxides (NO_x) are thought to be one of the most detrimental to oil functionality and is a major constituent of the exhaust species. NO_x can refer to any binary compound of nitrogen and oxygen, but in automotive applications refers to Nitric Oxide (NO) and Nitrogen Dioxide (NO_2) specifically, contributing to 90% and 10% of the total NO_x emissions respectively. NO_x species are usually termed together as

being toxic green house gases; however their environmental impacts are quite different, with NO_2 having a toxicity of roughly five times that of NO (Levendis et al. 1994).

NO_x emissions form from the oxidation of atmospheric nitrogen (N_2) and are dependent upon in-cylinder temperatures, pressures and access to freely available oxygen. The formation of NO is explained through the Extended Zeldovich mechanism (or Thermal NO) in which the atomic oxygen, hydroxyl radicals and N_2 are all in equilibrium. Formation of NO occurs through a chain reaction, initiated by atomic oxygen dissociated from O_2 molecules by the high temperatures reached during combustion (Lavoie et al. 1970).

$$O + N_2 \rightleftharpoons NO + N \quad \text{... (7)}$$
$$N + O_2 \rightleftharpoons NO + O \quad \text{... (8)}$$
$$N + OH \rightleftharpoons NO + H \quad \text{... (9)}$$

The Thermal NO formation mechanism was extended by Lavoie et al. (1970) to include the hydroxyl radical reaction with nitrogen (Equation 9). NO formation favours high temperatures due to the forward rate of reaction 7. When air/fuel mixtures are close to stoichiometric values, and combustion temperatures are sufficiently high, NO forms around the fuel spray flame zone in CI engines post-combustion shown later in Figure 2.6 (Bowman 1975). The overall reaction rate for this mechanism is slow relative to combustion and is very sensitive to localised temperatures.

NO_2 formation should be the final reaction of the NO_x series of emissions; however its formation may be quickly followed by its destruction as shown in the following reactions:

$$NO + HO_2 \rightleftharpoons NO_2 + OH \quad \text{(FORMATION)} \quad \text{... (10)}$$
$$NO_2 + H \rightleftharpoons NO + OH \quad \text{(DESTRUCTION)} \quad \text{... (11)}$$

NO_2 formation occurs through the reaction of thermal NO with hydroperoxyl (HO_2) radicals formed through the incomplete combustion of fuel. However, at very high combustion temperatures, typical of the flame zone, the destruction of NO_2 becomes greater than its formation. Unless the newly formed NO_2 is quenched by mixing with cooler fluids, the NO_2 will quickly decompose to NO. Typically, NO_2 **formation** favours lower peak combustion temperatures and NO_2 **destruction** high temperatures (Bowman 1975). Therefore the majority of NO_X emissions will be in the form of NO.

The absorption of nitrogen oxides in the oil is known as nitration and occurs when NO_x gases come into contact with the oil on the piston-cylinder liner interface as shown in Figure 2.5 (Uy et al. 2010). The mechanisms of how nitration affects oil are still not completely understood (Henderson & LeBarge 2013). One thought is that the NO_x acts as a free radical initiator that accelerates the rate of oxidation (Johnson & Korcek 1991). A consequence is the formation of peroxide and hydroperoxides radicals within the oil, which are able to further decompose or oxidise to form aldehydes, ketones and carboxylic acid (Rizvi 2009). Oil-borne oxidation intermediates are then able to further react with NO_2 and NO, leading to the formation of nitro-oxidation products. Alternatively the intermediates enable the destruction and/or formation of NO_2 within the oil depending on temperatures (Johnson & Korcek 1991).

Nitration of oil is temperature dependant, the initial formation of NO_x occurs when temperatures reach 137°C (Rizvi 2009), but can break down within the oil when temperatures exceed 150°C (Henderson & LeBarge 2013). The same is true within the sump,

where both oxidation and nitration occur concurrently. At relatively cooler sump temperatures (< 80°C), nitration is dominant, whereas when sump temperatures increase above 90°C, oxidation becomes dominant (Henderson & LeBarge 2013).

The second school of thought is that NO_x ions found in exhaust gas may hydrolyse within the crankcase to form nitrous/nitric acid which can attack the oil (Shimokoji & Okuyama 2009). These acids neutralize and consume the alkaline constituents in the oil which include several additives and detergents leading to a fall in Base Number (BN). This lends itself to a reduced additive performance and increased rate of oil degradation (Trujllo 2004).

The formation of deposits in and around the combustion chamber is also believed to be initiated by NO_x, organic nitrates and other oxidation-derived products entrained within the oil (Shimokoji & Okuyama 2009). These entrained contaminants are thermally unstable and are able to decompose and polymerise. However, a fall in BN is typically accompanied by a reduction in cleaning performance and so contaminants are able to accumulate forming several undesired polymerised substances such as sludge, varnish and resins (Trujllo 2004). Therefore nitration can be viewed as an initiator to deposit formation in engines.

Blowby condensate containing oil and water has been seen to have an increased NO_x ion concentration with engines utilising EGR (Exhaust Gas Recirculation) (Murakami 1995). There are two reasons why this is thought to occur, one is that the NO_x is reintroduced into the combustion chamber, increasing the likelihood of entering the crankcase as blowby. The second is the utilisation of EGR lowers the temperature of the oil and cylinder walls, which

will in turn increase the amount of NO_x able to be quenched by the oil, and transported to the sump (Murakami 1995).

2.4.2 - Biodiesel blowby gases

The variation in exhaust emissions between conventional diesel and biodiesel can again be attributed to differences in their respective properties as summarised in Table 2.1. The chemical composition of the two fuels is subtly different; RME has lower fuel-borne sulphate compounds present, producing lower SO_x emissions.

The increased surface tension and natural lubricity allows for an increased fuel charge spray to penetrate further into the combustion chamber increasing atomisation. In conjunction with a higher cetane number, oxygen content and lack of aromatics, biodiesel may in fact promote a more complete combustion leading to lower CO emissions and reduced unburned HC (Rounce et al. 2012; Sappok & Wong 2008; Agarwal & Das 2001; Giakoumis et al. 2012).

RME also has a high but distinct boiling range and flash point making it less volatile and less likely to evaporate unlike the ULSD which has a lower and broader boiling range. RME therefore requires increased in-cylinder pressures and flame temperatures for combustion, all favouring the production of NO_x. Overall the differences in exhaust emissions between RME and ULSD are a decrease in HC, SOx and CO species at the expense of increased NOx emissions (Rounce et al. 2012; Giakoumis et al. 2012).

2.5 - Particulate Matter

The emissions emanating from diesel engine exhaust will contain both gaseous pollutants and Particulate Matter (PM). The PM encompasses both the liquid and solid phase materials found in the exhaust, most recognisable as the black smoke emitted from diesel vehicles. Soot is just one element of PM, also referred to as the insoluble dry fraction; formed from clusters of microscopic carbonaceous particles (Gill et al. 2012). Soot formation is initiated via the pyrolysis of unburnt hydrocarbons, caused by the immense heat produced during fuel combustion (Kennedy 1997). Measurements by Clague et al. (1999) have shown diesel engine soots typically consisting of carbon (~90%), oxygen (~4%) and hydrogen (~3%) with remnants of nitrogen, sulphur and metallic elements (<1%).

Most research surrounding PM has thus far been the focus of aftertreatment research. However, these studies have revealed new levels of detail on soot morphology, chemistry and physical properties which is very relevant in determining the interactions that soot has within the engine. This section explores factors which contribute to the formation of soot and its properties from a tribological perspective.

2.5.1 - Formation and Microstructure

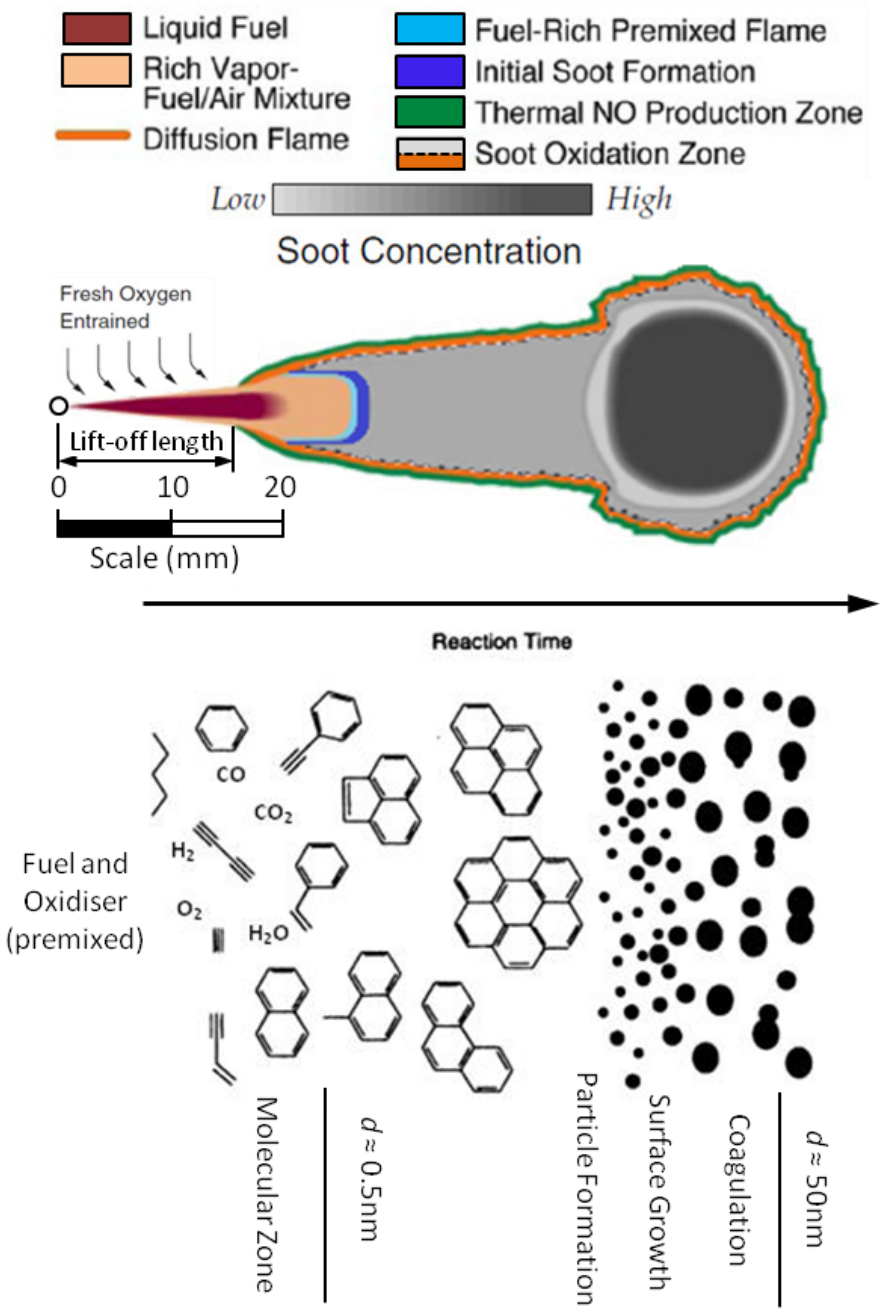

Figure 2.6 - Dec's Conceptual Model of Diesel Combustion during the Quasi-Steady Phase related to the structural formation of soot within the premixed flame, Adapted from Argachoy & Pimenta (2005); Dec (1997); Mueller et al. (2003); Musculus et al. (2002) and Richter & Howard (2000)

The formation of soot is described by Dec's conceptual model for direct injection diesel combustion during the "quasi-steady" period, illustrated in Figure 2.6. The model is an idealised cross-sectional slice through the midplane of a fuel jet plume, taken as a freeze frame between the end of the premixed-burn phase until the end of fuel injection (Dec 1997). This model is idealised due to the absence of external interactions such as the cylinder walls, multiple injection nozzles and swirl.

Within Dec's model, several stages are highlighted depicting the formation of soot. Fuel is injected into the combustion chamber at a high pressure forming a liquid jet (*burgundy*), entraining oxygen along its lift-off length. This forms a rich fuel/air vapour (*pink*), measured to be at temperatures between 700-900K for diesel fuels. A premixed combustion zone (*pale blue*) forms around the perimeter of the rich fuel/air vapour raising local temperatures further to 1300-1600K as any available oxygen is consumed (Mueller et al. 2003).

Downstream of the lift-off length, soot formation initiates beyond the fuel-rich premixed zone, where temperatures can reach 1300-2500K (Mueller et al. 2003). Soot increases in size and concentration the further from the injector nozzle, shown to be highest (*black*) at the centre of the jet plume (Musculus et al. 2002). Due to there being an abundance of oxygen from the surrounding air, a diffusion flame (*orange*) forms around the fuel jet's periphery, increasing the local temperature further (Flynn et al. 1999). Conditions on the lean side of the diffusion flame are ideal for NO formation (*green*), whereas inside the peripheral flame, nearby soot is oxidised (Dec 1997).

Figure 2.6 also depicts the structural formation of soot within the premixed flame. Soot particle growth occurs as a two stage process, the first being the nucleation of primary particles which grow from simple molecular components 1.5nm in diameter, to larger 'nanoparticles' up to 50nm in size (Kennedy 1997; Richter & Howard 2000). Secondary particles form through the collisions and cohesion of primary particles, creating large agglomerated structures 50-1000nm in size (Kittelson 1998).

Primary particles can grow by one of two mechanisms, chemically through surface growth, and/or physically by collision coagulation (Kennedy 1997). Surface growth is the more dominant mechanism whereby the nascent soot particles serve as nuclei for the deposition of gas phase species. The initial aromatic ring structures fuse with subsequently adsorbed Polycyclic Aromatic Hydrocarbons (PAH), forming bundles of polyacene platelets, increasing in particle size but not number (Richter & Howard 2000; Li et al. 2002).

Coagulation occurs through the sticking collisions of primary particles still undergoing mass growth. Particles collide and coalesce, significantly increasing in size whilst at the same time reducing in number. Within the post-flame zone the soot experiences further pyrolytic conditions where carbonization occurs, transforming the microstructure from an initially amorphous material to a progressively more graphitic one. This results in a small decrease in particle mass but no change in particle number (Richter & Howard 2000).

Carbonization typically indicates the end of the 'growth' stage of the primary particles, reducing the number of active sites on the surface for gaseous species to adsorb to. Any

further collisions between primary soot particles no longer results in coagulation, but agglomeration instead. These chain-like agglomerates form the structure of the secondary particles, composed of several tens to hundreds of primary particles clustered together by weak van der Waals forces (Ishiguro et al. 1997; Kuo et al. 1998; Lee et al. 2003).

2.5.2 - Factors

Soot formation occurs within the fuel jet spray with the most influential factors coming from the engine operating conditions. Increased oxygen within the soot-forming region of the fuel jet plume, either through entrainment of local air or additional fuel borne oxygen, reduces the production of soot. Available oxygen within the fuel burning regions increases local flame temperatures, which in-turn decreases the number of UHCs, increasing soot oxidation, resulting in a more complete combustion (Rounce et al. 2012; Ladommatos et al. 1996). With sufficient oxygen or oxygen-containing species, soot precursors will preferentially react to produce CO rather than aromatics and soot (Mueller et al. 2003; Flynn et al. 1999; Pinzi et al. 2013; Tsolakis et al. 2007).

Higher engine loads can lead to increased soot production, although this is primarily due to the increased fuelling rate required to maintain cylinder power (Tsolakis 2006). High engine speeds will also increase soot production, but this is due to the greater number of combustion cycles per second, leading to a reduced residence time of the particles within the combustion chamber available for oxidation (Daido et al. 2000). An increase in engine size has the opposite effect, as it increases soot residence time raising the level of soot oxidation, thus lowering soot production.

Increased fuel injection pressure will improve fuel atomisation, causing a greater number of smaller volume fuel droplets to form. It is thought that this causes a larger number of soot nucleating sites, increasing the number of primary particles and potentially reducing their average size (Tsolakis 2006). However, reduced primary particle size also decreases the likelihood of collisions and particle agglomeration, prohibiting the formation of larger secondary particles.

EGR also has an effect on soot formation, as a small portion of inlet air is replaced by recirculated exhaust gas, intended to reduce the level of available oxygen. Combustion temperatures are lowered, which in turn also reduces NO_x production. However, EGR reduces the oxygen to fuel ratio which in turn has the effect of increasing soot production whilst impairing soot oxidation. Therefore, with EGR systems, more soot remains un-oxidised, and will eventually appear in the exhaust (Ladommatos et al. 1996). Soot particles that re-enter the combustion chamber during EGR are thought to behave as particle nuclei; enabling the already formed soot particles to undergo further surface growth and coagulation, resulting in a net increase in emitted engine particle mass (Gill et al. 2012).

2.5.3 - Effects on oil

Only 29% of fuel-borne soot is thought to exit the combustion chamber through the exhaust valves, with the remainder forming deposits within the engine or accumulating in the sump. Soot is transported to the crankcase either with blowby gases or from the reciprocating action of the piston rings, scraping soot deposits from the cylinder walls which become entrained within the sump. However, soot is thought only to contribute to as little

as 3% of the total mass of sump oil in regular diesel engines. (Daido et al. 2000; Green & Lewis 2008; Dennis et al. 1999; Tokura et al. 1982)

Over time however, soot will alter oil performance, and any components which are reliant upon oil for lubrication. Most noticeably, soot affects the rheological performance and is seen to increase engine wear. In the past these problems have been attributed to oil oxidation, however a study by Bardasz et al. (1995) concluded that oil thickening was more dependent on the amount of soot present, and/or soot particle interaction than oxidation (George et al. 2007).

2.5.3.1 - Rheology

The effect of sooting on engine oil rheology is a complex balance and interplay between the chemical and physical properties of both the soot and the oil. Factors determining overall viscosity of the heterogeneous mix include primary particle and agglomerate size; particle density; polydispersity; colloidal stability; viscosity, temperature and shear history (Selby 1998; Antusch et al. 2010). Soot suspended within the oil would be expected to be Newtonian if the particles were to behave as independent spheres. However, the degree of thickening and rheological characteristics can vary due to the colloidal properties and rheology being interrelated. The state and form of the suspended particles will therefore affect the flow properties of the mixture. The wide range of influences means that soot-loaded oils can exhibit yield stress; shear thinning and thickening; and hysteresis behaviour (Bardasz et al. 1995; Selby 1998; Kornbrekke et al. 1998).

Ryason and Hansen (1991) carried out early investigations into the affects of sooting on used oil rheometry. Their studies showed that soot contamination levels below 1% w/w caused a linear increase in lubricant viscosity, but above 1% the viscosity rose rapidly (Green & Lewis 2008). The reason as to why soot loading increases oil viscosity is predominantly due to the stability of the colloidal system, and inter-particulate forces at work. The van der Waals forces between particles induce an attractive force; whereas any electrostatic forces cause the particles to repel. If the electrostatic barrier is lost through extreme compression or additive depletion; attractive forces will dominate causing the particles to agglomerate forming flocculated structures. These structures have a greater phase volume than dispersed particles, causing the overall fluid's viscosity to increase (Selby 1998; Kornbrekke et al. 1998).

However, oils containing highly agglomerated soot show a marked sensitivity to mechanical shear. In general, a suspension of agglomerated particles will be non-Newtonian, and the mixture will be "thickened". As shear stress increases, eventually the agglomerates will break apart, and the viscosity reduced, "thinning" in the process. Therefore the viscosity of soot loaded oil will not only depend on the flocculated structures, but also their breakdown under load. Viscosity measurements of highly flocculated oils are therefore less reliable due to the wide range of possible shear rates occurring. However, it is thought that oils operating under regular engine conditions experience a high enough shear stress that the soot-loaded oils are essentially in an unagglomerated state, behaving effectively as a Newtonian fluid (Kornbrekke et al. 1998; Selby 1998).

The behaviour of entrained soot particles will be determined by the particle size/film thickness ratio (Chiñas-Castillo & Spikes 2004). Increasing soot content is seen to increase fluid viscosity, with the entrained particles creating a thicker oil film and enhancing the film formation rate. This is due in part to the increased likelihood of particulates able to penetrate the Elastohydrodynamic (EHD) contact film, causing the soot to perform as a solid lubricant (Aldajah et al. 2007). However, when the oil film is less than the diameter of the primary soot particle, the effect on wear also increases (Green & Lewis 2008).

The lubricant's ability to deal with soot-induced thickening will also depend on the soot dispersancy and additive package. Once the dispersancy becomes too high or the additive package becomes depleted, the chemical balance shifts causing the oil to cease performing functionally. Increased viscosity will also cause pumpability problems leading to a loss of power and later to mechanical failure of components reliant on oil films to prevent metal-on-metal contact (Rounds 1977).

2.5.3.2 - Wear

Increased engine wear is more detrimental to overall engine performance and longevity than oil rheology. The reasons as to why soot reduces the oil's ability to prevent wear has been a topic of research for almost four decades. The debate began with the published paper: "Carbon: Cause of Diesel Engine Wear?" by Rounds (1977). With limited data on the hardness of soot particles, carbon black and graphite were used to simulate soot. With the Mohs hardness of graphite between 1-2, the prevailing opinion was that soot is too soft to abrasively wear engine components, going against the previously-held opinion.

There is little doubt that primary soot particles are harder than larger agglomerates, but the thought that graphitic particles could wear steel was thought to be ludicrous (Kuo et al. 1998; Ryason et al. 1990).

Rounds (1981) opposed the notion that surface coatings could be removed by soot abrasion, showing that the hardness of Carbon Black (a synthetic soot) was less than alumina, a known engine abrasive. Knowing that increased soot content increases engine wear, Rounds suggested that instead of acting as an abrasive, soot preferentially adsorbs active antiwear additives, reducing their effectiveness during film formation (Gautam et al. 1999; Green & Lewis 2008). The shortfall of Rounds' theory was that once the soot was removed from the oil, the antiwear performance returned to normal. If additive adsorption had occurred, soot removal would have also reduced the additive content and likewise the antiwear performance (Olomolehin et al. 2009).

Berbezier et al. (1986) did not rule out the possibility that soot preferentially adsorbs antiwear additives; just a failure of evidence concludes it to not be prevalent. Also that abrasive wear probably occurs due to the presence of soot, however these are not the only factors that contribute to wear, and alone do not explain the high engine wear rates caused by soot. To explain bore polishing, Berbezier thought there to be competitive adsorption between the antiwear additives and carbon to the metal surfaces. Surface coverage by carbon from soot occurs due to physical adsorption or the plugging of scratches by wear debris and deposits, decreasing the surface available for the antiwear additives to successfully adsorb to.

Berbezier and Martin (1988) hypothesised that soot may alter the physical and mechanical properties of the additive, depleting the additivised elements within the surface films. It was thought that the presence of sooty carbon would weaken the adhesion bonds between the antiwear film and the metal surface, weakening the film's mechanical strength (Kuo et al. 1998). Nagai et al. (1983) suggested that soot's influence on the destruction of the antiwear film was not through adsorption but abrasion, mechanically removing the film from metal surfaces.

Other research has shown that soot's influence on engine wear occurs through oil starvation to lubricated contacts (Kuo et al. 1998). There are two ways that oil starvation can occur; one is rheologically. With an increased oil viscosity, the pumping loss through small bore channels prevents a sufficient oil volume or pressure to maintain a lubricated contact resulting in wear. A secondary effect of soot agglomeration is thought to be the clogging of oil channels by soot, blocking lubricant entry creating dry contacts leading to rapid wear (Green et al. 2006b).

Ryason et al. (1990) revisited the original theory suggesting that soot particles do cause abrasive wear, contradicting the earlier findings of Rounds (1981). Ryason argued against the general opinion that soot is soft, as this was based on the assumption that soot had the same properties as graphite, which is not true. Graphite can be described as being anisotropic, as its properties change with direction in reference to the basal plane. Although soot is described as having a graphitic microstructure, it forms as randomly orientated polyacene platelets, stacked in amorphous bundles. Soot particles form as a spherical mosaic

of these 'bundles', with curved layers that do not yield as easily as the flat basal planes found in bulk graphite. The nano-sized non-planar microstructure of primary soot particles make it much harder than bulk graphite and potentially steel although no direct measurements of hardness had been made at the time of Ryason's studies in 1990 (Li et al. 2002; Ryason et al. 1990).

The hardness of primary soot particle was still questionable until Jao et al. (2000) demonstrated a technique to correlate carbon hardness and Plasmon energy using Electron Energy-Loss Spectroscopy (EELS). By utilising EELS on various carbon structures such as diamond and graphite which have known hardness values, a calibrated correlation could be made. Later experiments by Li et al. (2002) using this method proved that diesel soot is indeed harder than many corresponding engine parts. It was also shown that there is a marked difference in hardness among individual soot particles produced by the same engine (Li et al. 2002). After confirming what researchers had suspected all along, there finally was empirical evidence to prove that soot is hard enough to abrasively wear engine components. The additional verification that differing engine conditions also contributes to soot hardness was equally as important.

2.5.4 - Effects of Biodiesel PM

The majority of studies have found that biofuelled CI engines typically have reduced particulate emissions compared to diesel fuel. The main causes of this reduction is by both a decrease in soot formation and enhanced soot oxidation (Lapuerta et al. 2008). It is thought that improved combustion, especially in locally fuel-rich combustion zones, can occur due to

the additional fuel-borne oxygen of the biodiesel, reducing the number of soot precursor species formed such as acetylene and PAH (Tsolakis 2006; Flynn et al. 1999). These main precursor species are derived from the thermal decomposition of paraffinic, naphthenic, and aromatic fuel constituents, which are far lower for biodiesels (Llamas et al. 2013).

It is thought that the increased fuel density and lubricity of biodiesels results in better fuel atomisation. This causes an increased number of fuel droplets that are smaller in size, leading to a higher number of soot nucleation sites yielding a larger percentage of nano-sized particulates. It has also been shown that these nano-particulates are in fact liquid matter that contribute to the Soluble Organic Fraction (SOF) of the biodiesel PM (Rounce et al. 2012). Therefore, although the combustion of biodiesels yields a significantly lower proportion of solid PM compared to diesel combustion, it is accounted for with a considerably higher proportion of SOF originating from the from the unburned fuel (Tsolakis 2006). With sufficient oxygen available, the precursor species are more likely to react than produce soot (Mueller et al. 2003). Furthermore, the fuel-borne oxygen aids in the oxidation of any newly formed soot, resulting in biofuelled engines emitting smaller sized particles with a lower overall mass (Pinzi et al. 2013; Tsolakis 2006).

It is also thought that the lower sulphur content of most biodiesels contributes to lower PM emissions (Thornton et al. 2006; Tan et al. 2009). It is believed that sulphur causes a soot scrubbing effect, becoming an active centre for hydrocarbon adsorption. The importance of sulphur content though is becoming less relevant as fuels such as ULSD become the

convention (Lapuerta et al. 2008). However there is still currently a marked difference in sulphur content between RME (5 mg/kg), and ULSD (46 mg/kg) (Tsolakis et al. 2007).

Few researchers have specifically looked at the effects of biodiesel soot on engine wear in the same way as conventional diesel, with most research focussing on the effects of the fuel alone. Devlin et al. (2008) is one of few whose research has focussed on biodiesel soot, however the research looked at B20 blends only. The conclusions of this research were that the soot generated using B20 was of similar size and hardness to regular diesel; and there was no evidence of soot-induced oil thickening or oxidation concerns.

It has been seen that morphological features of soot generated by biodiesel produces more oxygenated particles both within its structure and upon the surface. A hypothesis proposed by Fang et al. (2007) is that soot generated from B100 results in a more polar surface that has an additional interaction with the dispersant additives. This leads to a more effective dispersion of soot colloids, prolonging the onset of viscosity increase by preventing agglomeration within the oil (Fang et al. 2007).

2.6 - Literature Summary

Engine oils during normal operation will degrade by undergoing continual reactions, changing both chemically and physically, detracting in performance from initial specifications and require changing. The main forms of oil degradation are evaporation, thermal degradation, oxidation, polymerisation, and deposit formation (Gatto et al. 2008). The rate at which oil degradation occurs is affected by several factors including: the age and condition

of the oil; the locations with which the reactions are occurring; and the presence of contaminants such as exhaust blowby, soot, and fuel (Lee et al. 2005). This thesis looks at the influence of each contaminant individually on the degradation of engine oils.

Fuel and oil come into contact with one another in and around the combustion chamber when the cylinder walls are wetted by uncombusted fuel. The oil and fuel mix are then transported to the sump by the scraping and reciprocating action of the piston rings, or with blow-by gases, or simply under gravity (Agarwal et al. 2003; Lee et al. 2005). Oil dilution is deemed critical once above 5% w/w for most diesel engines (Froelund & Ross 2005; Sappok & Wong 2008; Andreae et al. 2007). Diesel fuel dilution levels are known to increase in proportion with the number of aftertreatment devices which require regeneration through delayed injection strategies (Fang et al. 2006).

The common effect of fuel dilution is a change in oil viscosity, either as an increase with the fuel functioning as a substrate for oil oxidation (Gatto et al. 2008; Andreae et al. 2007). Or if fuel dilution dominates over oxidation, which is less viscous than oil, will cause an overall lower viscosity. This will in turn reduce the oil's load bearing capability, leading to increased friction and wear (Agarwal 2007; Andreae et al. 2007).

Within the sump, the most volatile fuel fractions evaporate, leaving heavier aromatic compounds behind. Therefore after a prolonged period, the fuel content remaining in the sump will have a different composition to the fuel that entered. This changes our understanding of oil/fuel interaction as previous work focussed on conventional fuels

interacting with sump oil. This suggests that the fuel found within the sump is compositionally different, and therefore should interact differently with the oil than previously expected.

The use of biodiesels has caused much confusion amongst researchers, whether its dilution helps or hinders oil performance. On the one hand, the polar nature of biodiesels enhances lubricity and its interaction with other hydrocarbons (Knothe & Steidley 2005). But in general, biodiesels have a lower oxidative stability than regular diesels which does reduce its capability for long term storage (Parsons 2007). And due to biodiesel's lower volatility, it enters the sump at a faster rate (Fang et al. 2007), and remains for longer than conventional diesel fuels (Andreae et al. 2007; He et al. 2011).

Much of the negative perception surrounding many biodiesels is due to 'poor' quality fuels, which either use non-transesterified fuels, or contain trace quantities of reactants which do not fully meet specifications (Fraer et al. 2005). There is also a suggestion that aged biodiesel interacts with antiwear additives, competing with and reducing their ability to protect the engine against wear (Fang et al. 2007). The lowering of the antiwear additives functionality competes with the increased lubricating capability of biodiesel, but eventually one must dominate over the other.

One agreed conclusion is that the influence that fuel dilution has on oil degradation is determined by both the age and condition of each fluid (Sappok & Wong 2008). This is an area usually assumed by many researchers, but has never truly been established. This asks

the question, at what point does the fuel content have the most influence on oil performance?

Harmful exhaust emissions are a result of incomplete fuel combustion; or the combustion of lubricating oil, additives and non-hydrocarbon compounds. Blowby is the leakage of exhaust by-products from the combustion chamber into the crankcase, circumventing the piston rings in the process. Several exhaust by-products are precursors of strong acids, which can lead to engine corrosion, but also act as a catalyst for oil oxidation (Murakami 1995). The difference between the exhaust emissions of RME and ULSD is a decrease in HC, SO_x and CO species at the expense of increased NO_x emissions (Rounce et al. 2012; Giakoumis et al. 2012). How influential these particular **pollutant** species are individually upon oil degradation is still questionable, especially with differences between the two fuels' emissions?

Soot formation initiates via the pyrolysis of unburnt hydrocarbons under the immense heat produced during the combustion of fuel (Kennedy 1997). Soot loading of engine oils has been shown to increase oil viscosity and engine wear, but how and why is still debated. How this compares for conventional and bio- diesels, which typically produce less particulate emissions, and the true effects and influence of engine oil soot loading, are also examined within this research.

CHAPTER 3 - EQUIPMENT & METHODS

This chapter contains descriptions of all the analytical test methods and equipment used within this research. The fuels chosen for use in all experiments were ULSD as the representative conventional diesel, and RME as the biodiesel. Both of which were provided by Shell Global Solutions UK with properties found in Table 2.1 of chapter 2.

The oil used within this research was a popular low-cost, store branded, part synthetic engine oil with an unknown additive package prior to experimenting. It was chosen to suitably represent what could potentially be a worst case usage scenario amongst common diesel engines, as well as being a useful comparison to the sump oil within the test engine. The oil meets many defined grades stipulated by several regulatory bodies, including SAE grade 10W/40; API grade SL-CF and ACEA grade A3/B3. Each regulatory body may have an emphasis on certain fluid properties over others, but for the purposes of this research, the ACEA standard was focussed upon which defines a grade A3/B3 oil as:

> *"Stable, stay-in-grade oil intended for use in high performance gasoline engines and car & light van diesel engines and/or for extended drain intervals where specified by the engine manufacturer, and/or for year-round use of low viscosity oils, and/or for severe operating conditions as defined by the engine manufacturer."* (ACEA 2010)

3.1 - Oil Ageing Rig

To simulate the effects of oil ageing within the engine, a test rig was developed to artificially age the oil. The rig enables the ageing conditions to be actively controlled and

finely tuned for parameters such as fuel dilution levels and engine exhaust. Figure 3.1 shows a side and front view of the ageing rig used within this study.

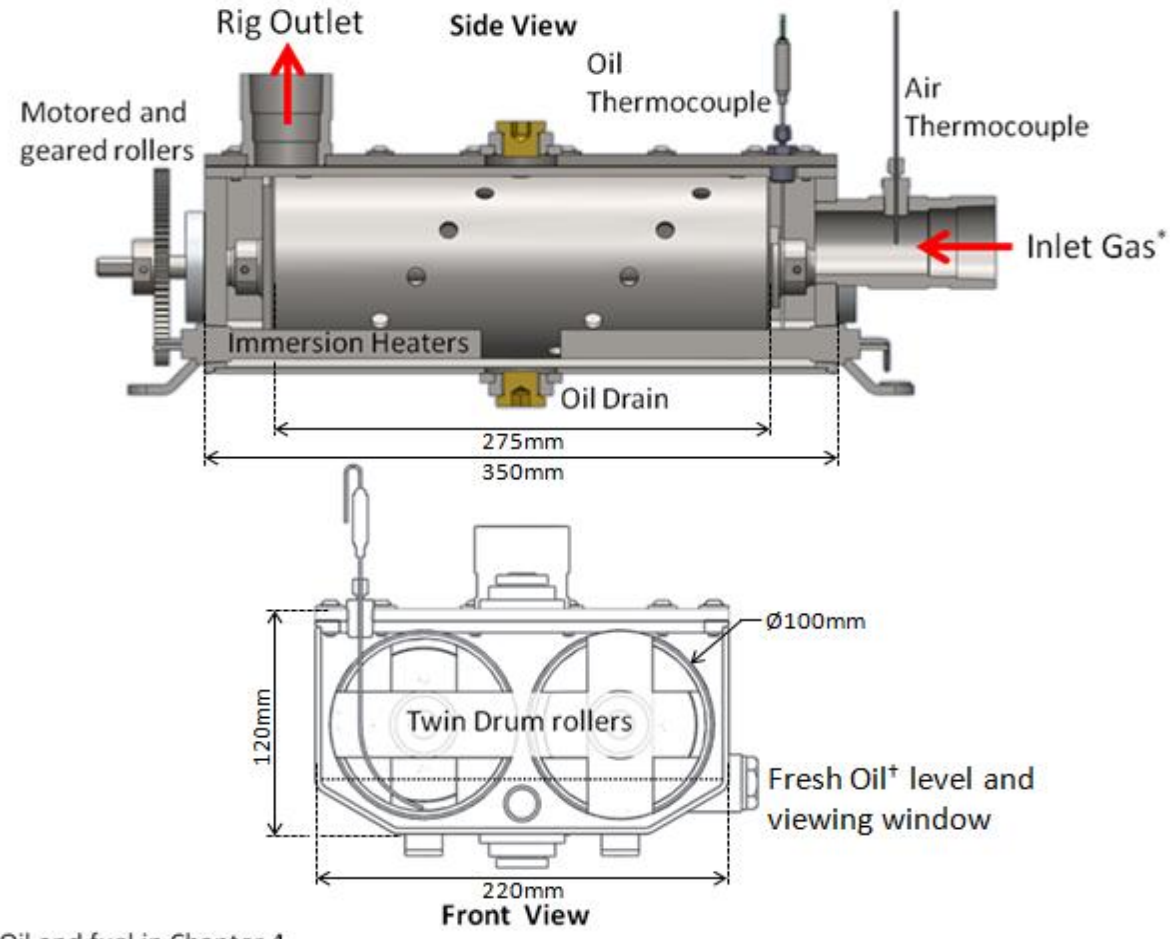

† - Oil and fuel in Chapter 4

* - Hot air in Chapter 4; Engine exhaust w/o PM in Chapter 5; Engine exhaust with PM in Chapter 6

Figure 3.1 - Oil Ageing Rig

The rig consists of an oil bath with two hollow drums immersed in a small volume of oil. The bath represents reactor 2, the sump as proposed by Lee et al (2006), maintaining the oil at an elevated temperature whilst continually churning and aerating it, simulating in-engine conditions. The drums represent reactor 1, the piston ring pack and grooves, where the oil forms a thin film and experiences high temperatures, abundant oxygen, and exhaust gases (for chapter 5 & 6) simulating the conditions in and around the combustion chamber.

3.1.1 - Rig Parameters

The ageing rig was setup to evaluate oil parameters using three different settings. These settings define the results found in chapters 4-6 with a summary of the test parameters shown in Table 3.1. For the three test variants, the rig was setup identically which included the bath being filled with 1.5 litres semi synthetic engine oil, with samples regularly extracted for characterisation in 10mL volumes and replaced by a fresh and equal volume of test fluid. Extracted samples would then be 'prepared' for characterisation by filtering through a series of different porosity filter papers, with only a small portion passing through a 0.8µm Millipore filter as required for testing on the USV (3.4.1).

Table 3.1 - Oil Ageing Rig Test Parameters

Chapter	4	5	6	
Measured Effect	Oxidation and fuel dilution	Exhaust emission w/o PM	Exhaust emission with PM	
Test Duration (hours)	100	20	20	
Rig Inlet connection	Hot air Gun	Engine exhaust @3bar + DPF	Engine Exhaust	
			@3bar	@5bar
Rig Inlet Temperature (°C)	150-250	130	130	160
Rig Inlet Flow rate (L/min)	600	753	753	878
Rig Oil Temperature (°C)	90	90	90	100
Roller Speed (rpm)	30	30	30	40

The initial test was run with fresh, unblended oil in the rig for 100 hours, with the hot air gun connected to the rig inlet, fluctuating between 150-250°C. At every hour, the rig was stopped and an oil sample was extracted and replaced with a fresh sample of equal volume.

This was continued every hour up until the test run was complete at 100 hours, when the remaining oil in the rig was also collected and stored.

The rig would then undergo an extensive cleaning process to prevent any build-up of partially oxidised residues which could affect any future experiments. Cleaning would involve an initial wash using a degreasing agent, followed by toluene to break down any stubborn oils, and then a final wash and scrub in warm soapy water. The whole rig would then be quickly reassembled and the next test fluid added to prevent the rig from corroding.

This process was repeated for two more test fluids for the fuel dilution tests (chapter 4). The fresh oil was pre-blended with 10% fuel by weight before entering the rig, amounting to a total test fluid volume of 1.5 litres. The first fuel dilution test used fresh oil blended with ULSD, and the second blended the oil with RME. Again each test ran for 100 hours each, with samples extracted regularly. The intentions for this test were to replicate in-engine conditions, whereby fuel would typically collect within the sump from exhaust blowby, but neglected the effects of other chemical content. This way the effects of sump dilution from fuel were compared between the unblended and pre-dosed samples to investigate their affects on the oil's thermo-oxidative degradation.

The second set of experiments included the effects from exhaust blowby (chapter 5), focussing on the exhaust's chemical content, but excluding PM. Here the rig was run in conjunction with a CI engine (section 3.2), with the engine's exhaust connected directly to the rig's inlet but with a physical filtration device fitted, known as a Diesel Particulate Filter

(DPF) detailed in section 3.2.1, to eliminate the effects of sooting. This time the engine and rig was run only twice, once per fuel for 20 hours each. The rig was filled with fresh unblended oil whilst the engine was firstly fuelled with ULSD only. Again oil samples were extracted from the rig on an hourly basis for further analysis. At the end of each test run, the rig went through an identical cleaning process as before, with the fuel lines feeding the engine also being cleaned and flushed. The second test was run using 100% RME (B100) in an identical fashion to the previous ULSD fuelled test.

The third set of experiments (chapter 6), again had the rig's inlet connected to the engine exhaust, but this time without the DPF, enabling the full exhaust to pass through the rig. There were three tests conducted with this setup, each lasting 20 hours per test. The two controlled variables were the fuel (ULSD or RME), and the Indicated Mean Effective Pressure (IMEP) of the engine (either 3 or 5 bar). This setup tested the effects of soot loading on the oil from the two fuels under two relatively modest engine loads. However, the heavier engine load of 5bar was conducted using ULSD alone as this was thought to produce the greatest amount of PM required to truly test the effects of soot loading on the oil.

3.1.2 - Soot Sampling

An additional aim for the test rig and the experimental setup was the collection of soot particles, which was achieved via three separate methods. The first utilised the oil bath, using the oil film formed upon the roller surfaces to entrain soot. This represented a more natural level of sooting found within the sump, which was attempted to be replicated by the rig.

The second method was a passive collection of soot onto steel wire mesh placed within an exhaust box in-line to the exhaust stream. This enabled a dry sooted form to be collected, which was later used to artificially dose the oil with a known mass of soot. This technique has a minimal impact on exhaust flow as the steel wire meshes were loosely packed and did not restrict the soot flow path to the rig.

The final method utilised copper mesh grids (Figure 3.2) to thermophoretically collect soot at the entrance of the exhaust manifold, perpendicular to the exhaust flow. The grids were also Formvar coated, enabling the soot samples to be viewed directly under Electron and Atomic Force Microscopes with no further preparation.

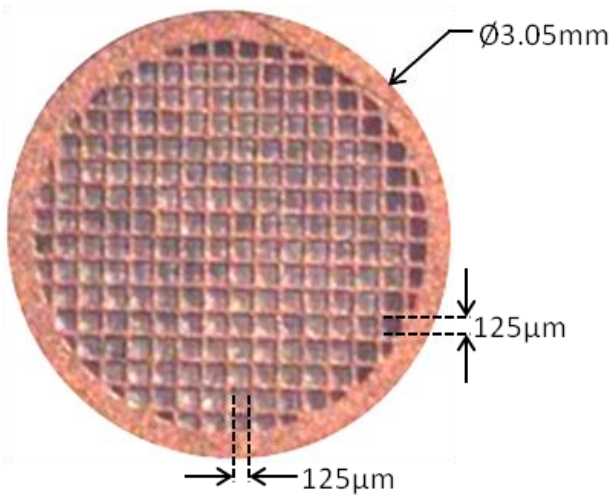

Figure 3.2 - Formvar coated copper mesh gilding grid

3.2 - Engine Setup

The test engine used within this research was a naturally aspirated single cylinder CI engine from Lister Petter (Figure 3.3), with parameters listed in Table 3.2. The engine utilises a pump-line-nozzle Direct Injection (DI) fuel system situated centrally at the top of the combustion chamber, directly fuelling into the piston crown bowl.

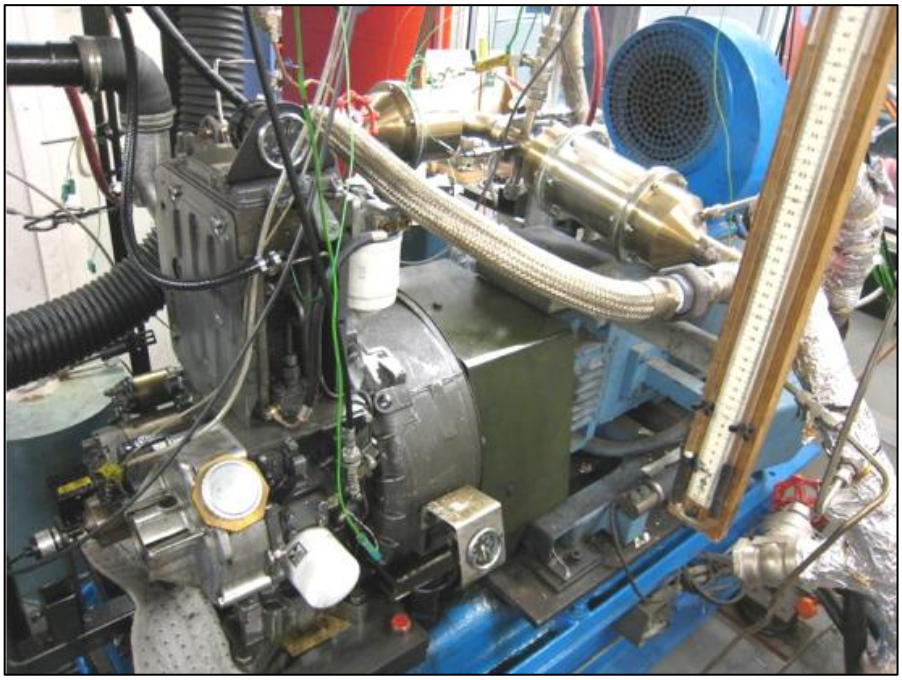

Figure 3.3 - Lister Petter TR1 Test Engine instrumented with dynamometer

The test engine is coupled to an air-cooled Thrige Titan DC electric dynamometer with a load cell and thyristor-controlled Shackleton Drive System that both loads and motors the engine. The engine is instrumented with a rotary encoder and tachometer attached to the flywheel to measure crank angle and speed. Engine inlet conditions were monitored using thermocouples, pressure sensors and a Romet rotary airflow meter. Likewise the exhaust and crankcase was instrumented to measure temperature and pressure. Mounted within the cylinder head was a Kistler 6125B pressure transducer to monitor in-cylinder pressure.

Table 3.2 - Test Engine Parameters

Engine Specifications		
Number of cylinders	1	
Bore/stroke	98.4mm/101.6mm	
Displacement volume	773cm^3	
Connecting rod length	165mm	
Compression ratio	15.5:1	
Related power	8.6kW @ 2500rpm	
Peak torque	39.2Nm @ 1800rpm	
Injection system	Three Ø0.25mm holes Pump-line-nozzle Bowl-in-piston	
Injection Timing (CAD)	22 bTDC	
Engine Test Conditions	**3 bar**	**5 bar**
Inlet Temperature (°C)	22-25	
Exhaust Temperature (°C)	220	320
Engine Torque (Nm)	12	20
Engine Speed (rpm)	1500	

3.2.1 - Diesel Particulate Filter

To eliminate the effects of sooting on the engine oil, the exhaust stream was fitted with a DPF provided by Johnson Matthey. The DPF is made from Cordierite and has been shown to remove 99% of PM by mass and 85-99% by particulate number for diesel fuel (Lakkireddy et al. 2006). The DPF is a wall-flow monolith filter and works by plugging adjacent cells downstream of the filter so the exhaust gas cannot exit cells directly, but must pass through the porous cell walls of the filter (Rounce et al. 2012). The solid PM becomes trapped within the walls and the inlet channel surface on the upstream side of the filter, allowing clean exhaust gas to exit downstream as shown in Figure 3.4.

PM will gradually fill the DPF, requiring removal to prevent blocking and increasing exhaust back pressure. This can be achieved by oxidation of the soot via a regeneration process, either actively by raising local temperatures or passively utilising the exhaust. Every 5 hours, the DPF was removed from the exhaust stream and actively regenerated by use of a furnace.

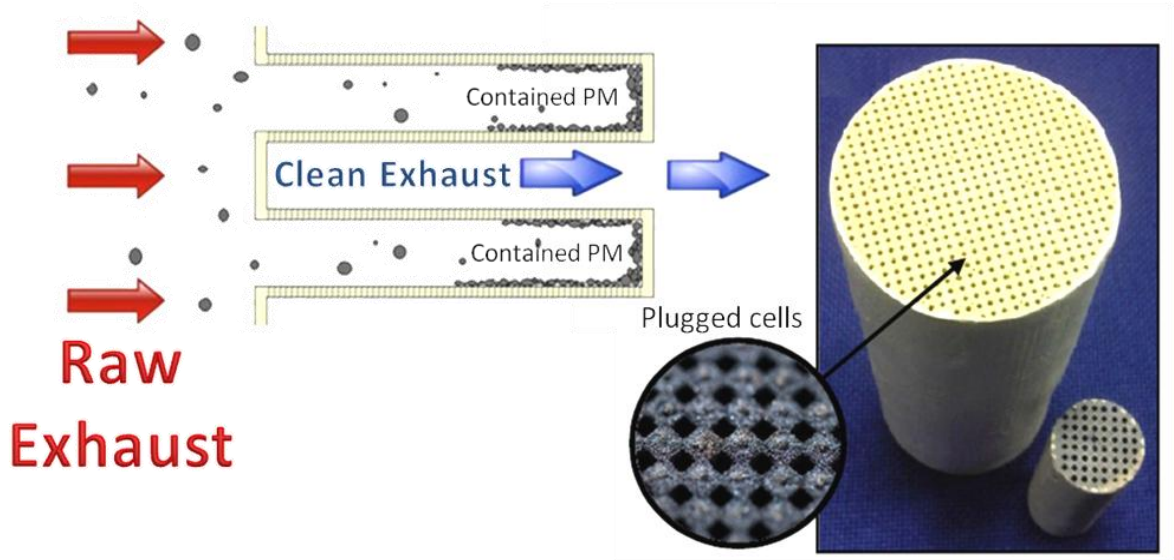

Figure 3.4 - Cordierite Diesel Particulate Filter (DPF) wall-flow monolith

3.2.2 - Exhaust Analysis

Exhaust gases were monitored using a Horiba Mexa 7100DEGR analyser sampled through a heated vacuum tube. The Horiba uses Chemiluminescence Detection (CLD) to measure concentrations of NO_x ($NO + NO_2$); Non-Dispersive Infrared (NDIR) for CO and CO_2; Flame Ionization Detection (FID) for Total Hydrocarbons; and Magneto-Pneumatic Detection (MPD) for Oxygen.

The size distribution and number of soot particles emitted from the engine is measured using a Scanning Mobility Particle Sizer (SMPS) Spectrometer, sampling from the exhaust

stream. The SMPS from TSI is comprised of an electrostatic classifier series 3080, a 3081 Differential Mobility Analyser (DMA) and a model 3775 Condensation Particle Counter (CPC). The SMPS measures particle size distribution based on the principle that a particle's ability to traverse an electric field, known as its electrical mobility, is directly related to the particle's size.

A heated rotating disc diluter (Thermo-diluter) is situated at the inlet of the SMPS to dilute the sampled exhaust whilst maintaining it at 150°C, minimising the potential for hydrocarbon condensation and nucleation. The sample and sheath flow rates were set at 0.5 and 5L/min respectively, enabling the range of measurable particle diameters to be between 12- 437nm when used with a dilution ratio of 200:1.

The particle mass distribution is then derived from the measured particle number and size distributions. By utilising *'The effective particle density exponential function'* formulated by Lapuerta et al. (2003). Each particle is assigned a mass that is more relevant to its size due to the relationship between particle density and measured particle size. The relationship states that as agglomerate particle size increases, the overall density decreases from 1.55 to 0.155 g/cm^3 in the equivalent diameter interval of 0.03-1.0µm.

3.3 - High Frequency Reciprocating Rig

Fluid lubricity was assessed using a High Frequency Reciprocating Rig (HFRR) consisting of a microprocessor control unit and the reciprocating friction and wear test system (Figure 3.5). The primary use for the HFRR is to measure the lubricity of fuels, but is also suitable for measuring wear and friction of engine oils, greases and other compounds (PCS Instruments 2009a).

Figure 3.5 - High Frequency Reciprocating Rig (PCS Instruments 2009a)

3.3.1 - Equipment Description

The HFRR is a simple tribometer that uses ball on disc contact in reciprocating motion to assess friction, film thickness and wear. Figure 3.6 shows a basic schematic of the HFRR which consists of an upper specimen (ball) that is loaded with a weight and forced to slide across the surface of the lower specimen (disc) with a fixed stroke length and frequency. The HFRR utilises the test fluid to lubricate the test specimen pair, enabling the assessment of several lubricating properties to be made in real-time such as the Coefficient of Friction (COF) and film thickness percentage.

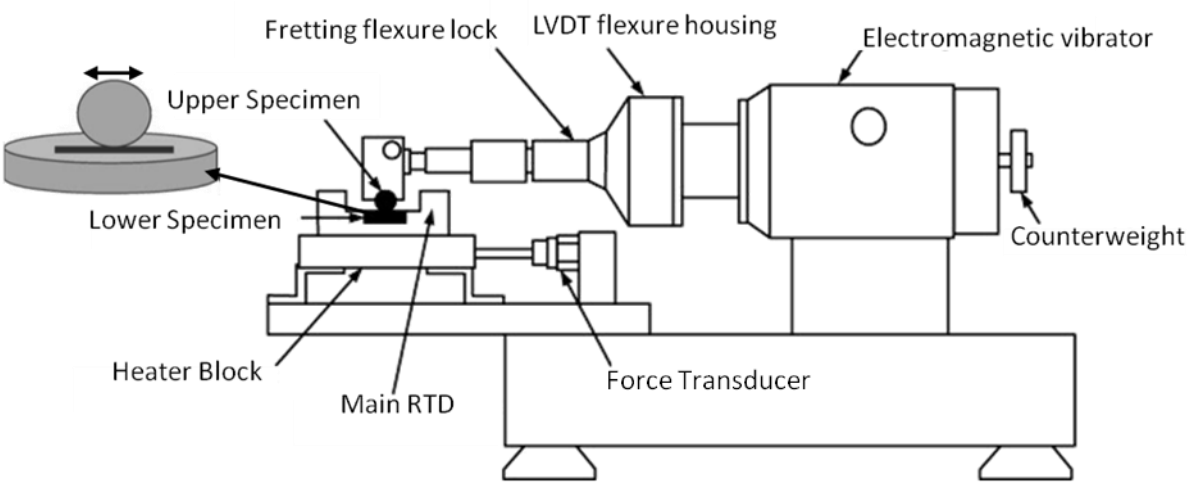

Figure 3.6 - HFRR Schematic (Sukjit & Dearn 2011)

Coefficient of Friction is measured by relating the transmitted forces between specimens to the fixed weight loaded to the upper specimen. Film thickness is measured by contact between the upper and lower specimens and is dependent upon the type of lubrication regime present. A current is passed through the two specimens and the amount of Electrical Contact Resistance (ECR) between them is proportional to the contact between surface asperities. If the lubrication regime present is fully hydrodynamic, there would be no contact between specimens and a 100% film thickness. If boundary lubrication is present, there would be full contact between specimens, no resistance to current and therefore 0% film thickness.

The Coefficient of Friction and film thickness fluctuate during testing; therefore all final readings are averaged over the total test time. The film thickness will also reach a steady state condition after a certain amount of time, which became a measureable parameter, referred to as the 'wearing in time'. The only manual measurement is the wear scar size taken from the surface of the ball which is achieved with the aid of a digital microscope.

Edges of the wear scar are measured along the x and y axis, which is then averaged to form the Average Wear Scar Diameter (AWSD) as shown in Figure 3.7.

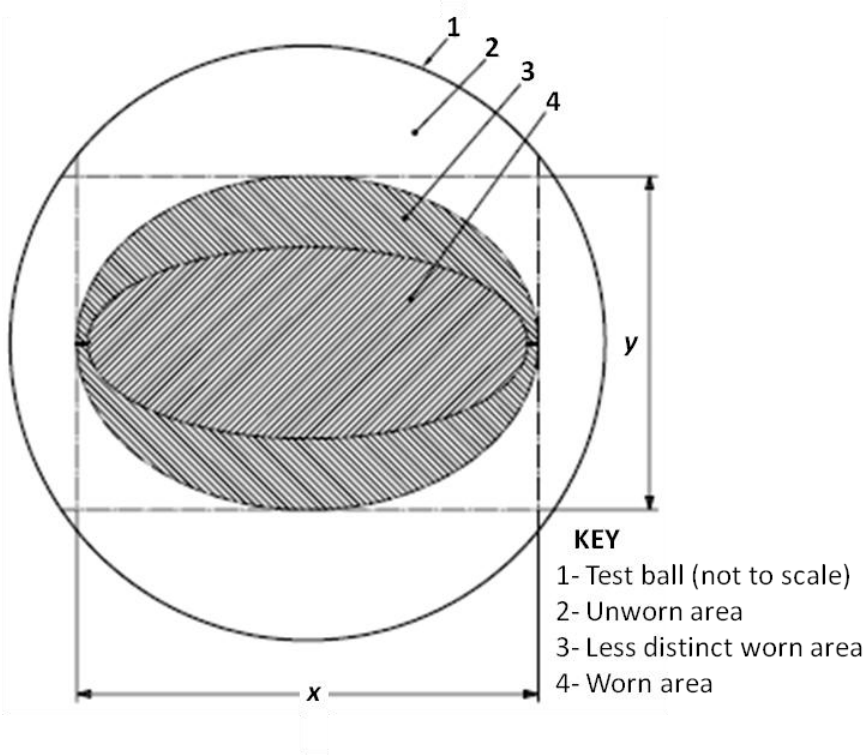

Figure 3.7 - Wear scar dimensions (BS EN ISO 12156-1)

Calibration of the HFRR is a simple process with a simple step-by-step guide built into the software. The HFRR is supplied with a combined calibration stroke/strain device and temperature calibration plugs used to calibrate the stroke length, force transducer and RTD thermocouple respectively. Contact resistance is set by the type of lower specimen holder chosen, and must be calibrated each time it is changed. The simplicity of the HFRR means the lubricating performance of fuels and oils can be quickly assessed with a high level of repeatability and reproducibility.

The HFRR specimens are manufactured to meet the following international standards CEC F-06-A-96; ASTM D6079 and D7688; ISO 12156-1; BS EN 590; JPI-5S-50-98; and IP 450/2000, the specifications of which can be found within Table 3.3.

Table 3.3 - HFRR test Specimen Specifications

Specimen	Upper	Lower
Shape	Ball	Disc
Dimensions	Ø6.00mm	Ø10.0 x 3.00mm
Material	AISI E-52100 steel	AISI E-52100 steel
Hardness	Rockwell hardness C (HRC) 58-66	Vickers hardness (Hv) 190-210
Surface Finish	0.05 µm R_a	0.02µm R_a

3.3.2 - Published Methods

There are presently several standards for the testing of fuel lubricity using the HFRR, developed initially to provide a correlation between the internal wear rates of diesel fuel pumps (Lewis 2009). These test standards however are intended for fuels alone and should not be adopted to measure the lubricity of engine oils which experience greater loads, temperatures and contact pressures. Trying to correlate HFRR wear scars and lubricity data to in-engine components is not a simple task. As there are no standardised methods, test parameters have been left to the interpretation of the researcher. Listed in Table 3.4 are examples of various research titles which use the HFRR to test an aspect of engine oil. Most test parameters are an attempt to replicate typical lubrication conditions of in-engine components operating under normal loads.

Table 3.4 - Summary of published HFRR oil analysis test parameters

Paper Title / Reference	Stroke (mm)	Frequency (Hz)	Velocity (mm/s)	Load	Hertzian Contact Stress (GPa)	Temperature (°C)	Time (mins)
The behaviour of Molybdenum Dialkyldithiocarbamate Friction Modifier additives							
Graham & Spikes (1999)	1	20	40	3.9N	1.03	50-200	60
Study of Zinc Dialkyldithiophosphate Using Electrochemical Techniques							
Xu et al. (2002)	1	20	40	400g	~0.51	60	30
Design of Functionalized PAMA Viscosity Modifiers to Reduce Friction and Wear in Lubricating Oils							
Muller et al. (2008)	2	20	80	200g	0.81	120	75
Wear effects and mechanisms of soot-contaminated automotive lubricants							
Green et al. (2006)	2	-	18 & 36	640g	-	24-100; 24; 100;	20
Extraction and tribological investigation of top piston ring zone oil from a gasoline engine							
Lee et al. (2006)	1	20	40	400g	1	40-140 +20 stepped	5/ temp
The importance of the Stribeck curve in the minimisation of engine friction							
Bovington et al. (1999)	1	20	40	10N	~0.35	40-140	
Interactions Leading to Formation of Low Friction Films in Systems Containing Molybdenum Dialkyldithiocarbamate and Zinc Dialkyldithiophosphate Additives							
S Korcek et al. (2000)	1	20	40	1000g	1.3 (final 0.5-1.0)	105	60
Fuel efficient engine oils, additive interactions, boundary friction, and wear							
Stefan Korcek et al. (1999)	1	20	40	9.8N	1.33	45 or 105	-
Friction and wear of tribofilms formed by zinc dialkyl dithiophosphate antiwear additive in low viscosity engine oils							
McQueen et al. (2005)	-	-	40	9.8N	~1.6	40-135 main@120	60
Effect of Different B20 Fuels on Laboratory-Aged Engine Oil Properties							
Uy et al. (2010)	1	20	40	9.8N	1.3 (final 0.5-1.0)	105	180
Characterization of anti-wear films formed from fresh and aged engine oils							
Uy et al. (2007)	-	20	-	9.8N	~0.85	-	-
Raman Characterization of Anti-Wear Films formed from fresh and aged engine oils							
Uy et al. (2006)	1	20	40	9.8N	1.3	105	60
Effect of Biodiesel (B20) on Vehicle-Aged Engine Oil Properties							
Zdrodowski et al. (2010)	1	20	40	1000g	1.3	105	180

Typical bulk oil temperatures from the engine sump are between 90-100°C, but will increase as oil travels through the crankcase towards hotter engine parts. Average temperatures found in piston ring landings for example are around 150°C during idling but can increase up to 350°C at full load (Smith et al. 2002). More reasonable temperatures are chosen to imitate engine warm up conditions or high sump temperatures of up to 120°C. Studying the effects of temperature on lubricity can also be achieved with ramped or stepped temperature increments over a single test run which has proved popular with some researchers. However it is more common to assess temperature by using the product of several averaged tests at separate temperature intervals to reduce the effects of hysteresis during testing.

The HFRR can be employed to identify different wear mechanisms present between specimens. Extending the stroke length will increases the wear scar size on the lower specimen, enhancing the visibility of features synonymous to specific wear mechanisms. This becomes important when testing samples that contain suspended contaminants such as soot and metallics which can exhibit abrasive and adhesive wear (Green et al. 2006a). However, as the stroke length is doubled, the reciprocating frequency must be halved to maintain the same sliding velocity.

Due to the highly localised contact geometry between HFRR specimens, the minimum possible Hertzian contact stress is 0.3GPa. This is one of the major drawbacks to using HFRR to analyse lubricity, as the contact stresses are more representative to rolling contact bearings or valvetrain components which do not experience reciprocating motion (Spikes

2006). However, it remains a good method to analyse lubricity by prematurely inducing wear.

A 1kg load suspended from the upper specimen holder will induce a Hertzian contact stress between 1.3–1.4GPa which will promote wear on both specimen surfaces changing the contact area in the process. This will consequently reduce the Hertzian contact stress until steady-state conditions are met, at which point contact stresses will lie in the region of 0.5-1.0GPa (Korcek et al. 2000; Zdrodowski et al. 2010). Whilst the specimens wear-in, the lubrication regime will fluctuate causing high levels of hysteresis. Wear scar growth will not remain constant during this phase which will influence the measured friction coefficient and film thickness. The HFRR can therefore be useful in measuring the wear-in times of specimens and the performance of anti-wear additives. One must be careful when using averaged values, as this also takes into account the time taken before steady-state conditions are reached.

In this study, each test fluid underwent identical test conditions enabling comparisons of fluid lubricity to be made. The finalised test parameters were as follows: the tested fluid was heated to 60°C and held for the entirety of the experiment. The upper specimen was loaded with a 1000g load, reciprocating with a stroke length of 2mm at a frequency of 10Hz for 60minutes. Once complete, a new specimen pair was used to repeat the test at a higher temperature of 120°C using the same test fluid.

3.4 - Viscometry

To measure the dynamic viscosity of the test fluids, an automated rheometer was preferred to give repeatable and reproducible results. Viscosity was measured by comparing the measured forces and rotational speeds of the rotor to reference fluids tested under identical conditions (ASTM D4683).

3.4.1 - Ultra Shear Viscometer Description

Figure 3.8 - Ultra Shear Viscometer (USV) (PCS Instruments 2009b)

The USV shown in Figure 3.8 is a 'Couette viscometer' which is a rotational rheometer consisting of two highly toleranced concentric cylinders which shear a thin fluid film within its annular gap. The USV utilises the viscous drag experienced by the rotating inner cylinder and measures the torque required to rotate it at a given speed (Haycock & Hillier 2004; Stachowiak & Batchelor 2005). The USV fulfils the criteria of being a High Temperature High Shear (HTHS) viscometer as it is designed to measure viscosities at shear rates in the range

of 1–10million reciprocal seconds, at temperatures up to 150°C, similar to those found within IC engines.

A drawback to high shear viscometers is the issue of shear heating the test fluids. At high shear rates, the effects are amplified which can lead to non-uniform film formation or a permanent drop in test fluid viscosity. Many viscometers are limited to shear rates below 3,000,000s^{-1} as a consequence, which is adequate for most test standards but does not cover the full range of shear rates experienced by many engine oils (PCS Instruments 2009b). The USV overcomes this issue by minimising the shearing interval as each viscosity measurement takes less than 100ms, reducing the permissible time for heating to take place. With the effects of shear heating virtually eliminated, the USV can attain very high shear rates (up to 10,000,000s^{-1}) but only with a very small annular gap.

Both the rotor and stator are manufactured to a very high tolerance, and surface finish (Rotor =0.05µm Ra; Stator <0.02µm Ra) so that both have a diameter of 12mm, and an annular gap width between the two of approximately 1µm. This is achieved by both being machined from tungsten carbide which has a high hardness (1610 [HV30]) and also a high resistance to thermal expansion. Consequently this means that all test fluids require filtering to less than the annular gap distance to prevent wearing of the rotor and/or stator.

The output of the USV is a viscosity map plotting viscosity (cP) against shear rate (s^{-1}). Each measured plot is the average of 3 individual measurements. If the standard deviation is

greater than 2%, the plotted point is replaced with an inverted triangle highlighting a 'measurement with high uncertainty'.

Calibration tends to be an issue with many viscometers due to thermal expansion of components altering the annular gap between the rotor and stator, which is common with tapered viscometers. The USV however does not require recalibration once setup due to the uniform shape of the rotor and stator, and the fact that both are manufactured from identical materials. Changes in the annular gap are therefore negligible with temperature change, and the rotor position is fixed and consequently has no influence over the gap size. Each rotor and stator comes as a matching pair with a set gap size, therefore calibration is only required when a new pair is installed, and will be valid for all temperatures and test fluids thereafter.

3.4.2 - AR Rheometer Description

The AR2000 Rheometer made by TA instruments (Figure 3.9), is a Low Temperature Low Shear (LTLS) rotational viscometer. It is popularly used to test the dynamic viscosity and the shear thinning properties of fluids at low shear stresses and shear rates. The AR Rheometer differs to the USV by being able to measure shear rates in the order of 10^{-4} to 10^{4} reciprocal seconds. This allows for viscosity measurements to be made between 5 and 10,000,000mPa.s.

Figure 3.9 - AR2000 Rheometer (TA Instruments)

A second viscometer was required after the limits of the USV were exposed, which was the requirement to filter all test fluids to under 1µm to fit within the rotor and stator's annular gap. Measuring the effects of soot thickened engine oils became a challenge as it was evident a lot of soot was inadvertently removed during filtration. The AR Rheometer was chosen to supplement the USV as it is ideal for measuring the viscosity of complex fluids such as suspensions, polymeric materials, pastes and dispersions.

The AR Rheometer has several rotor geometries to choose from, with each geometry requiring 'mapping' before use to measure it's inertia whilst freely rotating. During mapping, an optical encoder measures precise angular movements within a single revolution and compensates for these fluctuations and provides real-time corrections. The rotor geometry chosen was a 40mm diameter cone with 2° angle creating a minimal fluid gap of 54µm. Test fluids are injected onto a Peltier plate which heats the fluid through conduction to the

desired temperature in less than a minute. At very low shear rates, fluctuations in torque and friction can have a significant effect on viscosity measurements; however the Rheometer is designed to overcome this by use of air bearings, and digital torque management.

3.4.3 - Published Methods

Test standards established by the European Automobile Manufacturers Association (ACEA – Association des Constructeurs Européens d'Automotobiles) concerning engine and laboratory tests of in-service engine oils stipulates under laboratory Test 1.3 – *"Viscosity at high temperatures and high shear rates following CEC-L-036-90 demands dynamic viscosity tests to be undertaken at 150°C and a shear rate of $10^6 s^{-1}$".*

Table 3.5 - ACEA viscosity classes (ACEA 2010)

Oil class	A1/B1$_{-10}$	A3/B3$_{-10}$	A3/B4$_{-10}$	A5/B5$_{-10}$	C1$_{-10}$	C2$_{-10}$	C3$_{-10}$	C4$_{-10}$
Viscosity (mPa.s)	≥ 2.9 ≤ 3.5	≥ 3.5		≥ 2.9 ≤ 3.5	≥ 2.9		≥ 3.5	

Table 3.5 shows the minimum viscosity of new engine oils of different classes. The oil class indicates the intended use for a general type of engine oil, 'A/B' is for gasoline and light duty diesel engines; and 'C' is for catalyst compatible oils for light-duty engines with aftertreatment devices. Each class is followed by a two-digit number to identify the year of implementation (ACEA 2010).

Oil class differs from oil grade which depicts flow rates of engine oils, or more specifically kinematic viscosity, with a higher number indicating a higher viscosity. This was expanded to

include winter grade oils to indicate cold cranking capability. However, early multi-grade oils that performed well for both winter and normal grades would not perform well at high temperatures and shear stresses, important for an engine oil. In the early 1970s, the J300 high temperature oil specification was introduced to resolve this issue. Table 3.6 shows the most up-to-date version of the J300 specifications.

Table 3.6 - SAE J300 Engine oil viscosity classification (SAE J300)

SAE Viscosity Grade	High-Shear-Rate Viscosity (mPa.s)
20	2.6
30	2.9
40	3.5 (0W-40, 5W-40, 10W-40 grades)
40	3.7 (15W-40, 20W-40, 25W-40, 40 grades)
50	3.7
60	3.7

Although most test standards specify 150°C for measuring dynamic viscosity, most kinematic viscosity measurements are made at 100°C. Some researchers have chosen to report dynamic viscosity at 100°C (Lee et al. 2006), others at 40°C (Priest et al. 1999; Ofunne et al. 1989), and some at both 40 and 100°C (Green et al. 2006a). As engines fluctuate in temperature whilst in use, there is no set viscosity at which an engine oil will or must perform, as such there is no reason as to why one cannot report viscosity at all likely engine temperatures from 40-150°C such as Schmidt et al. (2006).

Equally can be said of oil shear rates, these are not fixed and will vary with engine speed and engine components, as shown in Table 3.7 which shows typical oil film conditions between in-engine components. What is clear from Table 3.7 is that engine oils will experience different film thicknesses, temperatures, pressures and shear rates depending on which

component it is adsorbed to. Although ASTM, CEC and ACEA test standards stipulate that dynamic viscosity should be reported at 100°C and 150°C and at a shear rate of $10^6 s^{-1}$, the reality is that oils will experience temperatures far lower than this and shear rates much greater. Therefore by creating a viscosity map, the overall lubricating performance of new and used engine oils can be assessed more effectively.

Table 3.7 - Oil film in gasoline engine components (Priest & Taylor 2000)

Parameter	Engine Bearing	Piston ring/liner (top compression ring)	Cam/follower (nose)
Minimum lubricant film thickness	< 1µm	< 0.2µm	0.1µm
Maximum temperature	120–150°C	200°C groove, 120°C liner	150°C
Maximum film pressure	250Mpa	70MPa	600MPa
Maximum shear rate	$10^8 s^{-1}$	$10^7 s^{-1}$	$10^7 s^{-1}$
Power loss (typical)	0.25kW	0.15kW	0.04kW
Minimum dynamic viscosity	2.5mPa.s	6.5mPa.s	EHL

All USV tested fluids had a viscosity mapping, first using a constant shear rate ($1x10^6 s^{-1}$); with the temperature ramped between 40-150°C at 10°C intervals. This was followed by a ramped shear rate ($1x10^6$-$1x10^7 s^{-1}$), at a constant temperature of 150°C. All tests conducted on the rheometer followed the test standard ASTM D6895. This method is specifically for heavily sooted oils with viscosities within the range of 12 to 35mPa·s, and has a repeatability of ±0.4 mPa·s. Tests were conducted at 100°C, with a shear rate ramped from 1 to $300s^{-1}$ and a shear stress between 0.1 to 10 Pa. This enabled rotational viscosity values to be compared at a shear rate of $100s^{-1}$.

3.5 - Gas Chromatography Mass Spectrometer

Gas Chromatography Mass Spectrometry (GC-MS) is an analytical technique used in chemistry to separate, detect and determine the elemental and molecular composition of a sample without it decomposing. Figure 3.10 shows the Clarus 600 GC-MS from Perkin Elmer used in this research.

Figure 3.10 - Clarus 600 GC-MS (Perkin Elmer 2009)

3.5.1 - Equipment Description

The GC-MS is comprised of two components, the Gas Chromatograph (GC) and the Mass Spectrometer (MS). The function of the GC is to take a compound of mixed substances and divide it into single molecules that are later characterised and quantified by the MS. The GC achieves this by vaporising the sample, transporting it via a carrier gas, also known as the mobile phase, through a capillary column that is suspended within an oven. As the sample traverses the column, it fractionates relative to both its physical and chemical properties, and its level of interaction with the column. The time taken for a compound to completely traverse the column and elute from the GC is known as its retention time. At the MS, the sample will undergo five stages: ionisation, repulsion, acceleration, filtration and detection. Together, the GC-MS is able to identify which functional groups a base oil has, and its

predominant structure. It is also able to identify any additives, impurities and contaminants whether it is fuel, acid or otherwise.

3.5.2 - Published Methods

Oil analysis by GC-MS is not new, current research has focussed on changes in composition and content through normal engine use or laboratory bench tests. These studies commonly look for characteristic peaks, such as those from a single additive or a collection of molecular peaks, and relate them to functional oil properties. The challenge is exacerbated by the number of peaks that comprise a base oil chromatogram, which being a blend of paraffins and naphthenes, can typically number over 1000 (Diaby et al. 2010; Wang & Stout 2007).

An approach chosen by Lam et al. (2010) to analyse engine oils was to separate the oil into five definable groups; linear paraffins with less than 24 carbon atoms ($<C_{24}$); linear and branched paraffins with more than 24 carbon atoms ($>C_{24}$); olefins (double bonds); cyclic compounds (aliphatic rings); and aromatic compounds. Lam et al. (2010) and Gómez-Rico et al. (2003) have both shown that the predominant hydrocarbon structures in most automotive oils are linear and branched paraffins lighter than C_{24}.

A typical technique used to correlate an oil's physical and chemical properties is to take a fresh oil and analyse it before and after it has achieved a certain number of hours or miles of continual engine usage. The benefit to this approach is that the oil will experience realistic conditions under a known timescale, the drawback however is that it is difficult to reproduce

the same conditions multiple times as there are too many variables. Another approach is to artificially degrade or age the oil via some laboratory based bench test whereby many conditions are known and can be controlled.

By using this technique, Lam et al. (2010) was able to assess fresh and used engine oils and determine from the respective chromatograms that oils scarcely change in peak intensity and retention times. The most noticeable difference being the reduced composition of species greater than C_{24} in the used oil compared to the fresh. The assumption being that heavier hydrocarbons break down to smaller, lighter fractions when exposed to high temperatures and pressures experienced in the engine.

The measurement of fuel content within engine oil is also possible via the GC; however chromatograms of fuels are equally as challenging to define as engine oils as they too have a similar number of low intensity peaks. Several methods have been developed using simulated GC distillation from ASTM D2887, or GC-FID following ASTM D3524 and DIN 51380, which can easily be transferred to GC-MS. The benefits of these methods are their applicability to used oil samples even when contaminated by other fuels, metallic impurities, and soot.

Before testing via GC-MS, samples were prepared by taking an aliquot of test fluid and dissolving it in Dichloro-Methane (CH_2Cl_2). A known mass of *n*-decane was then added to each used oil sample as an internal standard, relating the ratio of fuel peaks to the *n*-decane

peak. Fuel dilution mass was then interpolated against pre-dosed calibration mixtures up to 12% w/w, prepared in the same way.

Adams et al. (2009) and Zdrodowski et al. (2010) both attempted to develop GC techniques based on a modified form of ASTM D3524 to calibrate against diesel fuel and FAME components. Generally the intensity of FAME mass peaks will be greater than the sum of all the diesel fuel peaks making them easier to quantify. The challenge occurs with overlapping chromatogram peaks from the base-oil and the fuel, which for diesel may be significant at lower masses due when the two have similar boiling ranges. The overlapping from biodiesel occurs at a later elution time due to the higher boiling point of FAMEs, which may be masked by higher intensity base oil peaks. Depending on the degree overlapping, biodiesel dilution may not be reliably measured below 1% w/w (Adams et al. 2009). The level of repeatability assigned with this approach is ±0.3% w/w of the fuel.

The GC-MS was used to measure the effects of oil ageing from fuel dilution and exhaust gases by identifying entrained contaminants and exhaust species. Each test fluid was chemically analysed following test standards which includes the analysis of petroleum fractions, detecting and measuring diesel and gasoline diluents in used engine oil, and the determination of esters and acid content in FAMEs.

3.6 - Density

Oils were measured for changes in density following test standard ASTM D1298. In summary, a calibrated Hydrometer is used which correlates buoyancy to density within the range of 750-950 kg/m^3 with an accuracy of ±0.5. A 100mL sample was taken from each oil, before and after ageing. Each tested sample was contained within a measuring cylinder and held at temperature using either a water bath or environmental oven. The density of each sample was measured at 25, 40 and 100°C using the immersed hydrometer, avoiding sticking with the container walls as shown in Figure 3.11.

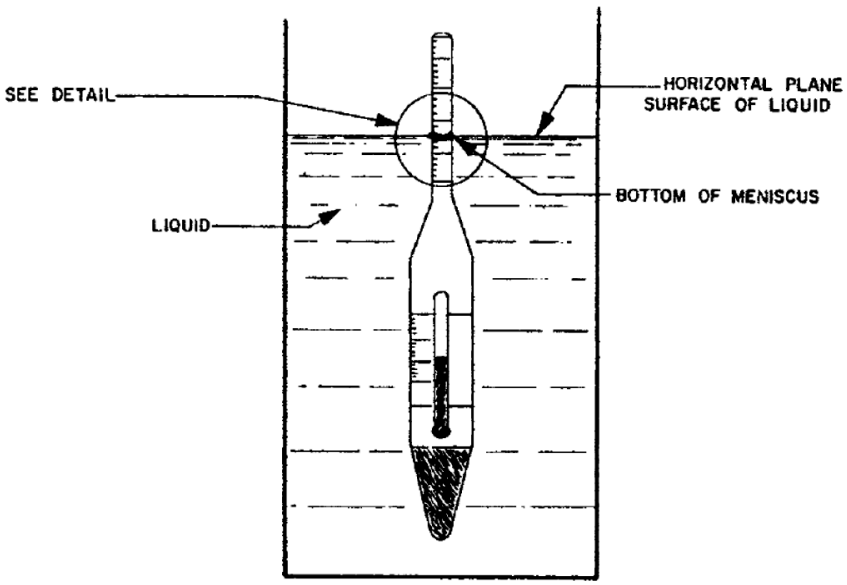

Figure 3.11 - Density Hydrometer (ASTM D1298)

3.7 - Acidity

The measurement of acidity or Total Acid Number (TAN) is a measure of how much Potassium Hydroxide (KOH) is required to neutralise one gram of oil as defined by test standard ASTM D974. The procedure involves taking a 2g sample of oil weighed in a beaker, and dissolving the oil using 100mL of titration solvent consisting of Iso-propanol and Toluene with the addition of 0.5mL of colour indicator solution (P-Naptholbenzein). A digital pipette containing 0.1 Molar alcoholic KOH is then introduced to the solution using a 'J-hook' delivery tube. The solution is then illuminated and gently agitated as titrant is added to the mixture. The mixture is neutralised when the solution first turns green or green-brown and remains for 15 seconds after the final addition of titrant.

3.8 - Microscopy

Soot samples were collected using the copper mesh grid shown in Figure 3.2 and observed using a Jeol 1200EX Transmission Electron Microscopy (TEM). Once the presence of soot particles was confirmed, the mesh grids were then further inspected using an Atomic Force Microscopy (AFM) from JPK Instruments, known as the NanoWizard II.

3.8.1 - Atomic Force Microscope

The AFM functions as a cantilever beam with a sharp probe stylus tip less than 10 nm in diameter located at its free end. By operating the AFM under 'Contact Mode', the probe can provide quantitative depth-sensing 3D map with nanometre-scale resolution as shown in Figure 3.12.

The AFM was utilised as a nano-indenter to measure the Young's modulus of soot particles from both diesel and biodiesel fuelled engines. The indenter tip was driven into the soot specimen's surface at nine different locations, 33nm apart shown by the numbered grid in Figure 3.12. The tip load was then decreased and retracted from the soot specimen, measuring load and displacement. From the resulting load-displacement curve, the Young's modulus is calculated as well as any residual stresses.

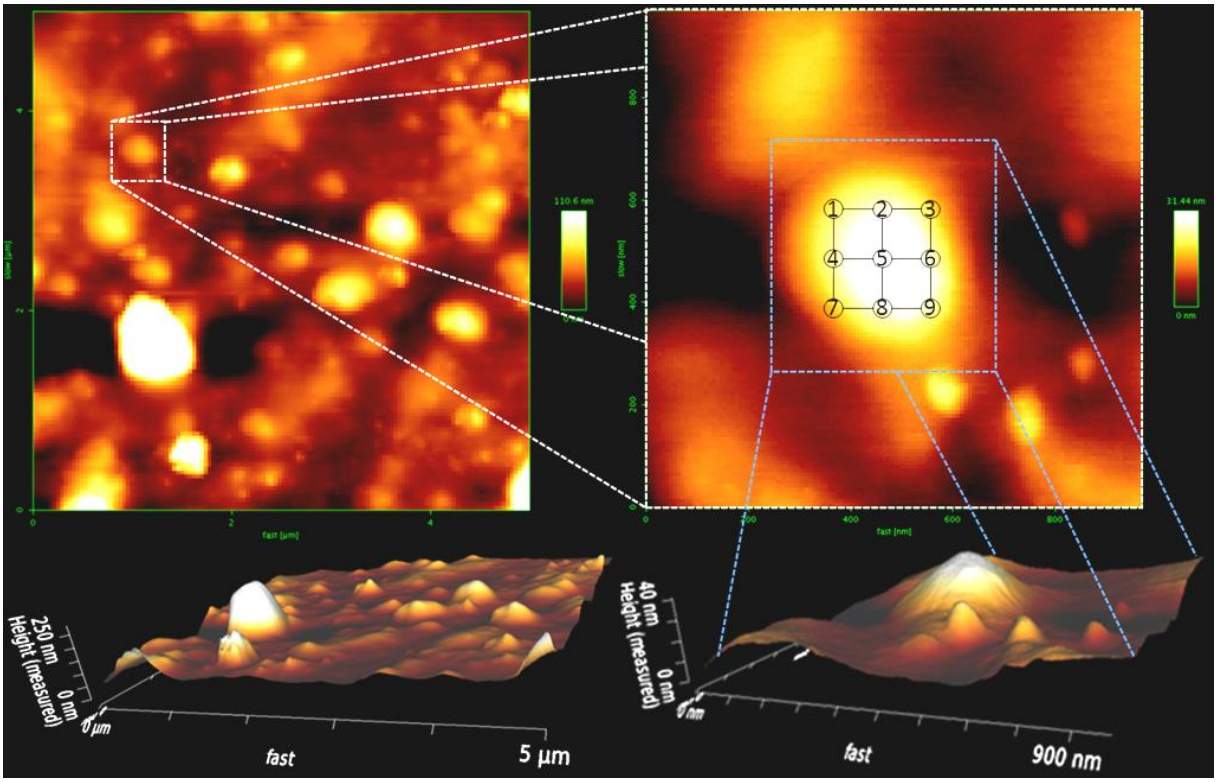

Figure 3.12 - AFM imaging with nano-indentation locations

CHAPTER 4 - EFFECTS OF FUEL DILUTION ON ENGINE OIL PERFORMANCE AND AGE

4.1 - Introduction

The purpose of this chapter is to investigate the ageing of engine oils whilst operated under similar conditions to IC engines. The causes and effects of oil ageing are well understood and documented, but the influence of fuels such as ULSD and neat biodiesels such as RME on the ageing of oil is not. This chapter analyses the influence of fuel dilution on the ageing of oils only, whilst eliminating the effects of other exhaust-borne contaminants such as combustion gases and PM.

This was achieved with the use of the ageing rig with the operating conditions described in section 3.1 of chapter 3. At the rig inlet, a hot air gun was connected to mimic exhaust gas conditions, minus the exhaust content. The rig was run three times with separate test fluids; an unblended engine oil; an oil/ULSD fuel blend (≈11% w/w); and an oil/RME blend (≈13% w/w). During each test run, samples were regularly extracted to characterise property changes. This chapter analyses the results of this test setup with changes in oil property measured against age, using the equipment and methods described in chapter 3 for viscosity, density, lubricity, chemical content and acidity.

4.2 - Results

Table 4.1 and Table 4.2 show the extracted 10mL and bulk oil samples respectively for the three test fluids depicting the visual changes brought on by ageing.

Table 4.1 - Extracted samples of oil and oil/fuel blends aged in rig

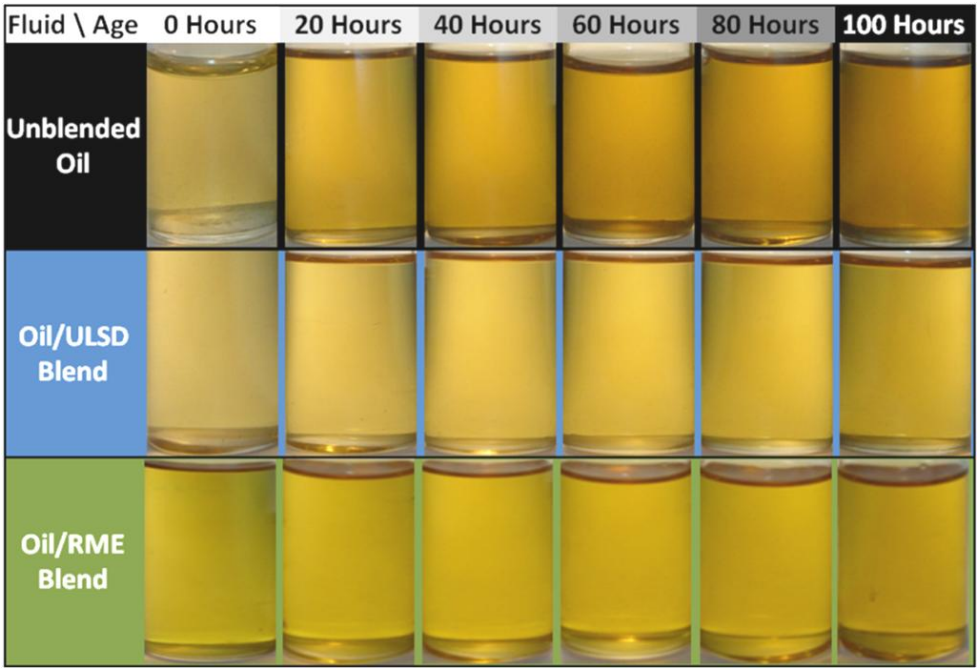

Table 4.2 - Bulk oil and oil/fuel blends colour change with age

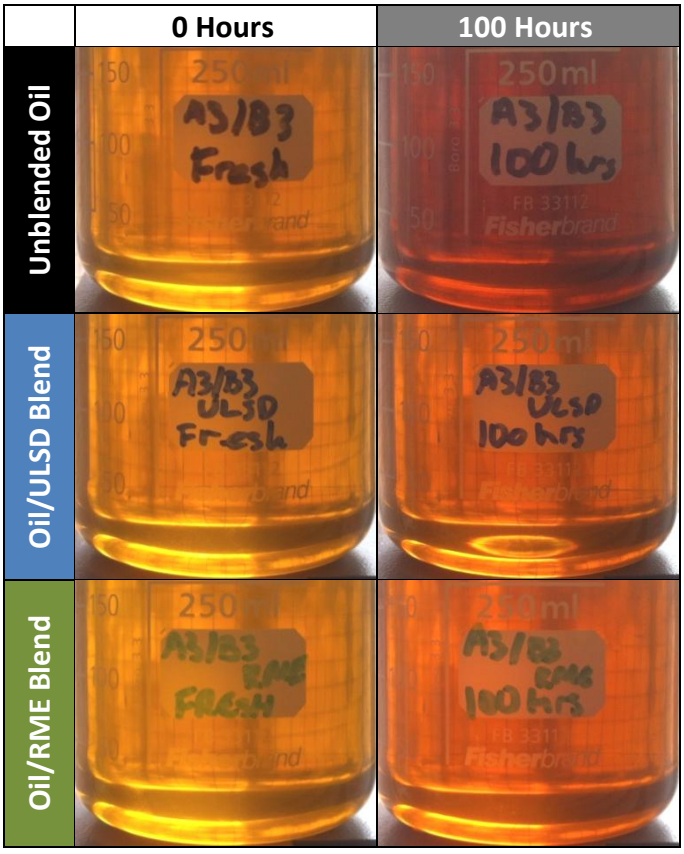

From both tables, it can be seen that the oil darkens with age. This is due to the oil oxidising and degrading, forming dark reddish-brown colours as the base oil chemistry changes. However, when diluted by fuel, the oil's initial colour changes in hue very slightly towards that of the diluted fuel. This can be seen with the oil/ULSD blend looking a paler yellow than the fresh unblended oil, and the oil/RME blend appearing almost a deeper, slightly green-yellow colour. The visible influence of the fuel after 100 hours in the rig shows a reduced darkening and reddening effect, which may suggest a delayed onset of ageing experienced by the base oil.

4.2.1 - Viscosity

Figure 4.1 illustrates the change in dynamic viscosity (in Centipoise) with ageing (in hours) of the fresh engine oil and two oil/fuel blends. Graphs A-C depicts the viscosity trends for the three test fluids measured using three different USV parameters. Table 4.3 gives a summary of results for these test parameters (defined in section 3.4.3 of chapter 3), and the percentage change in viscosity over the 100 hours of ageing. Each displayed point is formed from the standard deviation of three measurements.

Figure 4.1 shows that the trends for the three test fluids are similar across test parameters A-C, irrelevant of measured conditions. It was noticed that increasing the fluid temperature decreased the shear stress towards the minimal detectable limit of the USV, which increased the level of uncertainty for each measurement. However, as shear rate increased, so too did the shear stress, which in turn reduced the erratic nature of the measured trends. Although ASTM D4741 recommends that HTHS dynamic viscosity of engine oils to be measured at

150°C, this represents the performance limit of the USV, which in turn reduces the accuracy of these viscosity measurements. This is highlighted by the variability between individual measured points, which for graphs A and C varies by up to ±0.25%, whereas graph B is ±0.99%. This is still well within the 2% accuracy of the USV, but highlights the erratic nature caused by the ASTM parameters used for graph B.

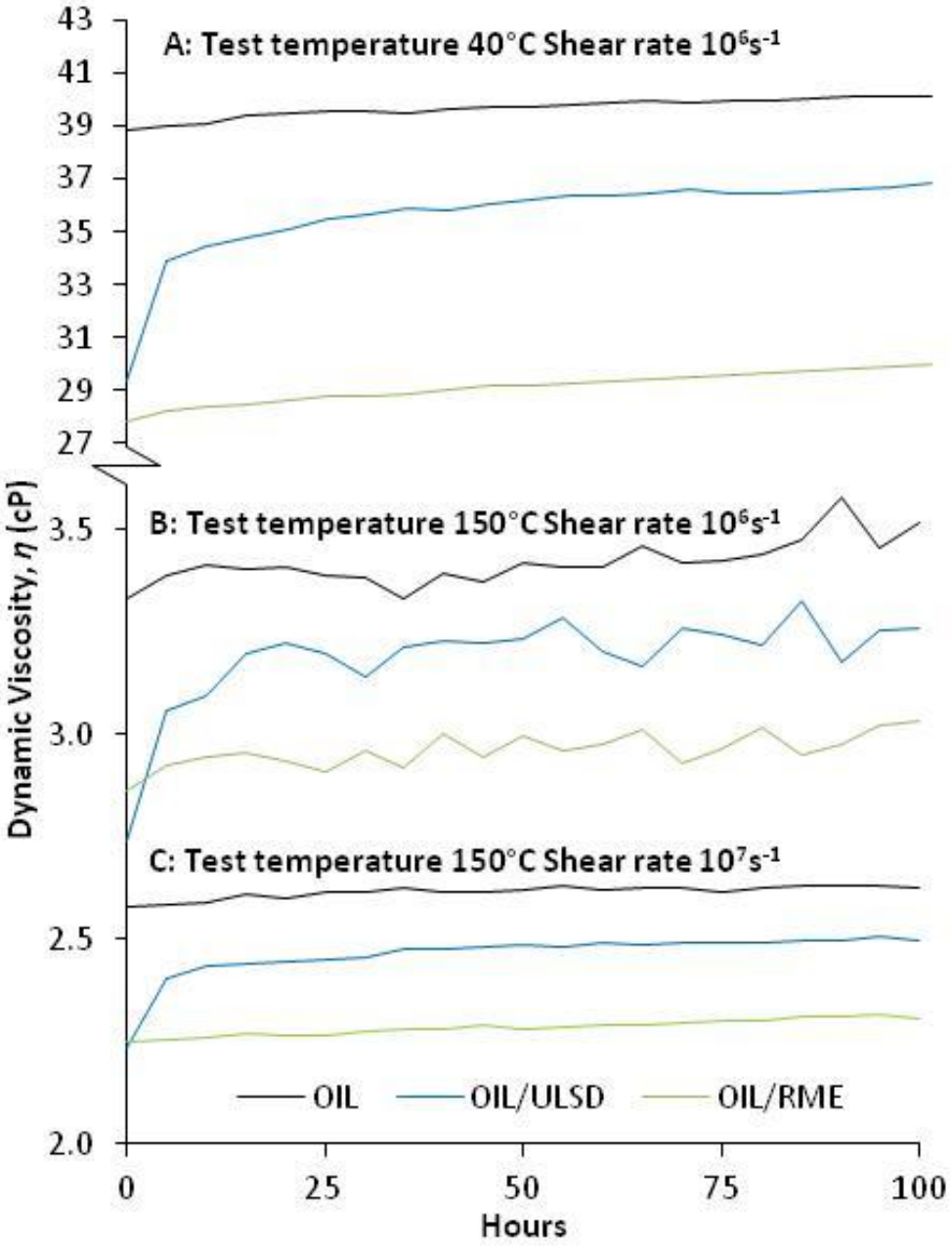

Figure 4.1 - Change in viscosity of oil and oil/fuel blends with age

The first difference between the three test fluids is the variation in initial viscosity. Both oil/fuel blends have an initial decrease in viscosity between 13-25% depending on temperature. This would be expected as typical viscosity ratios between the fuels and engine oil are 1:2:10 (ULSD: RME: Oil). The added fuel also brings the overall viscosity of the two blends below 2.9cP, the minimum ACEA specification for current engine oils. This has a benefit in that it reduces viscous drag, but a negative effect of reduced load carrying capability.

Over the 100 hours of ageing, the unblended oil has a steady increase in viscosity, finishing slightly above 3.5cP, the maximum ACEA specification for current engine oils. This has further implications on overall engine performance, especially if the trend were to continue and the oil not changed. For this experiment the unblended oil is used as a benchmark to measure trends against.

The oil/RME also exhibits a similar trend as the unblended oil over the 100 hours, whereas the oil/ULSD increases dramatically within the first 5 hours. This is due to the ULSD being more volatile than both the oil and RME, causing the lighter fractions to evaporate early on, reducing the overall fuel content and increasing viscosity. However, if all of the ULSD were to have evaporated from the oil, the blue lines of the oil/ULSD blend in Figure 4.1 would eventually meet the black lines of the unblended oil. As this does not occur, this would indicate that there is still a significant portion of ULSD remaining in the blend after 100 hours, or that the ULSD caused an irrecoverable change in the oil's viscosity.

Table 4.3 - Change in Viscosity of oil and oil/fuel blends during ageing (%$\Delta\eta$)

Fluid Graph	A	B	C
OIL 0-100hrs	3.3%	5.5%	1.8%
OIL/RME 0-100hrs	7.9%	6.0%	2.7%
OIL/ULSD 0-100hrs	25.4%	19.1%	11.8%
OIL/ULSD 0-5hrs	15.3%	11.6%	7.6%
OIL/ULSD 5-100hrs	10.1%	7.5%	4.2%
Temperature (°C)	40	150	150
Shear rate (x$10^6 s^{-1}$)	1	1	10

Table 4.3 summarises the change in viscosity between the three fluids from 0-100 hours. Oil increases in viscosity with ageing as the base oil slowly oxidises and thickens as described within the literature (Chen & Hsu 2003; Diaby et al. 2009) and confirmed by Figure 4.1. At first glance, the viscosity lines of the unblended oil and the oil/RME blend may appear to be almost parallel, but in fact the oil/RME increases in viscosity at a faster rate than the unblended oil during the 100 hours.

This is likely caused by the RME evaporating from the oil, increasing the overall viscosity of the blend whilst the oil itself oxidises at a normal rate, causing a greater increase over 100 hours than the unblended oil. There may also be the possibility that the RME itself was oxidised and thickened. However, with the fresh RME having a very low viscosity, the oxidised RME would have to increase in viscosity by a factor of five to account for the overall increase. Alternatively, the RME being a polar molecule rich in oxygen content could cause the oxidation of the base oil to accelerate, increasing the viscosity of the blend.

The change in viscosity for the oil/ULSD blend is the greatest of the three test fluids, with approximately $^{3}/_{5}^{th}$ of the overall rise occurring within the first 5 hours. A fairer comparison between test fluids is achieved by taking the viscosity change for the oil/ULSD blend after the bulk change in viscosity. The rate of change in viscosity with time, ($\Delta\eta/\Delta t$), was plotted for each temperature, shown in Figure 4.2. Each data point represents the gradient for each test fluid from 25 hours onwards, due to the oil/ULSD blend only reaching a steady rate of change at this time. The results are measured in centipoise per hour (cP/hour), averaged between 25-100 hours.

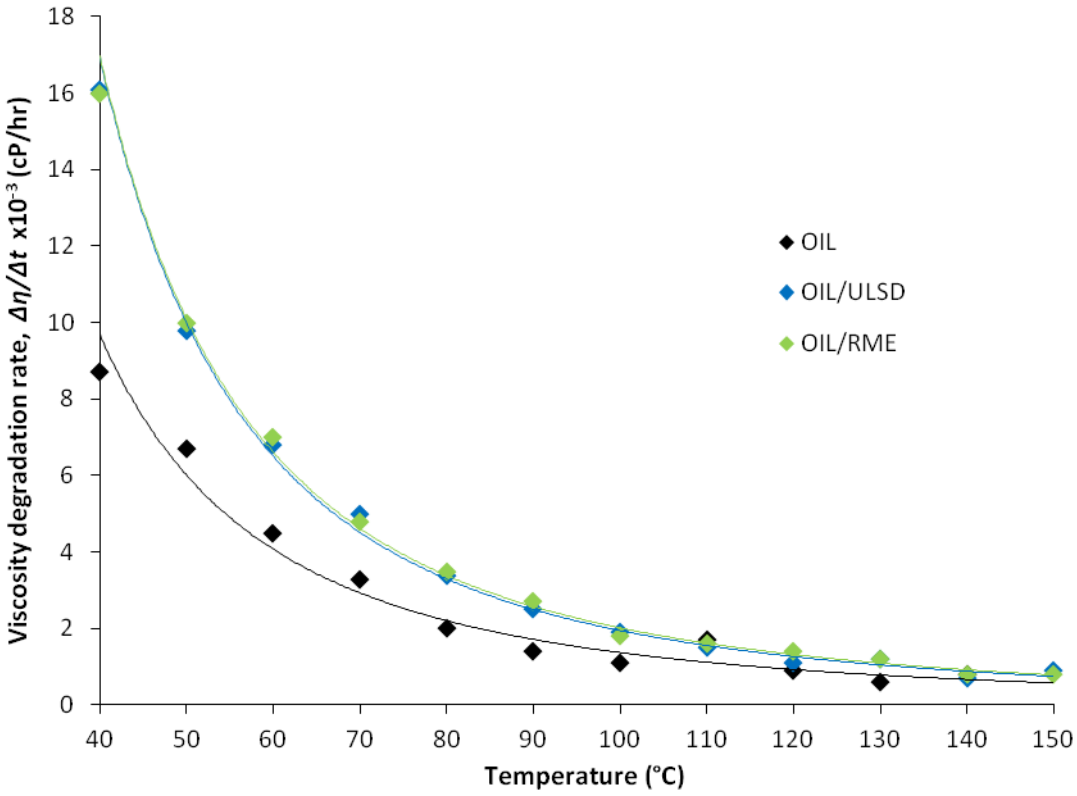

Figure 4.2 - Viscosity degradation rate of oil and oil/fuel blends with temperature

Figure 4.2 illustrates how each of the oil/fuel blends behaves over the measured temperature test parameters. What is now evident which wasn't before, is that both the

oil/fuel blends have almost an identical rate of viscosity degradation across test temperatures, which is higher than the unblended oil. From this experiment, it is unclear whether the mechanism behind the rate of viscosity degradation is the same for either fuels, or whether the evaporation of fuel (a viscosity diluent) in one blend equals the rate of oxidation and visco-thickening in the other.

Oil viscosity will contribute to the film thickness generated between moving components, which in turn will influence the level of metal to metal contact within an engine. Higher viscosity fluids tend to have increased load bearing capability, however a high viscosity will also increase drag, reducing the power output and increase fuel consumption. Therefore a trade-off between both oil functions is desired, a large film thickness with low viscous drag. Thus far from the viscosity measurements, it would appear that the added fuel content significantly reduces the viscosity of the oil, with RME maintaining this difference throughout the ageing process unlike the ULSD. However what affects this has on the load bearing capability will be analysed later in section 4.2.3.

4.2.2 - Density

The difference between dynamic and kinematic viscosity measurements is the inclusion of density in the latter. If the fluid density changes, this also causes a change in the kinematic viscosity. By separating these two fluid properties during the analysis helps to avoid any misinterpretations of trends which may be observed when the two measured properties are combined.

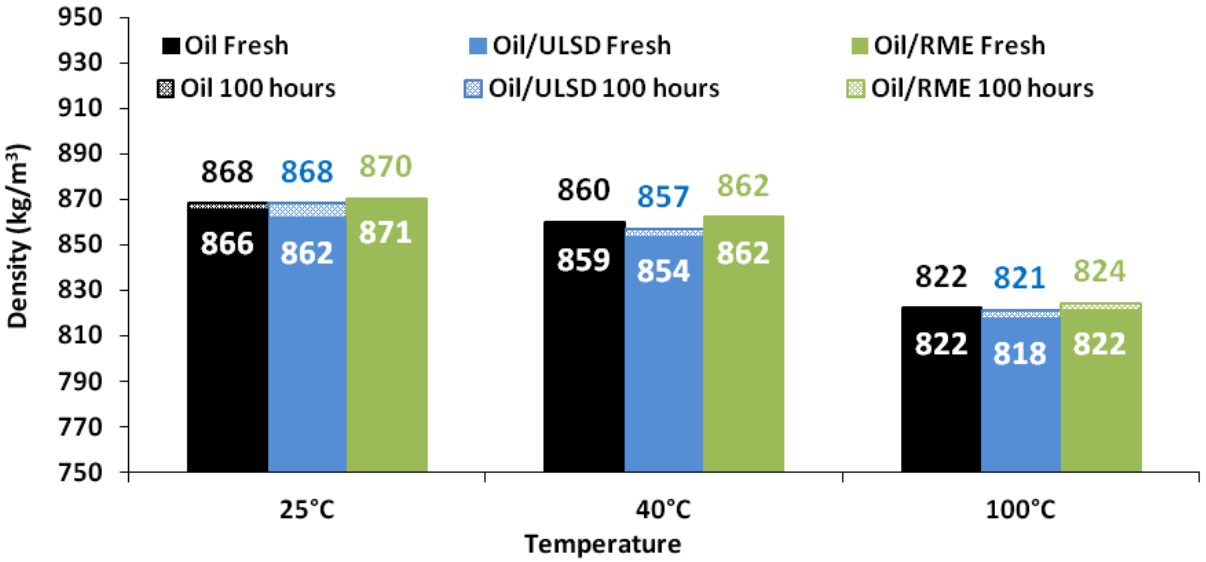

Figure 4.3 - Measured density for fresh and aged oil and fuel blends

Figure 4.3 shows a summary of measured densities for the oil and two fuel blends at three test temperatures. The differences in the initial density for the three test fluids across the measured temperatures, shows a shift from the density of the base oil towards the relative density of the fuel, as referenced in Table 2.1 from chapter 2.

The density-temperature relationship for the tested fluids decreases with temperature; however this relationship is not identical between fluids. Table 4.4 summarises the density thermal responses ($\Delta\rho/\Delta T$) for the three test fluids at both ages, taken from the gradient when plotting density with temperature. Using the fresh oil (*black*) as the benchmark, the addition of ULSD causes a very slight reduction in the thermal response of the oil/ULSD blend. This would indicate that there is a similar thermal behaviour for both the oil and the ULSD, even though there is a difference in overall density.

Table 4.4 - Density thermal response rate ($\Delta\rho/\Delta T$) for oil and fuel blends

$\Delta\rho/\Delta T$ ($kg/m^3/K$)	0 hours	100 hours
Oil	-0.595	-0.619
Oil/ULSD	-0.591	-0.619
Oil/RME	-0.657	-0.619

When blended with the denser RME, the thermal response rate has a sharper gradient indicating that RME is more susceptible to thermal expansion. This is seen when the oil/RME blend approaches 100°C, the density converges with the unblended oil which has a lower density throughout. This indicates that the RME itself must expand more than the oil at 100°C for the RME's greater density to be nullified.

Once aged, the three test fluids all have the same thermal response rate which is different from their respective fresh conditions. In the case of the unblended oil and the oil/ULSD, the thermal response increased making both fluids more susceptible to expansion with heating. This means that with ageing, the thermal behaviour of the test fluids' density increases, but also the influence of the fuel to the thermal response becomes nil. This is due to the evaporation of volatile compounds, leaving a heavier mass fraction within the base oil. Longer chained hydrocarbons are heavier and denser and are thought to be more susceptible to thermal expansion. A shift in hydrocarbon content could create a fluid with an overall higher density and larger thermal response rate, which would explain the observed behaviour of the aged thermal profiles at higher temperatures.

The opposite trend occurs with the ageing of the oil/RME blend which decreases in thermal response rate. The aged oil/RME begins to diverge from its fresh state, becoming less influenced by temperature, and closer resembling the aged unblended oil. This could be due to falling fuel content within the blend, or a fuel that has now been conditioned to have a lower thermal expansion. This would create an oil/RME blend in which the RME has less influence on the overall blend's density-temperature relationship. This has implications in lubricity as the rate of fluid expansion decreases with age, which could influence the film forming capability of the oil and rates of wear.

4.2.3 - Lubricity

The HFRR was operated under conditions described in section 3.3 of chapter 3 for the three test fluids taken at different states of ageing. Each fluid was tested in their fresh and 100 hour aged states, with an additional sample of the oil/ULSD blend aged at 5 hours due to the 'elbow' seen in Figure 4.1. Table 4.5 is a summary of the average film thickness measurements and coefficient of friction for the test fluids, which are also graphically summarised in Figure 4.4.

As each value is the average of a 60 minute test, it was thought important to add the minimum and maximum values for both the COFs and film thicknesses as both fluctuate during experimentation. This behaviour was seen for all the real-time film thickness plots, which would start at a maximum value for roughly the first minute, before dropping to its minimum for a further 1-5 minutes, steadily increasing over the remaining hour. This effect is most likely due to the oil only being able to temporarily protect the surfaces of the test

specimens, which is weakest towards the ends of each reciprocating stroke, allowing the two specimens to come into contact. As the fresh wear scar forms, a virgin surface of metal is exposed which attracts the polar additives within the oil to form a new, thicker film across the scar's surface. This occurs after some pre-set time, which has become defined as the 'wearing in time', the results of which are summarised later in Table 4.6.

Table 4.5 - Summary of lubricity properties of oil/fuel blends

Oil/Fuel Lubricating Properties		Film thickness (%)				Coefficient of Friction, μ			
		60°C		120°C		60°C		120°C	
Fluid	Aged state	Ave	Min Max	Ave	Min Max	Ave	Min Max	Ave	Min Max
Oil Unblended	Fresh	81.4	2% 100%	27.4	2% 100%	0.129	0.124 0.135	0.145	0.130 0.150
	100 Hours	59.2	1% 99%	25.2	2% 100%	0.130	0.123 0.140	0.142	0.123 0.149
Oil/ULSD Blend	Fresh	86.0	1% 100%	23.6	3% 100%	0.129	0.124 0.145	0.145	0.125 0.154
	5 Hours	73.0	1% 100%	24.6	3% 100%	0.132	0.126 0.141	0.146	0.126 0.154
	100 Hours	87.1	1% 100%	17.0	2% 100%	0.127	0.121 0.141	0.146	0.128 0.154
Oil/RME Blend	Fresh	85.4	1% 100%	95.9	8% 100%	0.124	0.118 0.133	0.106	0.097 0.135
	100 Hours	90.1	7% 100%	99.1	62% 100%	0.119	0.114 0.134	0.109	0.098 0.136

Another noticeable trend of the real-time data plots is the relationship between the COF and film thickness, when one reaches a maximum, the other will be at a minimum and vice versa, also seen in Table 4.5 and Figure 4.4. A fluid with good lubricity oil should have a high film thickness and low COF as it can sustain a higher load whilst losing a minimal amount of power in the process.

Using the unblended oil as a benchmark, ageing reduces the average film thickness from 81.4% to 59.2%. A consequence of ageing has been shown in Figure 4.1 to increase in viscosity which should in turn produce a thicker film. As the unblended oil shows the

opposite, it would be assumed that under these circumstances, the film thickness is influenced more by additive functionality, assumed to deplete with age.

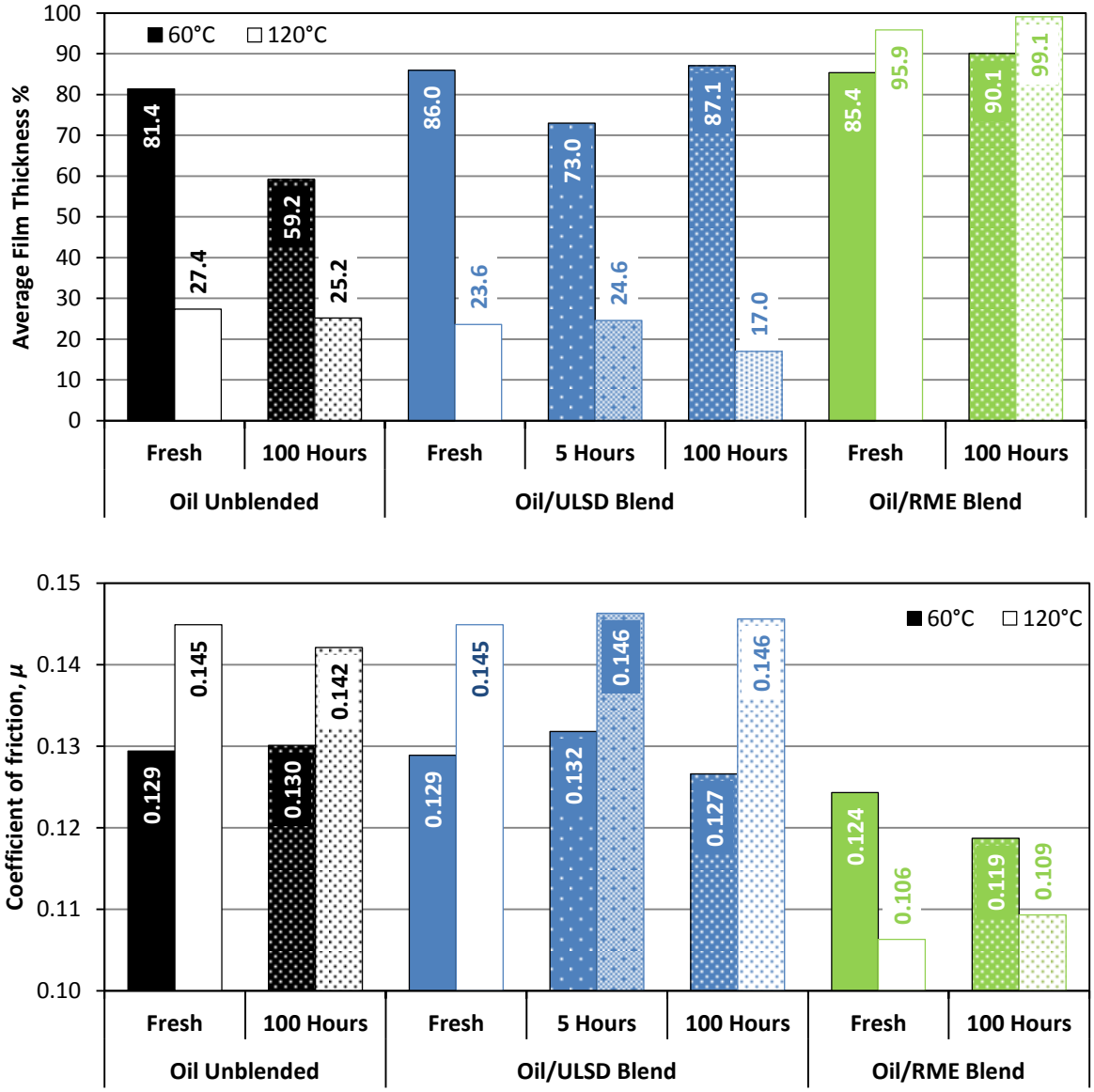

Figure 4.4 - Lubricity performance of fresh and aged oil/fuel blends measured as film thickness (top) and coefficient of friction (bottom)

At 120°C, the film thickness is lower for all fluids; this is due to the film being associated to the viscosity which is reduced at higher temperatures, as seen by the results from section 4.2.1. At 120°C, the oil's viscosity is roughly ¼ the value at 60°C, therefore the oil cannot

maintain a sufficiently thick film over the contact interface as it would at 60°C. The difference in film thickness performance with age at 120°C is a slight decrease, similar to 60°C, but with a lower proportioned loss. Similar trends with COF have also been observed, at higher temperatures the COF performance decreases showing greater levels of friction as the oil film is reduced, increasing specimen asperity contact. COF performance barely alters with age, suggesting that any friction modifiers are not yet depleted.

The addition of ULSD to the fresh oil exhibits no change in COF characteristics, but slightly alters the film formation. This is due to the inert nature of ULSD having little interaction with the oil's film forming capability, behaving as a filler at low temperatures that cause a thicker film to form. However, as the fluid's temperature is raised to 120°C, the initial film is thinner due to the fuel having a lower viscosity and lessened load bearing capability. When aged, there again is little difference in COF or film thickness, except that at 120°C the film thickness decreases further, which again is most likely due to additive depletion and/or the interaction of the fuel with the oil additives.

The largest change during the ageing of the oil/ULSD blend occurs at 5 hours which at 60°C has the lowest film thickness. This is peculiar as it happens during the 'elbow' shown in Figure 4.1 which coincides with the largest change in fuel content and viscosity. Whatever content remains from the fuel detracts only from the low temperature film formation as it is not evident at 120°C, where the film thickness increases. The 5 hour period depicts a point of transition for the blend, both physically and chemically. The blend goes from having a very high viscosity degradation rate to a very low rate thought to be due to a significant change

occurring within the blend's chemical content. This is manifested through the film thickness and COF, which at 5 hours is highest of all test fluids at both temperatures. It is thought at this timeframe, there is an imbalance in functional properties which eventually manages to stabilise itself during the remaining 95 hours.

The addition of RME to the fresh oil dramatically improves both the film thickness and COF (Knothe & Steidley 2005). However the two peculiar trends observed by the oil/RME blends are the improved lubricity both with age and at higher temperatures. The improved lubricity from the RME is thought to be due to the presence of more polar compounds such as the oxygenates within the FAME which create a naturally lower COF and greater additive interaction (Fang et al. 2006). With age, it would not be surprising that both the fuel and oil have oxidised, increasing the blend's overall polarity, adding to this natural lubricity behaviour.

The high temperature improvement is stranger as it not only creates a thicker oil film, but greatly reduces COF. The higher temperature may improve the surface adhesion of the oil/fuel with the metal surfaces, improving film formation and in turn reducing the COF. Alternatively, the high thermal response rate seen in Table 4.4 may cause the fuel to expand by a greater amount than the oil at a given temperature leading to an overall thicker film.

An improved film formation and low COF does not always result in reduced levels of wear. Table 4.6 summarises the average wear scar diameters (AWSD) formed on the surface of the upper specimens measured across the x and y axis. Also included is the wearing in times for

each test fluid, measured by the time taken for the film thickness to reach and maintain a stable peak.

Table 4.6 - Average Wear Scar Diameters and wearing-in times for oil and oil/fuel blends

Wear Parameters		AWSD (µm)		Wearing-in Time (mins)	
Fluid	Aged State	60°C	120°C	60°C	120°C
Oil Unblended	Fresh	236.5	300.0	24.15	60.00
	100 Hours	233.0	309.0	40.95	60.00
Oil/ULSD Blend	Fresh	221.5	303.5	15.77	60.00
	5 Hours	212.5	305.0	22.97	60.00
	100 Hours	237.5	296.5	13.07	60.00
Oil/RME Blend	Fresh	213.0	262.5	12.07	10.80
	100 Hours	241.0	287.5	6.50	2.20

When comparing AWSDs, it is unnecessary to compare between high and low temperatures, as with the other lubricity properties, the high temperature experiments cause a huge change in performance. Assuming the fresh unblended oil as the benchmark, ageing shows little difference in wear scars, which although are different, in reality they are within experimental error and can be adjudged to be the same.

The influence of ULSD dilution at 60°C initially reduces wear, indicating that perhaps the ULSD has a limited level of wear protection. With ageing, evaporation causes the blend to return to the same performance as the unblended oil. At 120°C, all oil/ULSD blends create similar AWSDs with any discrepancy being accounted for by experimental error.

RME dilution reduces wear at both temperatures, however with ageing, only the 120°C blend maintains at this reduced wear rate whereas the 60°C test shows the highest wear. RME is thought to dramatically reduce wear overall, with the benefits being greater felt at

higher temperatures giving the diluent additional antiwear performance reduced with ageing. The added antiwear performance may also be a consequence of the aged oil/RME blend having the highest average film thickness.

The final 'wearing-in time' for the test fluids, follows the trends of the average film thickness. Again using the fresh unblended oil at 60°C as the benchmark; ageing almost doubles the wearing in time for the same reasons as the reduced film thickness. The influence of ULSD decreases the wearing in time, as the oil film stabilises faster. Fuel-borne additives will aid in this parameter, benefitting the overall blend. However, the aged oil/ULSD has the shortest wearing in time, which may be due to the fuel evaporating and the additive remaining. This causes the overall aged blend to exhibit more of the positive attributes, and less negative attributes affiliated with ULSD dilution. At 120°C, the unblended oils and oil/ULSD blends do not ever reach a steady state, with the film thickness being too thin and weak to maintain a sufficient film, which also accounts for the increased levels of wear.

The addition of RME fuel to the oil also drastically improves the wearing-in time with both age and fluid temperature. All of the 120°C tests reach a steady state sooner than the 60°C tests. This is also seen with the minimum film thickness values in Table 4.5, which for the aged oil/RME at 120°C, never falls below 62%.

Overall, fuel dilution has been shown to improve the lubricity performance of the oil, with the influence of RME dilution being superior to ULSD dilution and the unblended oil. The

impact this might have in the long-term whether the oil will be able to sustain the improved performance both physically and chemically remains unknown and is a concern.

4.2.4 - Chemical Analysis

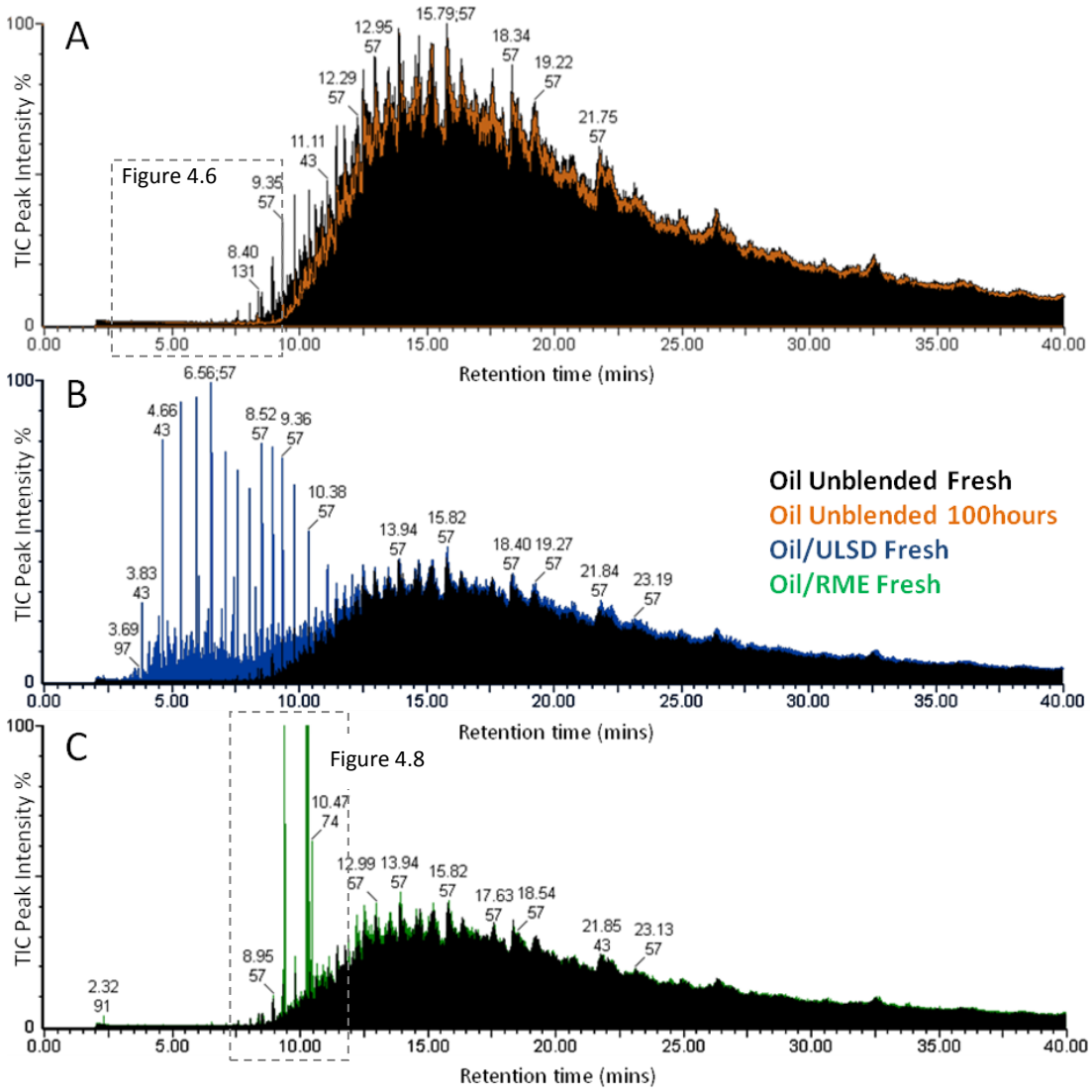

Figure 4.5 - Chromatograms of Fresh oil (black) overlaid with: A) 100 hour aged oil; B) Oil/ULSD blend fresh; C) Oil/RME Blend fresh

Each test fluid was chemically analysed using the GC-MS following test methods described in section 3.5 of chapter 3. The chromatograms in Figure 4.5 show the peak traces for fresh engine oil (*black*), overlaid with 100 hour aged oil (*orange*) (A); oil/ULSD (b*lue*) (B); and

oil/RME (*green*) (C). The x-axis represents GC column retention time, and the y-axis is the measured Total Ion Current (TIC) of detected mass fractions at the MS.

Chromatogram A in Figure 4.5 is typical for engine oils, with the earliest eluted peaks being light mass hydrocarbons. These peaks slowly grow in mass and intensity towards a 'bulge' comprised of linear and branched paraffins $>C_{24}$ as explained by both Lam et al. (2010) and Gómez-Rico et al. (2003). The overlaid peak trace in orange illustrates the change in peak intensity that occurs as a consequence of the ageing process, which has been magnified between 6 and 9 minutes and shown as Figure 4.6. This depicts the region to the left of the oil 'bulge' consisting predominantly of low mass linear paraffins with less than 24 carbon atoms ($<C_{24}$). The smallest paraffin peak within the fresh oil is just visible at 6.56 minutes, having a carbon number of 14 (Tetradecane). The identifiable peaks then increase in mass up until C_{24} (Tetracosane), before merging and overlapping with the branched paraffins within the 'bulge', which become more difficult to differentiate between.

Figure 4.6 shows a loss in peak intensity for all low mass molecules which contribute to the volatile fraction. The loss in peak intensity is reduced with increasing retention times, up until 12 minutes, when there is no visible peak loss for C_{24}. It would seem that ageing does not affect the heavier hydrocarbons, and that most of the change occurs through evaporation of the low mass fraction, which reduces in effectiveness with increasing boiling temperatures.

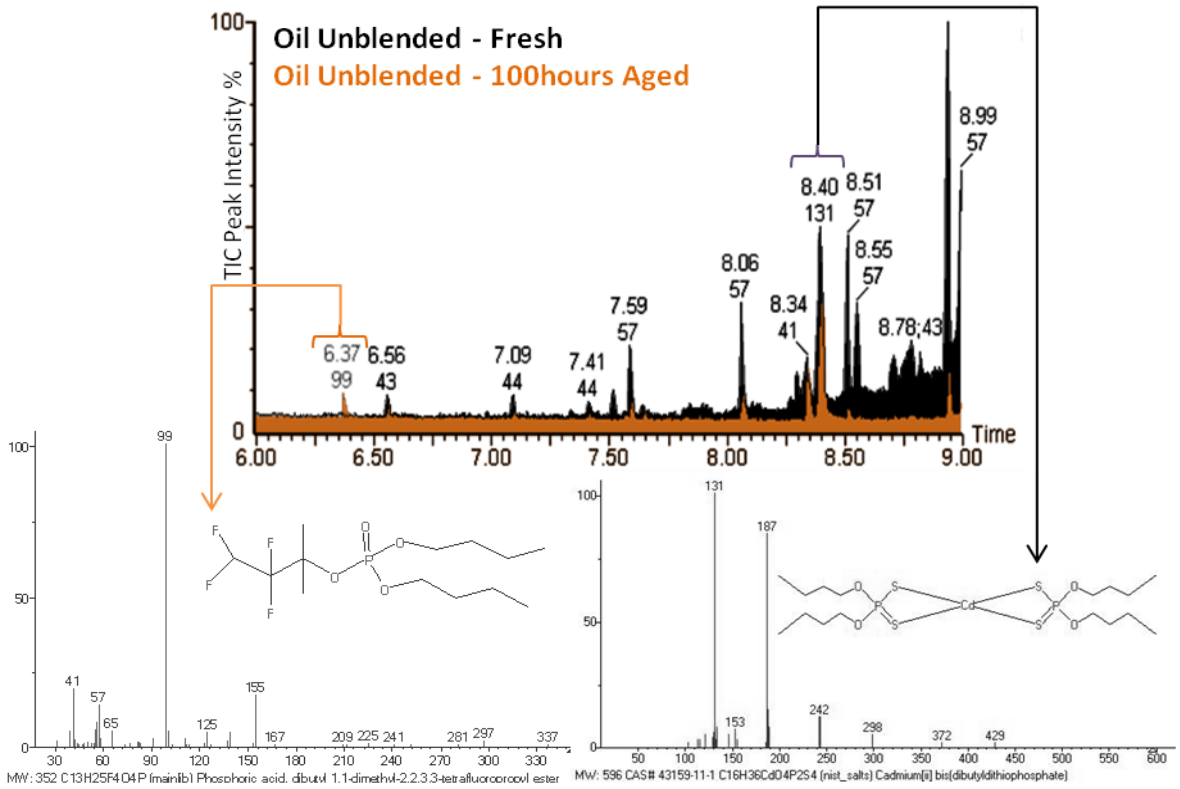

Figure 4.6 - Chromatogram of fresh and used engine oil showing mass spectrum peaks of degradation and Antiwear additive

Two chemicals highlighted in Figure 4.6 are represented by the peaks with retention times of 6.37 and 8.40 minutes, which are shown by their respective mass spectrums to have dominant masses of 99 and 131 respectively. The latter peak has been identified by the NIST search function to be Cadmium dibutyldithiophosphate, which shares a very similar structure to ZDDP. This peak is a cadmium based alternative, with similar antiwear functionality. The aged oil (*orange*) elutes the same peak, but noticeably smaller indicating a decrease in additive content, which may explain the decreased lubricity performance of the aged oil. The small peak at 6.37 minutes is only seen in the aged oil, and not the fresh, indicating a peak formed as a consequence of degradation. It is difficult to quantify and source this compound's origins; however it is thought to be a by-product of the depleted additive as it shares similar functional groups as well as being a fluorinated acid.

Chromatogram B in Figure 4.5 also shows engine oil overlaid with the peak trace for the fresh oil/ULSD blend. From 14 minutes onwards shows little to no difference in peak size and shape due to oil content within the blend being identical to the unblended oil. However, before 14 minutes the chromatogram differs as the ULSD fuel peaks overlap, increasing the intensity of the lighter mass peaks of the oil. Figure 4.7 shows offset chromatograms of the oil/ULSD blend at 0, 5 and 100 hours. The fuel peaks differ from the unblended oil due to the increased number of high intensity peaks which have a more defined shape and little fragmentation due to the greater level of refinement experienced by the fuel over the oil. This is seen with the ULSD peaks ranging from C_{10}-C_{24}, all having a greater intensity than the oil's largest peak found at the centre of the 'bulge'.

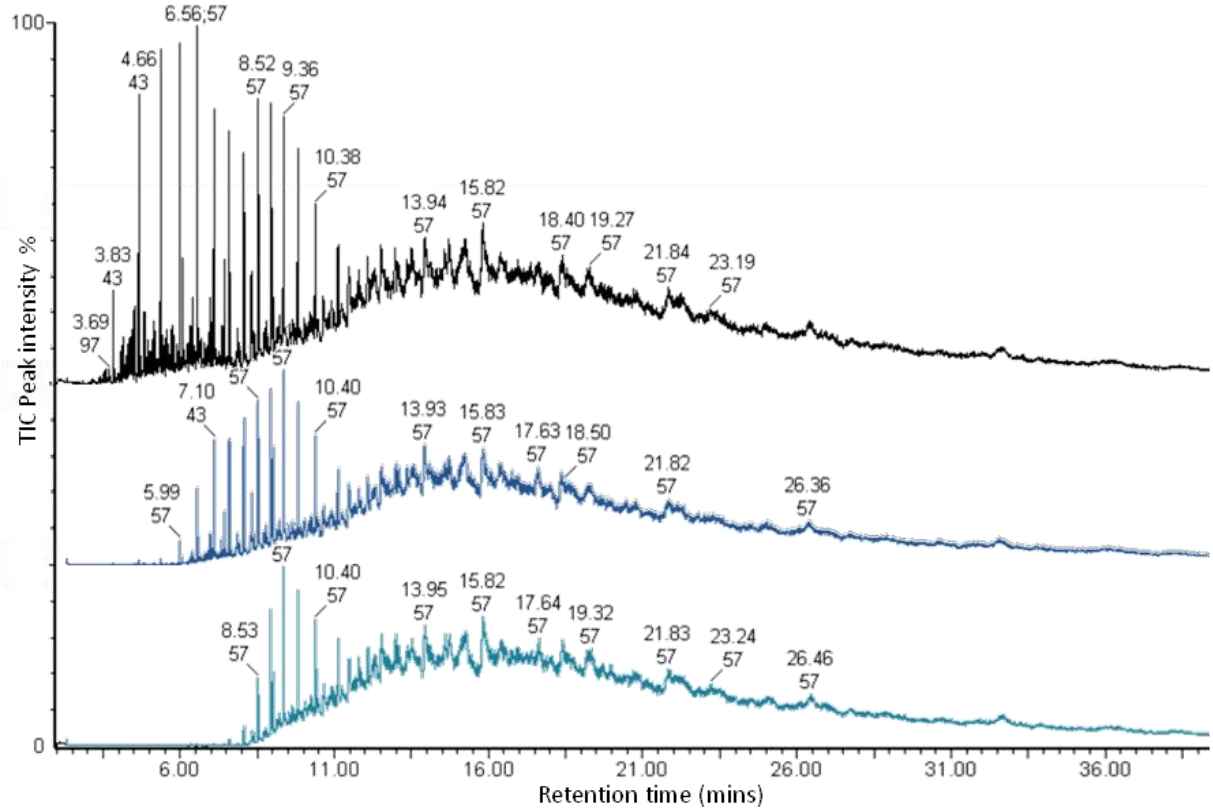

Figure 4.7 - Chromatograms of fresh and aged ULSD contaminated oil
Top – 0 hours; Middle – 5 hours; Bottom – 100 hours

Most noticeable in Figure 4.7 is that the low mass paraffin peaks change in intensity between the fresh blend and aged blends. Within the fresh fluid, the dominant peaks occur between C_{10}-C_{14}, but after only 5 hours these are narrowed to C_{16}-C_{20}, and at 100 hours to C_{18}-C_{20}. A qualitative assessment of these chromatograms shows that with each ageing interval, the ULSD peaks decrease in intensity by roughly a half. The challenge arises when attempting to quantify ULSD content as there is no discernible 'fuel peak' as the ULSD is spread, reducing the intensity of any one measurable peak. Fuel peak intensities also vary with age, making the process to establish fuel content more difficult.

Chromatogram C in Figure 4.5 is for the fresh oil/RME blend (*green*) overlaid with the peak trace for fresh engine oil. Unlike the ULSD which has mass peaks spread over a large retention time, RME has very distinguished 'fuel peaks' as shown in Figure 4.8. Table 4.7 provides a breakdown of the RME's four peaks comprising the FAMEs from the rapeseed triglyceride. The intensity of the FAMEs is so great, that they completely dwarf any of the oil peaks which are no longer visible. Differences in peak intensity are less noticeable for the oil/RME than for unblended oil, with changes being most significant for peaks $<C_{24}$. The oil/RME blend does not show many signs of ageing or similar shifts in peak intensity like previous chromatograms. The RME hence behaves as a non-volatile sacrificial additive, degrading whilst the oil continues to function.

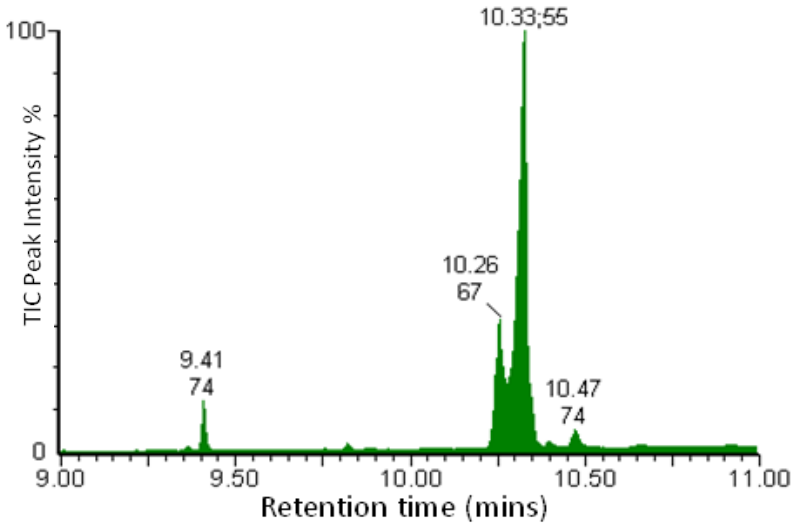

Figure 4.8 - RME chromatogram

Table 4.7 - RME chromatogram and constituent mass peaks

Name	Methyl Hexadecanoate	Methyl Octadecadienoate	Methyl Octadecenoate	Methyl Octadecanoate
Synonym:	Methyl Palmitate	Methyl Linolelaidate	Methyl Oleate	Methyl Stearate
Retention time:	9.41	10.26	10.33	10.47
Largest mass peak:	74	67	55	74
Molecular weight:	270	294	296	298
CAS #	112-39-0	2566-97-4	112-62-9	112-61-8
Formula:	$C_{17}H_{34}O_2$	$C_{19}H_{34}O_2$	$C_{19}H_{36}O_2$	$C_{19}H_{38}O_2$
Linear Formula:	$CH_3(CH_2)_{14}COOCH_3$	$CH_3(CH_2)_4CH{=}CH.CH_2CH{=}CH(CH_2)_7COOCH_3$	$CH_3(CH_2)_7CH{=}CH(CH_2)_7COOCH_3$	$CH_3(CH_2)_{16}COOCH_3$
Saturation:	C16:0	C18:2	C18:1	C18:0
Structure:	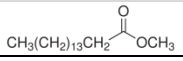	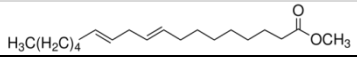	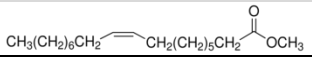	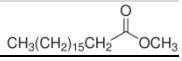

Figure 4.9 shows the changing fuel dilution levels for the two oil/fuel blends with age. Although fuel content was aimed to be roughly 10% w/w of the total blend, errors during sample preparation led to initial fuel dilutions of 12.8% and 11.3% for the ULSD and RME respectively. This level of inaccuracy however was not seen to alter the resultant trends.

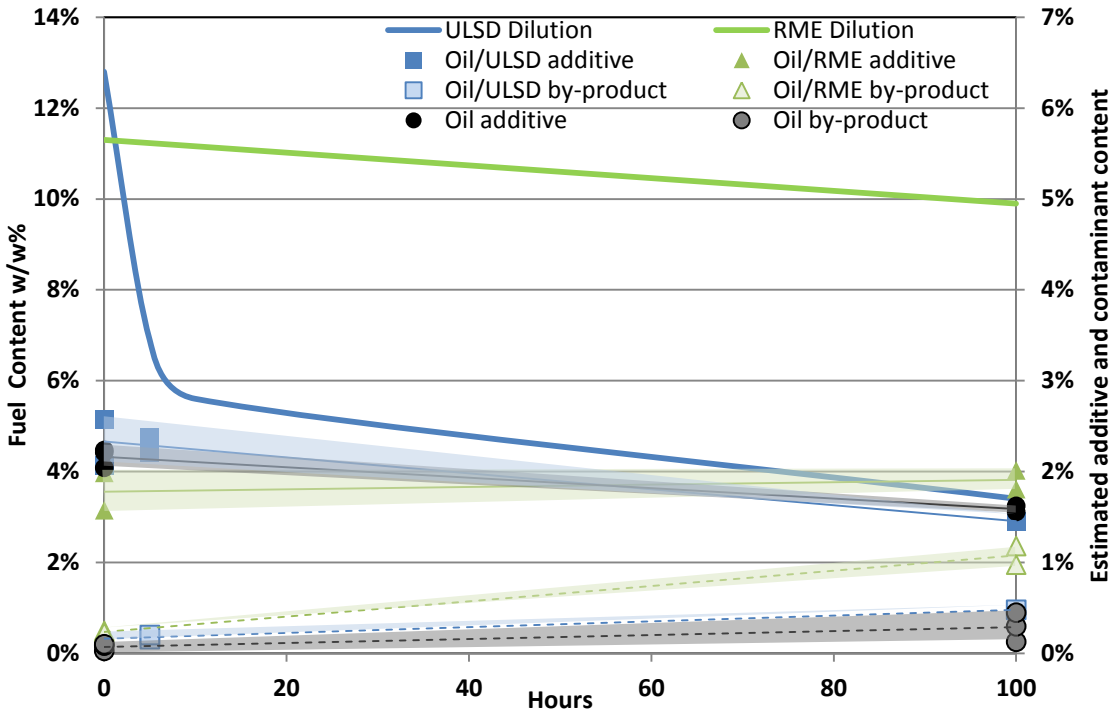

Figure 4.9 - Fuel, Additive and by-product content in oil/fuel blends with ageing

The ULSD content is seen to mirror the viscosity performance in Figure 4.1, decreasing at a rate of around 1.18% w/w per hour for the first 5 hours followed by 0.04% w/w per hour in steady state. This represents a halving in fuel content within the first 5 hours, with a further halving over the remaining 95 hours, leaving a quarter of the initial fuel content after 100 hours. This confirms the previous qualitative assessment, and many assumptions that were made when measuring other fluid properties which were overshadowed by the ULSD. By comparison, the RME content fell by an $\frac{1}{8}^{th}$ over 100 hours, with the fuel maintaining a strong presence throughout ageing, hence why the lubricity performance did not degrade. This is also in agreement with the literature that biodiesels are less volatile than conventional diesels, and will remain within sump oil for longer and in larger quantities (Andreae et al. 2007; Fang et al. 2007).

The additional data shown in Figure 4.9 is measured against the estimated additive and degraded by-product content which were highlighted in Figure 4.6. As mentioned earlier, the monitoring of these two compounds is difficult to accurately achieve due to peaks being masked by the fuel and/or oil which have greater intensities at similar retention times. The estimated values are shown relative to one another for both species. The shaded triangles are areas of possibility where the content of either the additive or by-product could be at any point during the ageing process. This shows a high level of inaccuracy to this assessment, but as it is very difficult to quantify these species without an external standard to calibrate against, assumptions must be made. A summary of results are shown in Table 4.8.

Table 4.8 - Assumed Fuel, additive and aged by-product content in oil/fuel blends

Test Fluid	Age	Fuel	Additive	By-Product
Oil	0	-	2.0%	-
	100	-	1.6%	0.4%
Oil/ULSD	0	12.8%	2.0%	-
	5	6.9%	2.0%	0.2%
	100	3.4%	1.5%	0.5%
Oil/RME	0	11.3%	2.0%	-
	100	9.9%	1.8%	1.0%

Overall additive content has been shown to deplete by $^{1}/_{10}{}^{th}$ – $^{1}/_{4}$ over the course of the 100 hours of ageing. The oil/ULSD shows the greatest loss in additive content, with the oil/RME having the highest additive content after ageing. This could potentially explain why the oil/RME also has the highest lubricity of all the test fluids after ageing, as the additive content remains highest for longer than the other test fluids. However the oil/RME has the highest aged by-product content of the three test fluids after 100 hours; double that of the oil/ULSD. If indeed this by-product is a result of the degraded additive, this would correlate

well with the findings of Sappok & Wong (2008) and Fang et al. (2007) who both observed a decrease in functionality of ZDDP with increasing biodiesel content. Although the approximate values of the by-products may not correlate exactly with the additive content, these values reflect trends that are significant and are felt require further investigation.

4.2.5 - Acidity

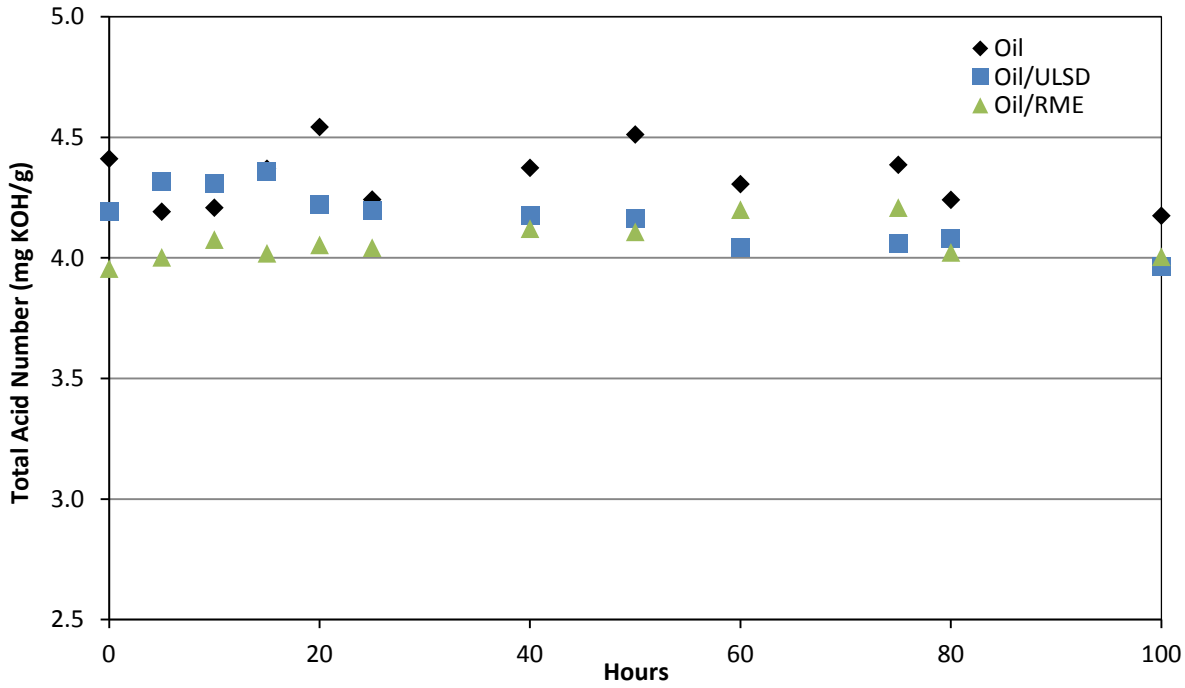

Figure 4.10 - Oil and oil/fuel blends TAN with ageing

Figure 4.10 shows an array of TAN measurements for the three test fluids at different points of ageing. Each displayed TAN value is the average of 3 measurements, with the standard deviation never exceeding ±2% per measured point. Overall the test fluid acidity seems to be higher than literature would predict, this may be due to a slighter weaker titrant solution, however trends are correct as they are proportional to one another.

The main weakness when measuring the TAN of engine oils using a colour-indicator titration method such as ASTM D974 oppose to a Potentiometric method such as ASTM D664, is the additional human error in determining the precise point of colour change. When titrating, the mixture at first assumes a yellow-orange colour, and at the point of neutralising, turns green or greenish-brown. This in itself can be difficult when the orange and brown appear similar in hue, and is also required to be held for a minimum of 15 seconds.

Due to the immiscibility of oil within an aqueous acid, the oil must first be dissolved using an alcohol based solution containing both Iso-propanol and Toluene. This is then titrated against an alcoholic potassium hydroxide (KOH) solution with an alcoholic colour indicator. Each solution was formulated and mixed manually within the laboratory, and titrated against standardised acids and alkalis to approximate their molarity. Each of these processes gives rise to its own level of error, which can accumulate.

With the difficulties in TAN measurements highlighted, it is unsurprising that between the three test fluids, there are little to no discernible trends. This is especially true for the unblended oil which would be expected to gain in acidity due to oxidation of its base. This would likely produce organic acids which may be more volatile and be expected to evaporate (Chen & Hsu 2003), causing there to be little overall change in TAN, but only small fluctuations during its ageing.

The oil/ULSD blend appears to shown a more obvious trend with an overall decline in TAN with age, whereas the oil/RME blend shows a slow increase up until 75 hours, when there is

again a decline. The addition of either fuel will dilute the blend's overall TAN, but unlike ULSD, RME is slightly acidic contributing to TAN by +0.15mgKOH/g. As the fuel content of the blend decreases, TAN would be expected to increase, unlike that of the oil/ULSD blend. This may be due to fuel additives within the ULSD which do not evaporate with the main hydrocarbon portion of the fuel.

4.3 - Conclusions

The aim of this chapter was to investigate the influence of fuel dilution on the ageing and performance of diesel engine oils. When oils age, there is a natural loss to both the base content as well as the additive package. This has an effect of increasing viscosity, density and diminishing the lubricity properties of the unblended oil.

By comparison, the dilution of oil with ULSD has both short and long term effects. The fuel 'dilutes' all of the properties, reducing the viscosity, density and acidity. However the initial fuel levels are quickly lost through evaporation, leaving the heavier fuel constituents behind. This changes the lubricity which is at its worst at this point, but over time these effects settle as the oil finds a natural balance of fuel content, with the density and viscosity returning to more normalised levels. At comparable aged states, the lubricity is improved over unblended oil and the viscosity is much lower. Both of which have benefits to overall engine performance, indicating that the effects of ULSD dilution are not as detrimental as previously thought.

Similar results are also seen with the dilution of RME, showing an initial dilution of all measured properties but indicating a clear benefit to oil performance. The added fuel drastically reduces viscosity and has the largest benefit on lubricity. The benefit of RME dilution is also greater at both higher temperatures and with age. With a lower volatility, biodiesel remains in the sump at similar quantities throughout ageing. This can be a positive as the benefits of the fuel are constantly maintained. But also a negative in that over time the dilution levels may become dangerously high and the oil may no longer be able to maintain other functions.

Overall the effects of fuel dilution can be seen as a positive, with the slight addition of diesel fuel acting as a self-governing system, and biodiesel a lubricity additive. If the biodiesel were slightly more volatile, the self-governing dilution levels could make it a more attractive alternative, as such, the risk of heavy dilution makes it not so favourable for a B100 fuelling option. As an alternative, this natural dilution cycle could be utilised to maintain the performance of engine oils, by depositing additives into the sump oil, extending the length between drainage intervals.

CHAPTER 5 - EFFECTS OF EXHAUST BLOWBY ON ENGINE OIL PERFORMANCE AND AGE

5.1 - Introduction

This chapter examines the effects of diesel fuel combustion and its by-products on the ageing of sump oil. This builds on chapter 4 which investigated the effects of oil ageing and the direct influence of fuel dilution, establishing the influence of exhaust-borne contaminants from the combustion of ULSD and RME. This chapter studies the effects of oil entrained contaminants from the blow-by such as water, unburnt hydrocarbons and nitrous oxides, but excludes the influence of Particulate Matter (PM) and soot.

This was achieved by artificially ageing the oil within a bespoke ageing rig described in section 3.1 of chapter 3 which was connected to the exhaust of a single cylinder diesel engine (section 3.2). To eliminate the effects of sooting, fitted upstream to the rig within the exhaust was a DPF (section 3.2.1) which prevented PM from reaching the rig. The effects of ageing by exhaust gases were compared by combusting two fuels, ULSD and neat RME. The rig was run twice for 20 hours, once per fuel, with samples regularly extracted to characterise property changes. This chapter analyses changes in oil property measured against age using the equipment and methods described in chapter 3 for viscosity, density, lubricity, chemical content and acidity.

5.2 - Results

Table 5.1 - A comparison of the extracted exhaust aged oil samples from the test rig

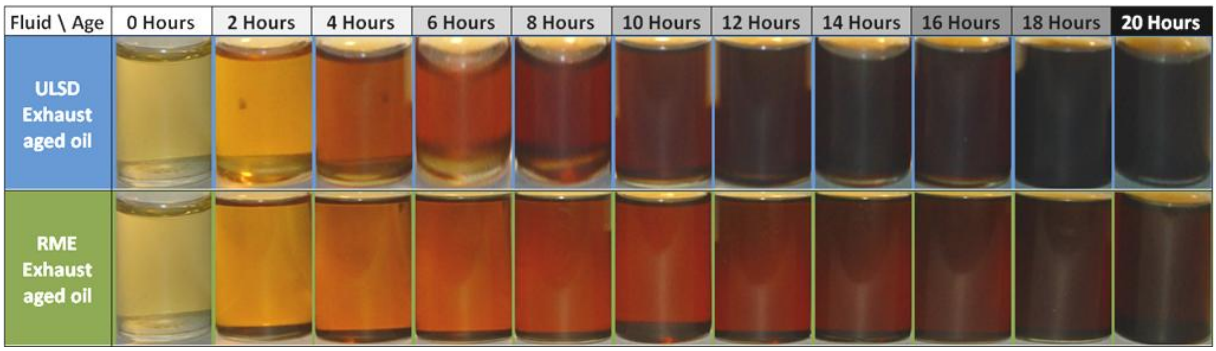

Table 5.1 is a visual comparison of 10mL exhaust aged oil samples for the two test fuels with age. Combustion by-products are collected by the oil, causing a chemical degradation to occur which manifests itself visually as a colour change. It can be seen that the oil gets darker with age, starting a pale yellow turning different shades of reddish-brown with a fairly constant colour change throughout.

The effects of ULSD appear worse than RME as the samples show a difference in both colour and opacity. As a colour comparison, it would seem that the level of ageing experienced by the oil from RME exhaust after 20 hours appears to be similar to the ULSD exhaust aged oil after only 12 hours. This may not actually be the case as will be seen in this chapter which demonstrates how these colour differences are influenced by multiple oil properties.

5.2.1 - Exhaust

The test engine was run using ULSD and B100 RME with exhaust emissions from the combustion of the fuels analysed using the Horiba Mexa 7100DEGR analyser (section 3.2.2, chapter 3), the results of which are shown in Table 5.2.

Table 5.2 - Test Engine exhaust speciation

Exhaust content	ULSD	RME
NO (ppm)	480	600
NO_2 (ppm)	60	50
NO_X (ppm)	540	650
Propylene (ppm)	2	1
Ethylene (ppm)	6	5
Methane (ppm)	2.5	1
Ethane (ppm)	1	0
Acetylene (ppm)	2	1
Formaldehyde (ppm)	7	5
Total HC (ppm)	350	200
CO (ppm)	185	130
H_2O %Vol.	3.57	3.42
CO_2 %Vol.	3.9	3.83
O_2 %Vol.	15	15

Differences in exhaust emissions between the two fuels are noticeable in total HC and CO being lower for RME at the expense of increased NO_x, comparing well with the literature (Rounce et al. 2012; Giakoumis et al. 2012). They highlight the differences in combustion conditions for the two fuels and the effects that the emissions have on the ageing and condition of the oil. This should not be confused with the influence of engine oils on exhaust emissions.

5.2.2 - Viscosity

Figure 5.1 illustrates the change in dynamic viscosity of the aged oils with graphs A and C representing the lower and upper temperature bounds of the USV respectively. Graph B is the viscosity measured at 90°C, the temperature at which the bulk volume of the oil is maintained within the ageing rig. The trends for the two test fuels are similar across test parameters A-C, irrelevant of measured conditions. Like Figure 4.1 of chapter 4, graph C

follows ASTM D4741 and shows the highest level of distortion, less than ±0.98% between measurements, whereas graphs A and B produce the same trends but with less distortion, ±0.21% and ±0.52% respectively.

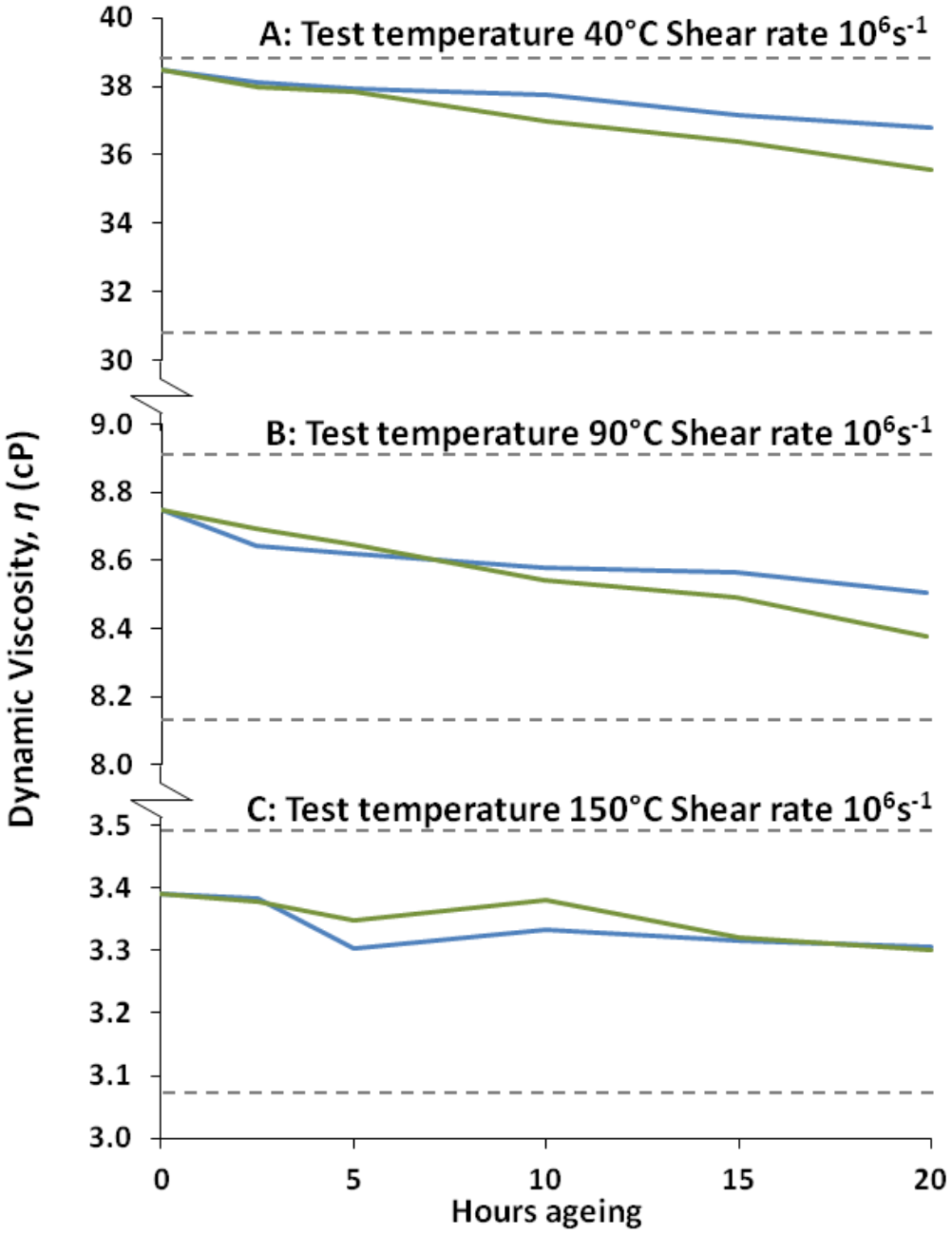

Figure 5.1 - Dynamic Viscosity of engine oil aged due to exhaust emissions from the combustion of ULSD (*blue*) and RME (*green*)

What remains unclear from figure 5.1 is whether this change in dynamic viscosity for the two aged oils is constant. In graph A, the ULSD exhaust aged oil would seem to deteriorate at a near constant rate, but is slightly more staggered in graphs B and C. Whereas the RME exhaust aged oil degrades at a constant rate in graph B, and is staggered in graphs A and C. This may illustrate more the weakness of the USV rather than the individual temperature characteristics of the oils. However, there does seem to be some consistencies within all of the measured data sets to indicate that neither of the exhaust aged oils have a constant viscosity degradation rate, and that the RME exhaust aged oil degrades faster overall.

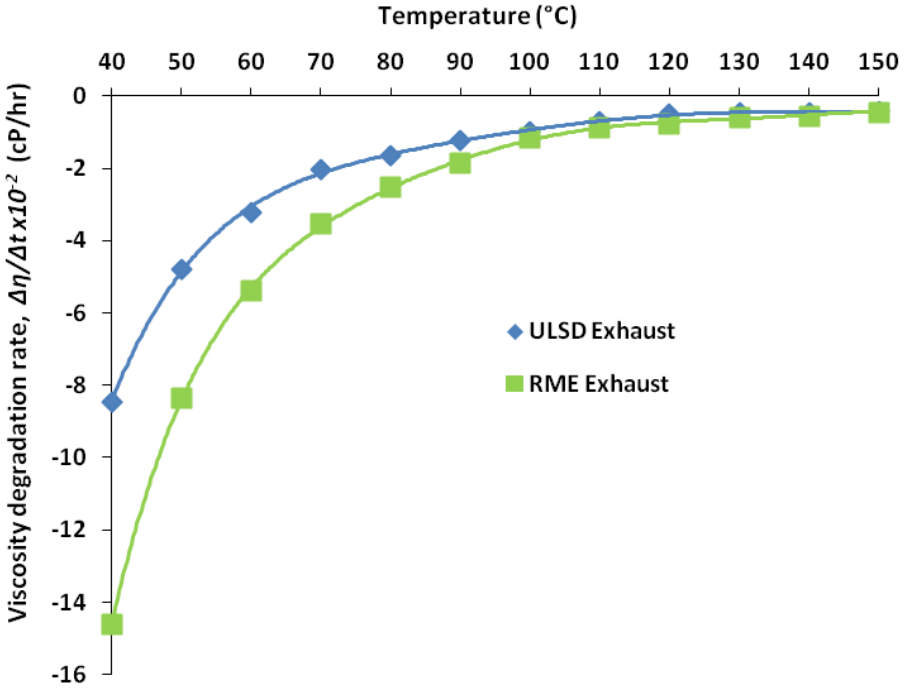

Figure 5.2 - Exhaust aged oil dynamic viscosity degradation rate per temperature

Figure 5.2 shows the total viscosity loss at each measured temperature, and compares the overall degradation rates for the two fuels. As the oil temperature increases, the loss in oil viscosity decreases. Comparing these losses for the exhaust aged oils shows that overall RME causes a greater loss than ULSD at each measured temperature. The expected trend would

be that the viscosity increases with age due to evaporation, oxidation, and polymerisation of the base oil. However, as the oil decreases in viscosity, this would indicate that there is some level of contamination which is the most influential in altering the oil's viscosity than other forms of thermo-chemical degradation triggered by the exhaust emissions. In this instance, the contaminants thin the oil, reducing the overall viscosity, and are more dominant in RME exhaust aged oil than ULSD.

Similar trends are seen in Figure 5.3 which is a summarised form of the Viscosity Index (VI) described by ASTM D2270. The Viscosity Index (VI) is a widely accepted measure of the Viscosity-Temperature (*η-T)* relationship and the level of dependency of viscosity with temperature for petroleum products (ASTM D2270). VI is measured from referenced fluids at both temperatures, and measures the proportional viscosity difference of a fluid from these values. If a fluid has a higher viscosity change at 100°C than at 40°C, this would indicate a high temperature dependency and will have a low VI number; likewise a high VI number indicates an oil viscosity with a low temperature dependency.

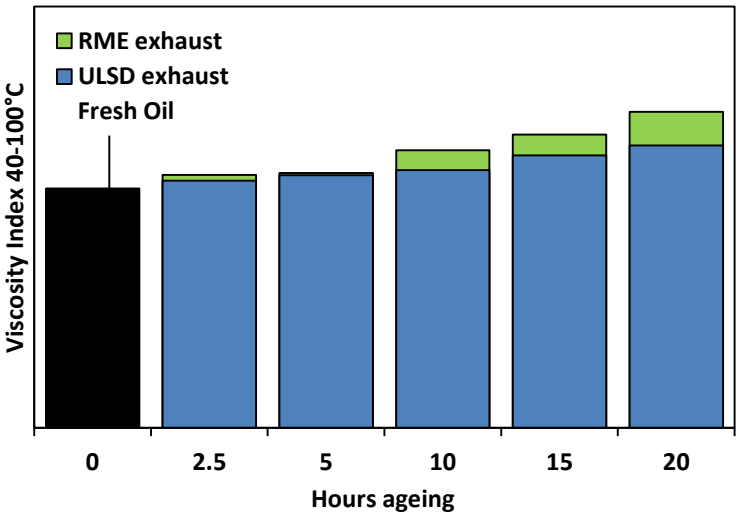

Figure 5.3 - Viscosity Index for exhaust aged oils

Figure 5.3 shows that the VI increases with age and is greater for the RME exhaust than the ULSD, confirming the already seen trends in Figure 5.1 and Figure 5.2. Because the VI increases with age, this would indicate a decreasing η-T relationship suggesting either the aged base oil or the collected contaminants have less of a thermal relationship than the uncontaminated oil. In reality, ageing of base oil as shown in section 4.2.1 of chapter 4 is shown to proportionally increase with age at all measured temperatures, showing little change in VI. However the contamination of the oil with fuel shows an increased VI, therefore it would be no surprise if the collected contaminants from the exhaust cause a similar effect.

Oils must maintain performance across all potential operating conditions including cold engine start-ups and during high engine loads which cover the two temperature extremities. Oil which exhibits a high VI will perform adequately across all sump temperatures. From the viscosity results, it would appear that both exhaust aged oils perform better than the fresh oil across the measured temperature regime, with the RME exhaust aged oil slightly better than the ULSD. Whether these differences are a result of changes in the base oil or due to the entrained contaminants will require deeper chemical analysis, however both will have an effect on the oil's overall lubricity.

5.2.3 - Lubricity

Each exhaust aged oil was split into aged increments up to 20 hours, and tested at 60°C and 120°C. Table 5.3 shows a summary of the average film thickness measurements and coefficient of friction for the test fluids which are also graphically summarised in

Figure 5.4. As each value is the average of a 60 minute test, the addition of minimum and maximum values for both the COFs and film thicknesses are also included.

Table 5.3 - Summary of lubricity properties for exhaust aged oils

Oil/Fuel Lubricating Properties		Film thickness (%)				Coefficient of Friction, μ			
		60°C		120°C		60°C		120°C	
Fluid	Age	Ave	Min Max	Ave	Min Max	Ave	Min Max	Ave	Min Max
Oil	Fresh	81.4	2% 100%	27.4	2% 100%	0.129	0.124 0.135	0.145	0.126 0.151
ULSD Exhaust	2.5 Hours	59.6	6% 100%	75.7	17% 100%	0.132	0.123 0.140	0.147	0.125 0.155
	5 Hours	50.5	6% 100%	69.9	13% 100%	0.125	0.124 0.145	0.146	0.125 0.1555
	10 Hours	40.7	8% 100%	62.1	34% 100%	0.140	0.126 0.141	0.146	0.126 0.157
	15 Hours	24.4	9% 100%	49.3	28% 100%	0.136	0.121 0.141	0.148	0.124 0.164
	20 Hours	44.9	18% 100%	48.0	27% 100%	0.141	0.126 0.141	0.148	0.128 0.168
RME Exhaust	2.5 Hours	82.8	6% 100%	75.7	10% 100%	0.127	0.118 0.137	0.146	0.123 0.153
	5 Hours	64.1	6% 100%	69.5	18% 100%	0.126	0.116 0.140	0.139	0.120 0.155
	10 Hours	38.9	7% 100%	82.9	32% 100%	0.128	0.120 0.139	0.139	0.120 0.149
	15 Hours	61.7	6% 100%	92.1	32% 100%	0.125	0.120 0.143	0.135	0.119 0.150
	20 Hours	89.1	6% 100%	86.7	11% 100%	0.124	0.120 0.141	0.135	0.125 0.150

The three graphs in figure 5.4 show the change in film thickness, COF and wear with age for both test fluids at two temperatures. Figure 5.4A shows the average film thickness, both exhaust aged oils perform the same up to a certain period before diverging. At both temperatures the two fluids show a steady decrease or thinning of film thickness with the RME exhaust aged oil diverging and increasing with age. This shows the differing effects of the two fuel's exhaust conditions, most likely due to contamination. The ULSD's exhaust causes the oil film to continually decrease, lowering the overall lubricity, with the effects being greater felt at higher temperatures. This should be expected as the oil is seen to have a lowered viscosity (Figure 5.1) with age, reducing the film thickness. The contaminant's thinning effect is likely to be less influential as the oil increases in temperature which has also been seen with the VI in Figure 5.3.

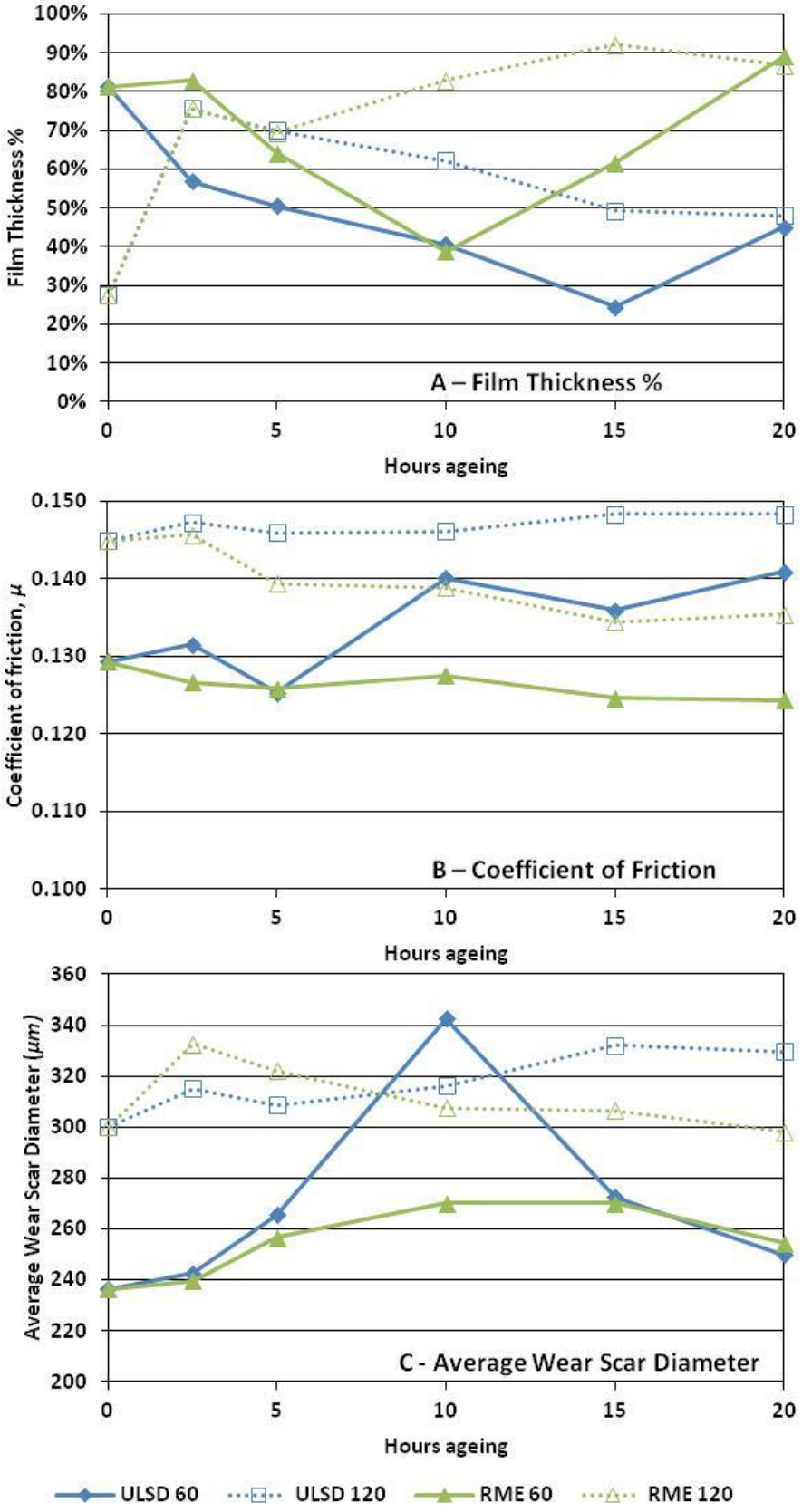

Figure 5.4 - Oil Lubricity properties with exhaust ageing, Film thickness (A); Coefficient of Friction (B) and Average Wear Scar Diameter (C)

The contaminant from the RME's exhaust however causes an improvement to the film thickness, and is a positive influence on lubricity. This is peculiar as it also shows a lowered viscosity which should cause a reduced film thickness. The entrainment of the RME exhaust contaminant in the earlier timeframes does reduce the oil film, but with increasing age (and content) shows a drastic improvement. The point at which the two fluids diverge also differs with fluid temperature, with the RME exhaust contaminant diverging at an earlier timeframe at 120°C. This contamination may be temperature dependant, and at the low quantities found at 10 hours has a greater influence on film thickness at 120°C than it does at 60°C, which again goes against the VI data results.

At 120°C, both fluids exhibit an initial increase in lubricity up to 2.5 hours before following the previous described trends. This is likely due to the evaporation of lighter oil fractions from both fluids whose overall contribution to the film thickness detracts at higher temperatures. The removal of the volatile fraction shows an increase in film thickness in the early timeframes but only during the high temperature test.

Considering Figure 5.4B for the COF, the two fluids again show opposing trends throughout ageing. This graph highlights the relationship between the lubricity properties, with the COF being directly reliant upon the film thickness. The ULSD exhaust aged oil is seen to increase the COF with age, with a greater change at 60°C than at 120°C. Like the film thickness, this identical trend shows that the oil is progressively worsened whilst aged by the ULSD exhaust, with the difference in temperature blamed on the lessening influence of the entrained exhaust contaminants. The opposite trend is observed for the RME exhaust aged oil which

again shows a marked improvement in COF for both temperatures, but with the change being greater at higher temperatures than at low temperatures. Again this is most likely due to the exhaust contaminant affecting the COF, but this time having a significantly greater affect at high temperatures.

The AWSDs are shown in Figure 5.4C and show similar trends to the other two lubricity parameters. At 60°C, both the ULSD and RME exhaust aged oils exhibit their lowest wear scars, peaking around the 10 hour mark before reducing again, mirroring the film thickness performance. However at 120°C the trend resembles more the COF performance with the RME exhaust aged oil initially producing larger wear scars than the ULSD, but reducing in size with age. The ULSD exhaust aged oil increases in wear scar size with age, showing the two opposing trends crossing over at roughly the 8 hour mark. These trends reemphasize the importance of the two fuel's exhaust contaminants and their respective influence on the oil as described earlier. The trends are also shown in Table 5.4, which includes the wearing-in time established as the time taken for the film thickness to reach a stable peak in the real-time film measurements.

Using the fresh oil as benchmark, the oil reaches a steady-state for the film thickness, and is measured by having a 'wearing-in time' of 24 minutes at 60°C, but at 120°C it never reaches this steady-state within the 60 minute test. When aged by the ULSD exhaust, this steady-state is again never reached by the oil for either test temperature. However when aged by the RME exhaust, the oil reaches steady state at both temperatures for the least and most aged oil samples. However this isn't reached for the middle aged range (5-15 hours),

depicting a period of transition as the oil shifts in lubricity properties, shown as a pivotal period in all of the HFRR results.

Table 5.4 - Average Wear Scar Diameter and wearing-in time for exhaust aged oils

Wear Parameters		AWSD (µm)		Wearing-in Time (mins)	
Fluid	Age	60°C	120°C	60°C	120°C
Oil	Fresh	236.5	300.0	24.15	60.0
ULSD Exhaust	2.5 Hours	242.5	315.0	60.0	60.0
	5 Hours	265.5	308.5	60.0	60.0
	10 Hours	342.5	316.0	60.0	60.0
	15 Hours	272.5	332.0	60.0	60.0
	20 Hours	250.0	329.5	60.0	60.0
RME Exhaust	2.5 Hours	239.5	332.5	40.8	50.45
	5 Hours	256.5	322.0	60.0	60.0
	10 Hours	270.0	307.5	60.0	60.0
	15 Hours	270.0	306.5	60.0	48.7
	20 Hours	254.5	298.0	21.57	41.3

The steady state is a reflection on the oil's ability to maintain a maximum oil film, which: a) increases with age; b) is never reached and is worsened when exposed to ULSD exhaust; and c) is improved in part by the RME exhaust. This is in agreement with earlier lubricity trends highlighting the balance in performance between the exhaust degrading the oil and the entrained contaminants which also affect performance.

Overall what these data trends show is that the contamination from the ULSD exhaust is fairly inert, diluting performance with age (and content), detracting from the oil's behaviour. In contrast the contamination from the RME exhaust is shown to be a very active element in the fluid's lubricity, improving performance with age, content and temperature.

For both fluids a turning point is observed where the measured property reverses the trend, due to the conflicting factors from the exhaust (thermal and contamination) acting on the oil. Base oil degradation reduces performance as shown in section 4.2.3 of chapter 4, whereas the entrainment of exhaust-borne contaminants has been shown to be both positive and negative. When one factor begins to outweigh the other, a reversing in trend is observed. However, when reversing is not seen, the trend will have significantly slowed or stopped altogether by the time the test reaches 20 hours. Either no further measurable change is taking place, or the trend reversal is most likely to occur after this measured timeframe.

5.2.4 - Chemical Analysis

Each test fluid was chemically analysed using the GC-MS following test methods described in section 3.5 of chapter 3. The chromatograms shown in Figure 5.5 and Figure 5.6 are of the exhaust aged engine oil from the combustion of ULSD in (*blue*), and RME (*green*). The peak trace for fresh engine oil is overlaid in black for both chromatograms to show any changes with age.

Figure 5.5 shows the chromatogram for oil aged by ULSD exhaust for 10 and 20 hours, with the region between 6-11 minutes magnified to highlight any changes. It would be expected that with age, the peaks within this region would reduce in intensity due to evaporation; however these peaks are observed to grow instead. The peaks specifically seen to grow the most are the volatile mass fraction identified as being unburnt hydrocarbons (UHC) from the fuel, matching the peak trace for ULSD. This would indicate that the predominant entrained

exhaust contaminant from the combustion of ULSD is the fuel itself. This explains some of the trends seen for the viscosity and lubricity which degrade with increasing age and fuel content, similar to those seen in chapter 4 for the oil/ULSD blend.

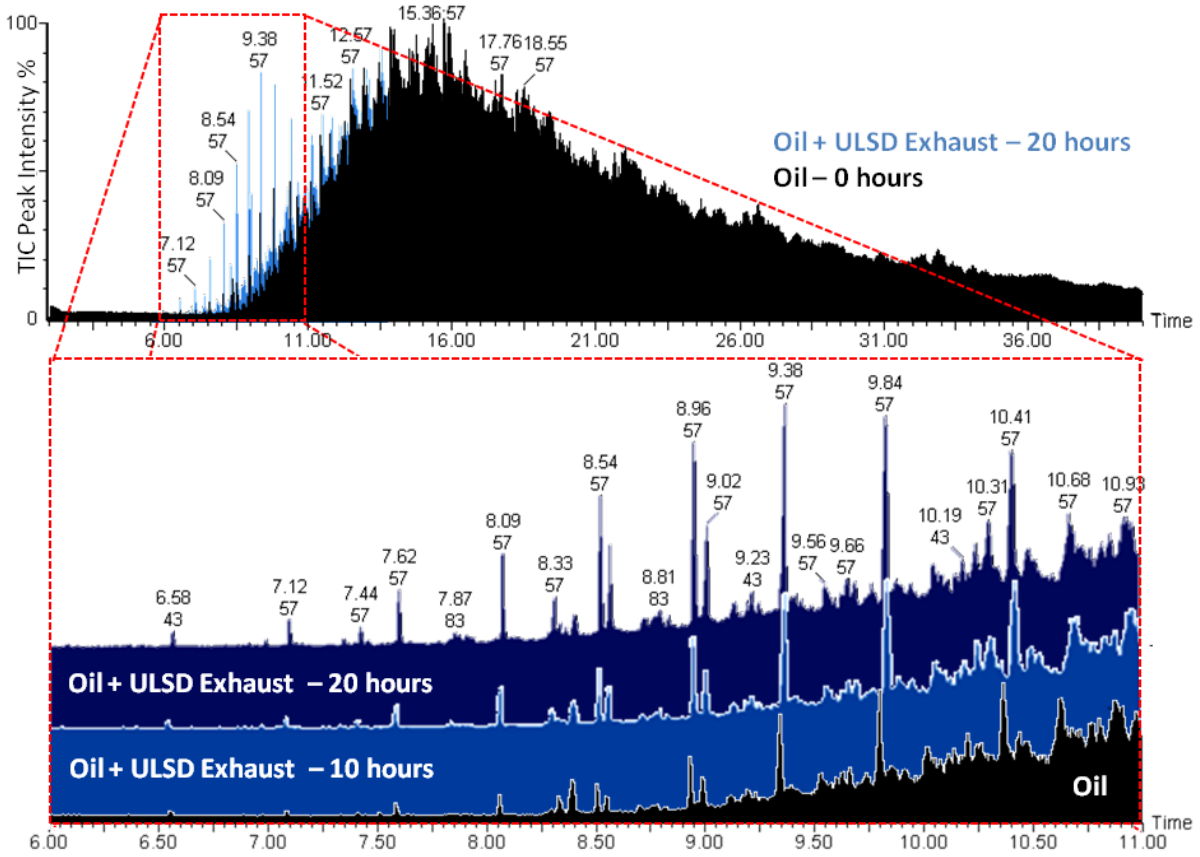

Figure 5.5 - Chromatograms of exhaust aged engine oil from ULSD

Figure 5.6 shows the chromatogram for oil aged by RME exhaust, also overlaid with the peak trace for fresh engine oil. The noticeable trend is the growth of the main contaminant which after 20 hours dwarfs the intensity of any other mass peak found in the oil. The contaminants are seen as four distinctive peaks which are magnified between 9-11 minutes in the final chromatogram and are seen to grow in intensity with age. The four peaks are seen at retention times of 9.40, 10.24, 10.29 and 10.46 minutes, and are FAMEs from the RME with details of each peak detailed earlier in Table 4.7 in section 4.2.4 of chapter 4. The

trend again is the same as before with the main contaminant being the unburnt fuel. This simplified the quantifying of the exhaust contaminants as the calibration fluid was known to be unburnt fuel residues. By repeating the procedure described in section 3.5 of chapter 3 for measuring fuel dilution levels in fresh engine oils, contaminant levels for the two exhaust aged oils were measured.

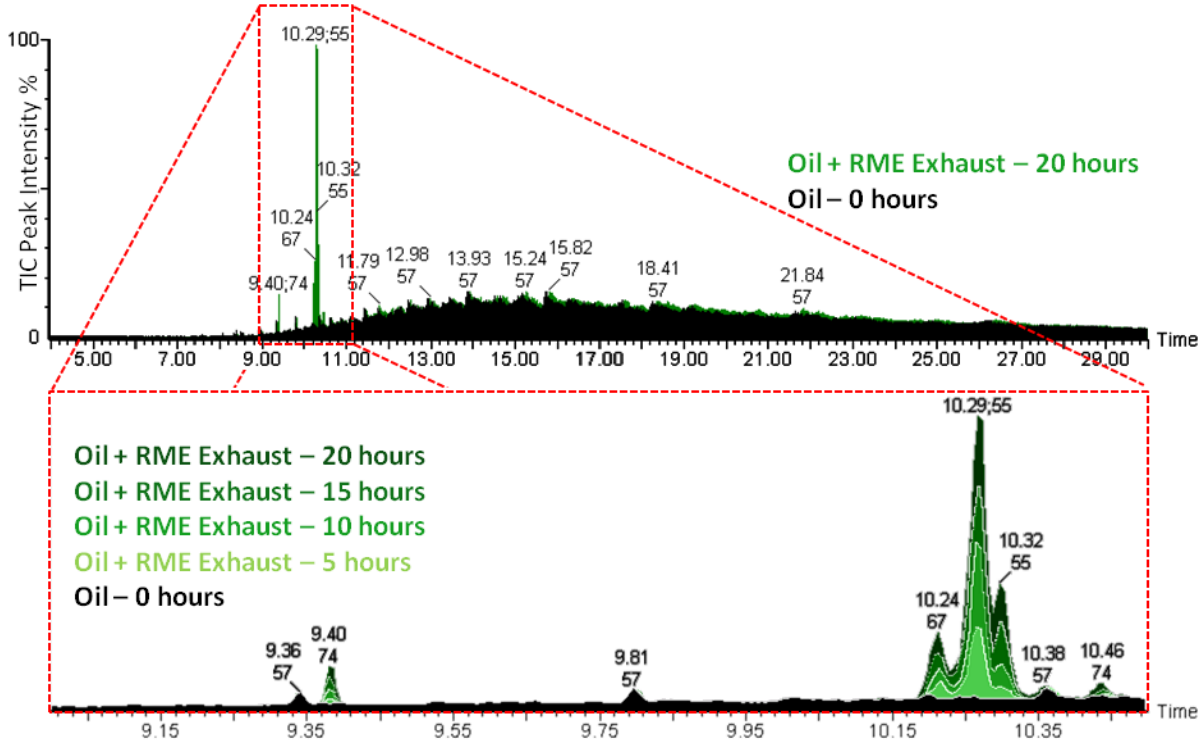

Figure 5.6 - Chromatograms of exhaust aged engine oil from RME

The RME content within the oil is seen to increase linearly with a near constant rate of roughly 0.11% w/w per hour, whereas the ULSD fluctuates between 0.05%-0.28% w/w per hour. This can partly be explained by RME having a higher boiling point than the ULSD, which has been seen to remain in sump oil for longer periods (Fang et al. 2007). ULSD would therefore not be expected to remain in the sump for as long as RME, however it is only the

light mass fuel fraction that evaporates, causing the higher mass constituents to remain and accumulate at a slower rate.

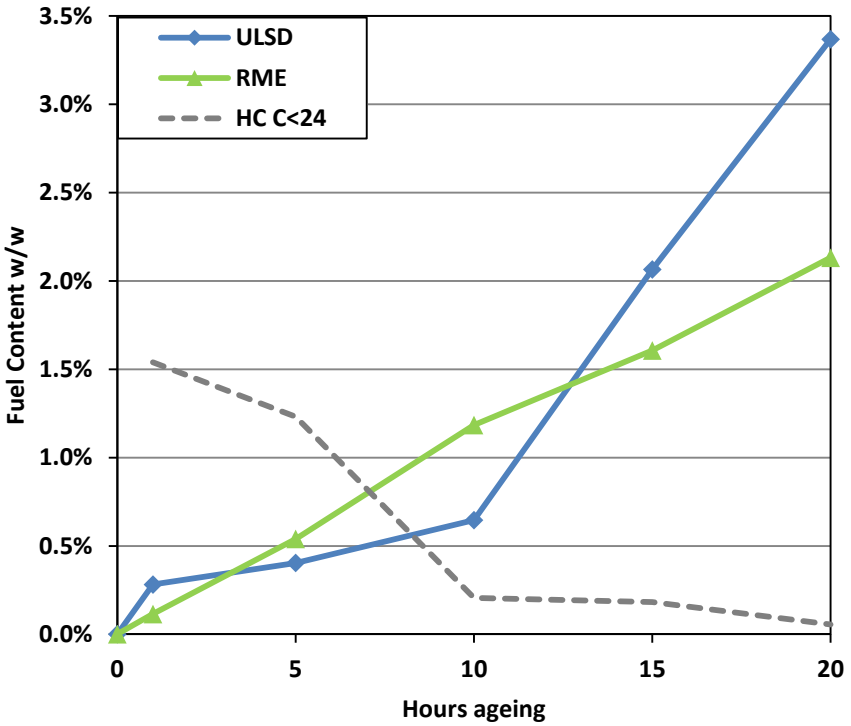

Figure 5.7 - GC measured contaminant content from exhaust aged oils

As the ULSD peaks match the volatile mass fraction of the base oil, it was thought that the change in measured fuel content might be influenced by the oil's evaporation. As both share similar intensity peaks between C_{10}-C_{24}, the loss in these lighter mass peaks may be at fault for the low gain in measured fuel content. The calibration fluids used to measure fuel content utilised fresh oil only; eliminating the contribution of the oil to the fuel peaks. However, as the oil ages, evaporation occurs lowering the respective mass peak intensities within the chromatogram, skewing the aged results. To explain the fluctuating ULSD content, a balance is formed between the increasing ULSD peaks and the decreasing base oil peaks. Between 1-10 hours, the loss in mass peak intensity for the base oil must be at its severest for the ULSD content not to increase at a constant rate like the RME.

To test this hypothesis, the oil that was aged by RME exhaust was measured for typical 'ULSD' peaks, or the low mass fraction. As both exhaust aged oils experienced identical experimental conditions and differ in exhaust content only, any change in base oil composition should be the same. Therefore any observed change in 'ULSD' content for the RME exhaust aged oil is due entirely to base oil evaporation. The grey dashed line in Figure 5.7 shows the apparent change in 'ULSD' content for the RME exhaust aged oil, and as predicted, the greatest loss in volatile mass fraction occurs between 1-10 hours. Beyond this point, most if not all of the volatile peaks had evaporated from the base oil. This gave a trend between 10-20 hours where very little evaporation took place resulting in the highest gain in 'ULSD' content.

The overall content from UHCs found in both exhaust aged oils is higher for ULSD than RME. This does not agree with the literature which suggests that fuel content within sump oil should be higher for RME than ULSD. However, it is emphasised that this experimental setup is not the actual engine sump but an external ageing rig and the mechanism of fuel entrainment is not the same. This rig collects unburnt fuel that enters the exhaust stream, which is higher than the rate of fuel entering the sump via blowby. The purpose of the rig is to accelerate the chemical interactions which naturally occur in the sump so that the same trends may be discovered during a shorter timeframe.

What this experiment does show is that under the same conditions, RME will continually enter the sump at a constant rate, whereas ULSD may appear not to. Depending at what timeframe is sampled, the fuel content within the oil may appear greater for RME than

ULSD. Additionally the measured fuel content will depend on how the calibration curve for ULSD content is established. Due to the similar nature of ULSD and oil, this can lead to misleading measurements of actual fuel content.

5.2.5 - Density

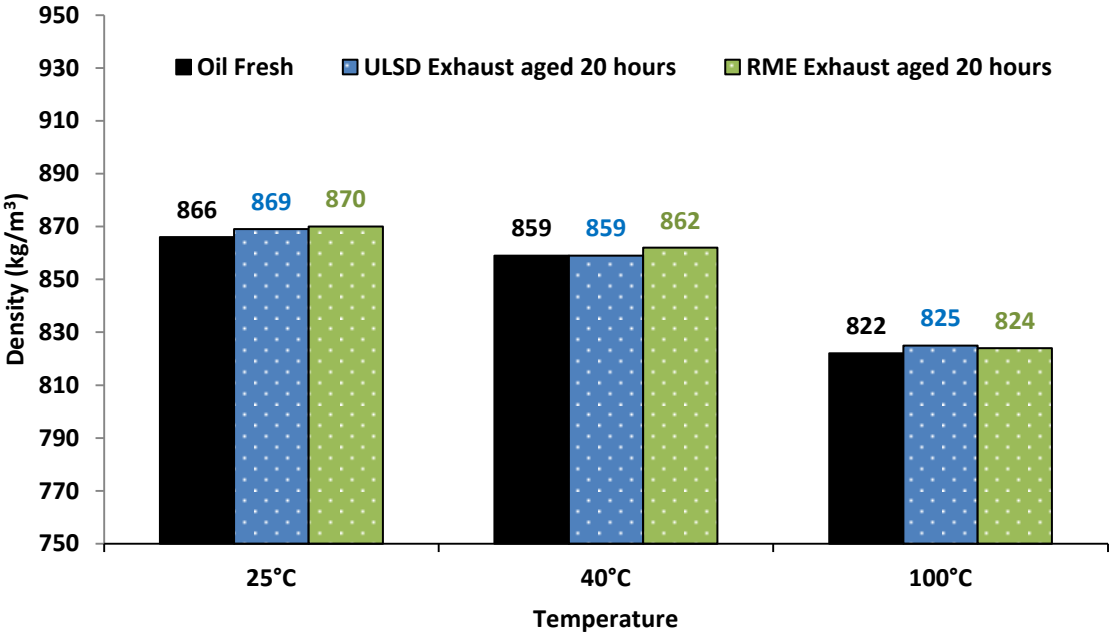

Figure 5.8 - Measured density for fresh oil (*black*), and oil aged for 20 hours by engine exhaust from ULSD (*blue*) and RME (*green*)

Figure 5.8 is a summary of measured densities for the fresh oil and the two exhaust aged oils after 20 hours measured at three temperatures. Using the fresh oil as a reference, it is evident that both the ULSD and RME exhaust cause an increase in lubricating fluid density. With the knowledge that the main exhaust contamination is the unburnt fuel, the addition of RME as seen in Figure 4.3 of chapter 4, demonstrates an increased fluid density. Here the RME exhaust aged oil matches the oil/RME blend after 100 hours, showing similar effects for both fuel entrainment plus degradation. The addition of ULSD would be expected to decrease the oil's density; however it is seen here to increase in density, more so than the

aged oil/ULSD blend from chapter 4. This behaviour is accounted for by the lower fuel content, and the increased evaporation of fuel and the oil's volatile fractions as shown in Figure 5.7, which all contribute to the higher overall fluid density.

Table 5.5 summarises the density thermal responses ($\Delta\rho/\Delta T$) for the three test fluids. The values represented were found in the same way as Table 4.4 in section 4.2.2 of chapter 4. Using the fresh oil as a reference, the influence of the ULSD exhaust causes a very slight reduction in thermal response for the oil. This would indicate that there is a similar thermal response rate for both the fresh oil and the ULSD exhaust contaminants, even though there is an increased density at each temperature measurement. As the thermal response is lower, this indicates that the aged oil and fuel are less susceptible to thermal expansion, with the ULSD again 'diluting' the oil's properties. The thermal response for the RME exhaust aged oil has a sharper gradient indicating that this aged oil is more susceptible to thermal expansion. This again was seen in Table 4.4 of chapter 4 showing that the collected RME has a higher thermal expansion, which has a strong influence on lubricity as seen in section 5.2.3 and section 4.2.3 of chapter 4.

Table 5.5 - Density thermal response rate ($\Delta\rho/\Delta T$) for fresh and exhaust aged oils

	$\Delta\rho/\Delta T$ (kg/m^3/K)
Oil	-0.595
ULSD Exhaust	-0.581
RME Exhaust	-0.619

The trends from the thermal responses ($\Delta\rho/\Delta T$) appear to conflict with the trends concerning Viscosity Index shown in Figure 5.3. It was stated that for the VI, both the RME

and ULSD are less susceptible to thermal change than the oil, but for density the opposite is true, especially for RME. This is because the dynamic viscosity and density are unrelated, whereas kinematic viscosity includes density within its measurement. Separating these two fluid properties during analysis was thought to be important as it is possible to have a fluid that is thermally influenced in one property, but not another.

5.2.6 - Acidity

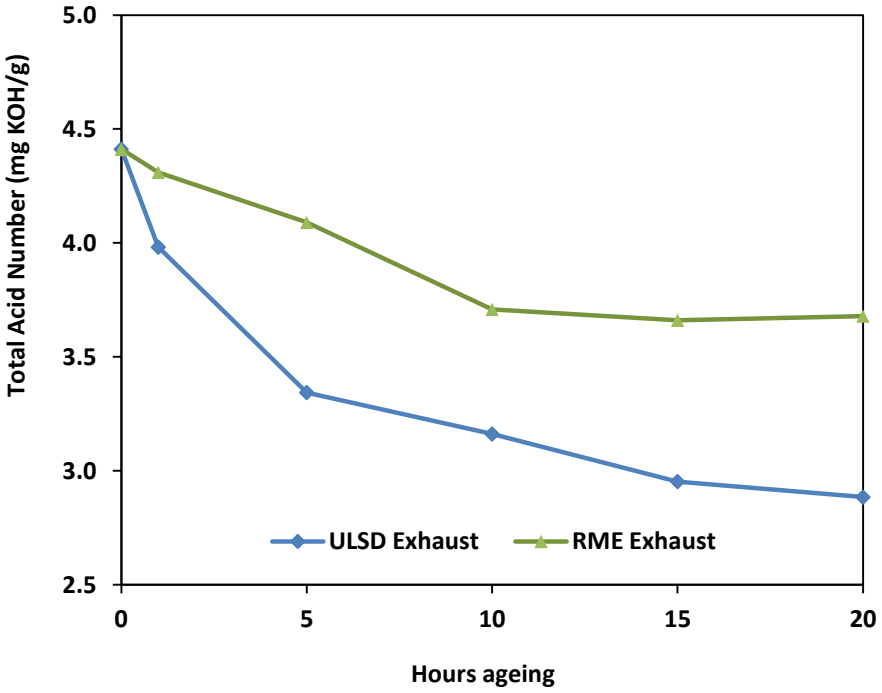

Figure 5.9 - TAN of exhaust aged oils

Figure 5.9 shows an array of TAN measurements for the two test fluids at different points of ageing, with each value being the average of 3 measurements, with the standard deviation for each measured point being less than ±1%. Both exhaust aged oils exhibit a steady decrease with age, curtailing for the final 10 hours. The main difference between the two fluids is the overall drop in TAN, which for the ULSD exhaust drops by 35% from its initial value, whereas RME falls by only 17%.

There are several factors which contribute to these trends, firstly the accumulation of fuel which has a far lower TAN (RME ≈0.1-0.2; ULSD ≈0), diluting the oil's acidity. The slightly acidic RME also causes a fall in TAN, less though than the ULSD which is also shown. However, from the fuel content graphs of Figure 5.7, it is seen that this dilution is only very small, which would not account for such a significant drop in TAN. The accumulation of fuel has also been shown to occur at a near constant rate, but the loss in TAN is not constant. If acidity were directly influenced by fuel content alone, then the overall TAN trend would mirror the fuel content graph of Figure 5.7. Therefore other factors must also be affecting TAN which include base oil oxidation (Chen & Hsu 2003), additive depletion (Fang et al. 2007; Sinha & Agarwal 2008; Thornton et al. 2009) and any exhaust-borne contaminants (Rizvi 2009; Shimokoji & Okuyama 2009).

The TAN graphs from section 4.2.5 of chapter 4 show that the influence of ULSD causes a negative trend, whereas RME both increases and decreases in TAN with age. However, unlike the experiments of chapter 4, the oil was not pre-dosed with fuel, just naturally accumulated with age. Therefore the effects from fuel dilution alone will be different to those seen in chapter 4, but still influential nonetheless. As earlier property trends within this chapter have shown, there is a balance between the oil ageing and it's accumulation of exhaust contaminants, causing two conflicting conditions, which may also be true for the TAN.

From the literature, it was stated that the main effect of exhaust contaminants on engine oil is the entrainment of acids, acid forming by-products and free radicals (Haycock & Hillier

2004; Henderson & LeBarge 2013; Johnson & Korcek 1991; Rizvi 2009). All of which accelerates the degradation of oil, increasing acidity. However within the sampled timeframe of 20 hours, none of this is seen from either fuel, and the opposite is seen. If the rate of loss in TAN was determined by fuel dilution alone, then test fluids should have similar TAN levels throughout, differentiating only by the RME's natural acidity and the relative fuel content. But as both fluids divert away from this negative trend, slowing and maintaining a constant TAN, it is thought that there may be additional acidic affects from exhaust by-products.

Both test fluids negative TAN trends slow as the experiment approaches the end of its test duration, with the RME exhaust appearing to have almost a visible vertex at around 15 hours, with the TAN beginning to rise again at 20 hours. This could be the first visible effects from the exhaust by-products, which is in conflict with the increasing fuel content. The reason as to why this is more visible from the RME exhaust over the ULSD is likely to be due to both lower fuel content within the oil, and higher acid content entering the oil directly from the exhaust stream. However, for this experiment, the effects are very small in comparison to the effects of total fuel contamination over the same timeframe. It is envisaged however that with an extended experimental timeframe of 20+ hours, these effects may become more evident and that experiments run for <20 hours, at best only the apex between acid/fuel effects are visible.

5.3 - Conclusions

The aim of this chapter was to measure the influence of differing exhaust emissions from two diesel fuels on the measureable properties of engine oil. Slight differences in exhaust composition were measured with total HC and CO content being lower for RME at the expense of increased NO_x emissions. However chemical analysis using the GC-MS showed the predominant entrained exhaust-borne contaminant within the oil was unburnt fuel. This chapter differs from the previous chapter 4 in that fuel is naturally accumulated with time, whilst also lost through evaporation. With a shorter experimental timeframe, the effects were heightened for fuel contamination, which in turn masked those from the other exhaust contaminants.

The gain in fuel was seen to dilute all properties in a similar fashion as chapter 4 such as viscosity, lubricity, density and acidity. The influence of the fuel dilution is rapid and more evident in the earlier timeframes, but curtails with age indicating that other factors are contributing to the change, but have a slower response. This is most likely due to the thermo-chemical action of the exhaust species causing a significant change in the base oil through evaporation, degradation and entrainment.

This was observed with several properties exhibiting trends thought to be influenced by more than one factor. Typically at some point during the ageing, a property trend will either slow, stop or reverse. It is thought that with a longer experimental time, some of these secondary influences from the exhaust may be more visible had the fuel content not saturated most of the measurable oil property changes.

CHAPTER 6 - EFFECTS OF PARTICULATE MATTER ON ENGINE OIL PERFORMANCE AND AGE

6.1 - Introduction

The purpose of this chapter is to further investigate the effects of IC engine exhaust emissions on the properties of sump oil. Exhaust generated by the combustion of diesel fuels contains both gaseous pollutants, investigated in chapter 5, and Particulate Matter (PM) studied within this chapter. The PM encompasses both the liquid and solid phase materials found in the exhaust with soot being just one element, also referred to as the insoluble dry fraction. The formation of soot from the pyrolysis of unburnt hydrocarbons is well understood and discussed in section 2.5 of chapter 2. This chapter looks at the soot formed from different diesel fuels such as ULSD and RME and its interaction with engine oil.

This was achieved by artificially ageing the oil using the ageing rig (described in section 3.1 of chapter 3) which was connected to the exhaust of the diesel engine without a DPF. This allowed the entirety of the PM to enter the rig. The effects of exhaust ageing on the oil including soot entrainment were compared again for two fuels, ULSD and RME. Each fuel was run at a low engine load with an Indicated Mean Effective Pressure (IMEP) of 3 bar, before being run at 5 bar to increase the effects of soot loading for the ULSD only. Each test run lasted 20 hours with samples regularly extracted to characterise property changes.

This chapter analyses the results of this test setup with changes in oil property measured against age using the equipment and methods described in chapter 3 for density, chemical content, acidity, viscosity and lubricity. Soot was also passively collected from the exhaust

stream as described in section 3.1.2 to analyse the soot using both scanning electron and atomic force microscopy. The collection of bulk soot was also used to artificially dose the engine oil with known soot masses and tested for viscosity and lubricity alone.

6.2 - Results

Table 6.1 - Extracted samples of exhaust and soot aged engine oil in rig

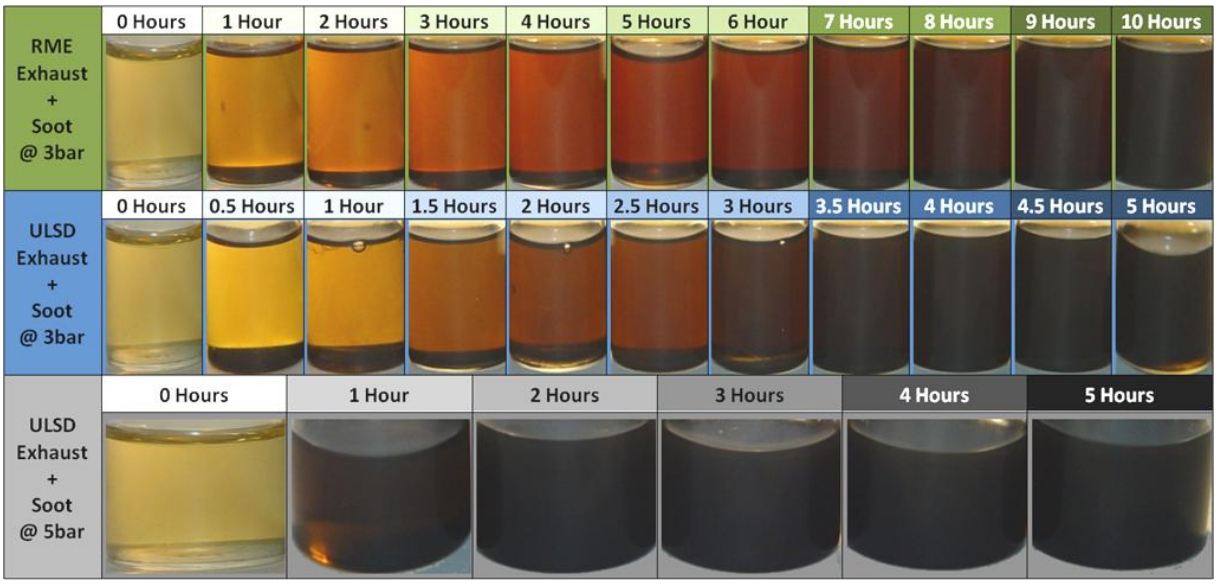

Table 6.1 a visual comparison of the extracted 10mL exhaust and soot aged oil samples for the three tests. The oil collected the same combustion by-products as before, as well as soot, also contributing to the colour change. Table 5.1 from chapter 5 showed the oil becoming more opaque and turning different shades of reddish-brown with age; however this transition occurred over the entire 20 hour cycle. The extracted oils within the chapter still exhibit the same colour change; however the opacity is worse in a shorter time due to the additional entrainment of soot.

The RME exhaust aged oil is shown to lose all clarity after 10 hours, showing the slowest colour change and also the lowest rate of soot accumulation. The ULSD exhaust at 3 bar has a higher rate of sooting, and loses clarity in half the time of the RME exhaust. The ULSD at 5 bar has the highest rate of sooting, and becomes the familiar black of used engine oil within only 2 hours of ageing.

6.2.1 - Exhaust

Emissions from the combustion of the two fuels were sampled from the exhaust stream and analysed using the Horiba Mexa 7100DEGR analyser, the results of which are shown in Table 6.2.

Table 6.2 - Test Engine exhaust speciation

Exhaust content	RME @ 3 bar	ULSD @ 3 bar	ULSD @ 5 bar
NO (ppm)	600	480	880
NO_2 (ppm)	50	60	50
NO_X (ppm)	650	540	930
Propylene (ppm)	1	2	1
Ethylene (ppm)	5	6	4
Methane (ppm)	1	2.5	0.5
Ethane (ppm)	0	1	1
Acetylene (ppm)	1	2	1
Formaldehyde (ppm)	5	7	5
Total HC (ppm)	200	350	450
CO (ppm)	130	185	120
H_2O %Vol.	3.42	3.57	5.31
CO_2 %Vol.	3.83	3.9	5.65
O_2 %Vol.	15	15	-

The exhaust speciation results shown in Table 6.2 differ from Table 5.2 of chapter 5 with the addition of the ULSD exhaust data at 5 bar. There is a significant increase in NO_x, CO_2 and total HCs at higher engine loads due to higher combustion temperatures which favour

oxidation and the production of thermal NO and compares well with the literature (Mueller et al. 2003; Flynn et al. 1999; Rounce et al. 2012; Ladommatos et al. 1996). They are included to highlight differences in combustion parameters, which will in turn influence the formation of PM and how it interacts with the oil.

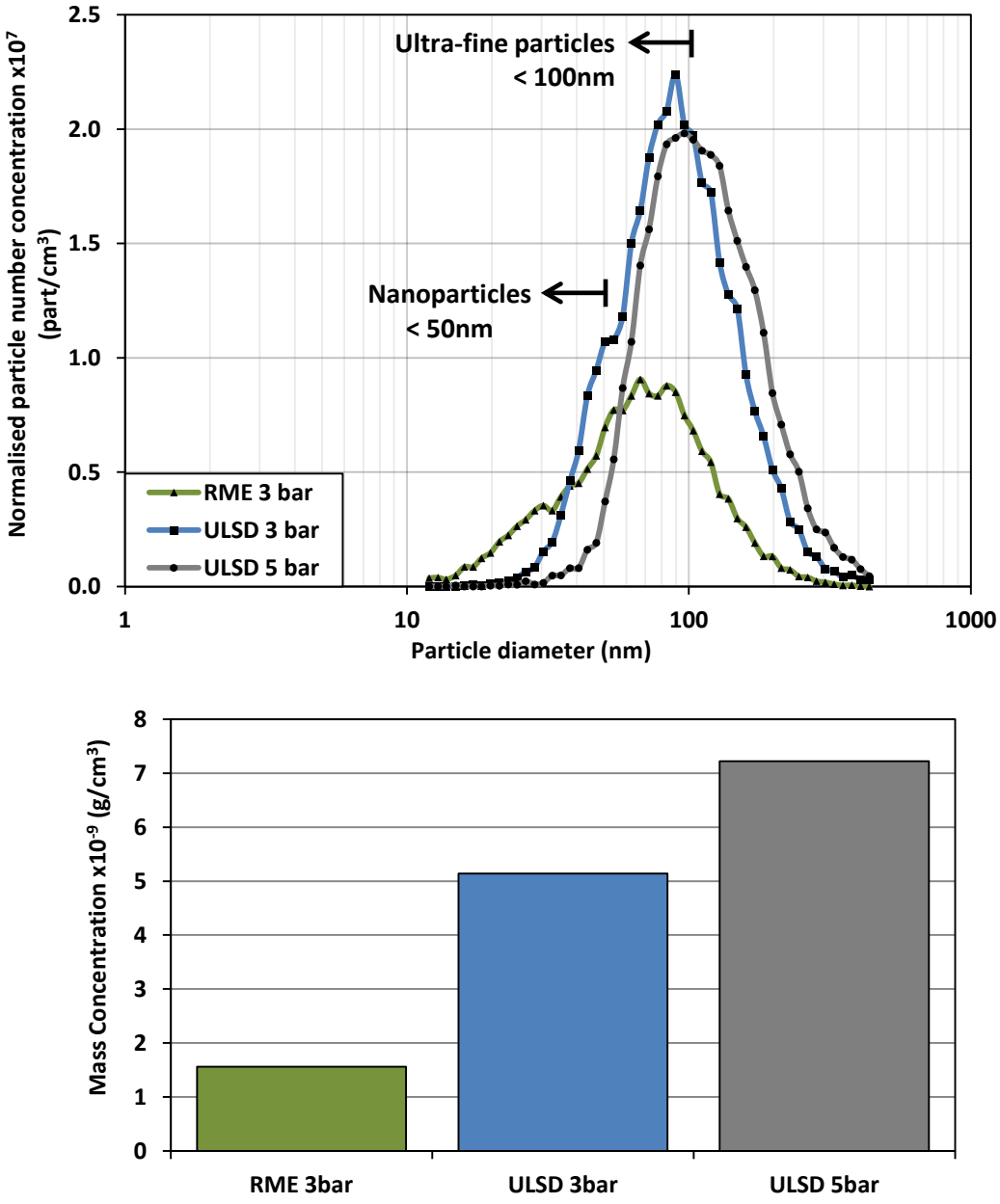

Figure 6.1 - SMPS data particle sizing (top) and Exhaust PM mass concentration (bottom)

Data from the Scanning Mobility Particle Sizer (SMPS), which measures particle number and size distribution for the three test runs is shown in Figure 6.1. Also displayed is the derived particle mass concentration which utilised the *'The effective particle density exponential function'* formulated by Lapuerta et al. (2003). Results of the PM emissions compares well with the work done by Ladommatos et al. (1996), Daido et al. (2000) and Lapuerta et al. (2003).

Differences between the two fuels are noticeable with RME producing far lower particle numbers, a lower total PM mass, and a higher proportion of nano-sized particles in comparison to the ULSD as expected. Likewise it was stated that higher engine loads increases soot production as seen with the comparison of ULSD combustion at both 3 and 5 bar. From the particle count and size distribution however, it appears that there is a slightly lower particle number concentration at higher loads. This is countered by an increased proportion of larger diameter particles greater than 100nm which contributes to the greater mass concentration seen at higher engine loads.

The extracted oil samples of Table 6.1 matches well with the above PM mass concentration, this shows the oils with the fastest changing colour also having the highest PM mass. Most of the PM that enters the rig will not become entrained within the oil; however as a proportional scale the two data sets match well even though one is only qualitative. Determining the degree of soot loading experienced by the oil for the three test conditions will have a large bearing on the results hereafter, and the influence that the two fuel derived soots have on the oil.

6.2.2 - Density

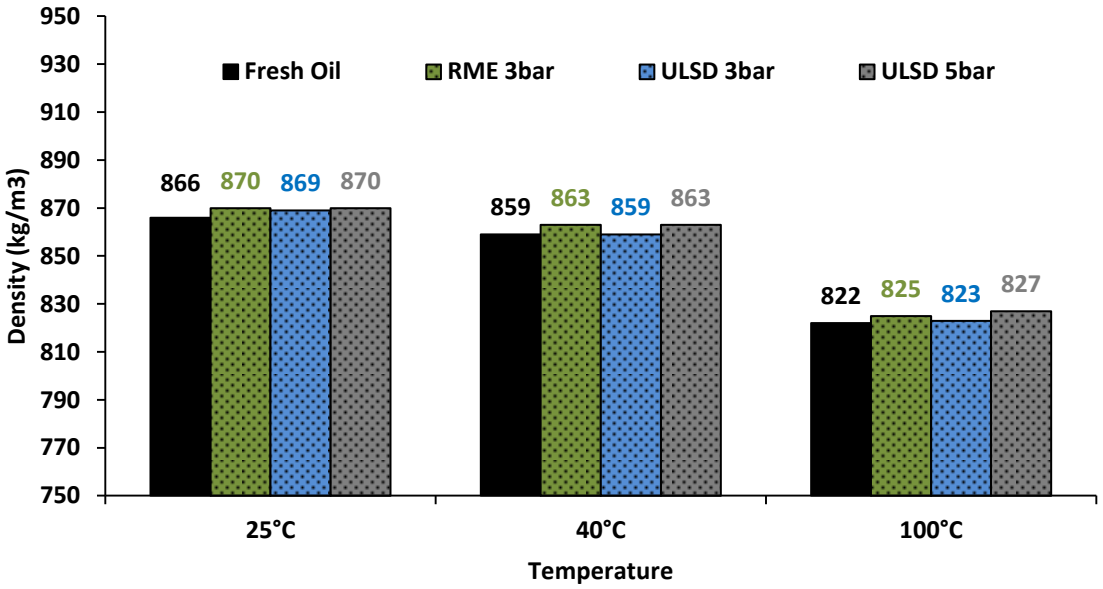

Figure 6.2 - Measured density for fresh oil, and 20 hour aged oil from sooted exhaust

Figure 6.2 shows the measured densities for test fluids. Using the fresh oil (*black*) as a reference, it is evident that the exhaust from the two fuels increases the oil density. As seen in Figure 5.7 of chapter 5, the entrainment of exhaust contaminants causes an increase in fluid density. This again is repeated but with the addition of soot which is significantly denser than the oil, contributing to a higher overall density, however this is only seen when the soot contamination levels are significant.

Table 6.3 - Density thermal response rate ($\Delta\rho/\Delta T$) for fresh and sooted exhaust aged oils

$\Delta\rho/\Delta T$ (kg/m^3/K)	
Fresh Oil	-0.595
RME 3 bar	-0.610
ULSD 3 bar	-0.609
ULSD 5 bar	-0.581

Table 6.3 summarises the density thermal responses ($\Delta\rho/\Delta T$) for the four test fluids. If the trend for the fresh oil is again used as a reference, the influence of the RME exhaust increases the thermal response gradient whereby the density decreases at a faster rate than the fresh oil. This is a repeated trend from the earlier chapters indicating that RME is more susceptible to thermal expansion. The entrainment of soot particles increases oil density, but reduces the thermal response due to being solid with an assumed limited thermal expansion within this temperature range. Due to the low soot content seen in Figure 6.1, it is unlikely that the RME soot has any effect on either the overall density nor the thermal response of the RME exhaust aged oil after 20 hours.

The ULSD exhaust aged oil under low engine loads has an almost equal thermal response rate as the RME exhaust aged oil. This is surprising as the ULSD oil has a lower measured density at each temperature, indicating that its overall density due to contaminant entrainment must be less. In Table 5.5 of chapter 5, the ULSD exhaust aged oil is seen to have a lower thermal response rate than the base oil, however now it is seen to be similar to the aged oil/ULSD blend of chapter 4. This would indicate either a greater level of base oil degradation than was seen in the chapter 5 results, or that fuel contamination is lower.

From the SMPS data in Figure 6.1, it can also be seen that the soot content should be higher for the ULSD which in turn would increase the overall density. Under these engine conditions, the influence of soot loading on the overall oil density is negligible after 20 hours; therefore changes in density are thought to be from other sources. Either both aged oils have a similar level of oxidation as each have identical thermal responses, or that the

entrained contaminants from the RME exhaust have a greater influence than ULSD exhaust on fluid density.

Comparing the ULSD exhaust aged oil at higher engine loads; the oil has the lowest thermal response and highest measured density at each temperature than any of the measured test fluids. Under these engine conditions, the influence of soot entrainment on the overall oil density is likely to be higher, which as expected increases density and lowers the thermal response. Also the overall oil density is likely to be influenced by the exhaust conditions which at higher engine loads differ (as shown in Table 3.1 & Table 3.2). This reduces the volatile content entering the rig, and increases the evaporation rate of fuel and other volatiles from the oil.

6.2.3 - Chemical Analysis

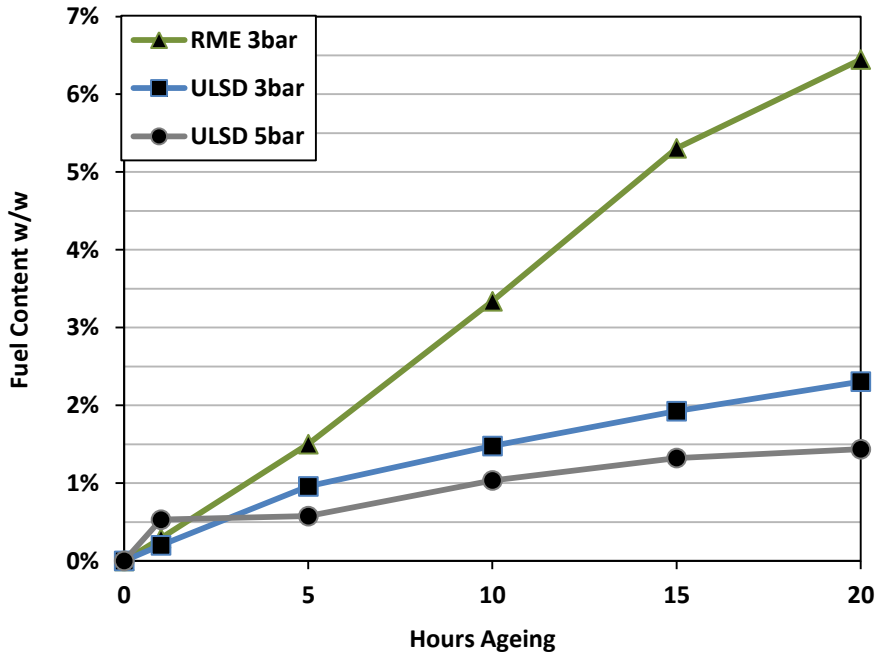

Figure 6.3 - Fuel content within sooted exhaust aged oils

Each test fluid was chemically analysed using the GC-MS following test methods described in section 3.5. During ageing, the oil evaporates which decreases the volatile content, but at the same time the oil accumulates fuel which increases the volatile content. This is seen for both the ULSD and RME, with the dilution levels shown in Figure 6.3. Soot content however cannot be tested using the GC-MS as it tests fluids only, with samples requiring filtering beforehand.

Figure 6.3 shows fuel contamination levels for the three exhaust aged oils, which was expected to be the same as Figure 5.6 of chapter 5 for both the RME and ULSD content at 3 bar. The difference between the two test setups is the inclusion of the DPF in chapter 5, which should only alter the PM content and not the fuel. As seen in Figure 6.3, the RME content increases linearly with a near constant rate of roughly 0.32% w/w per hour, which is far higher than the accumulation rate in chapter 5. Likewise the ULSD content at 3 bar now increases linearly at roughly 0.12% w/w per hour, but in chapter 5 showed huge levels of fluctuation. Why the lack of a DPF reduces ULSD content but increases the RME is unknown, however this does highlight a weakness of the test setup as the DPF has no direct influence on the fuels path to the engine's sump.

Of more importance is the difference in fuel content when operated at higher engine loads. The rate of ULSD accumulation is reduced to 0.07% w/w per hour on average and is the only oil with a slightly fluctuating content. Within the first hour, there is a huge gain of 0.53%, before dropping down to a more subdued rate of only 0.01% w/w per hour between 1-5 hours. This may be due to the rig still warming, quenching a greater amount of exhaust-

borne UHCs. But as the rig warms, and paired with the hotter exhaust at higher loads, the rate of evaporation of both the fuel and the oil increases, which results in a very low net gain in fuel content for the duration of the experiment.

The observed difference in fuel content is important as it shows that there are now two differences in input characteristics from this chapter's test setup to that of chapter 5. Without the DPF in the exhaust stream, all test fluids accumulate PM which was the desired effect; however both fuelled exhausts have an undesired change in the level of fuel entrainment. Both will influence the measured property changes of the oil, but in reality have no further relevance in the real world due to the rig not being an actual engine. Knowing the effects of fuel dilution from chapter 4, the difference in fuel content can be offset to further investigate the effects of sooting on the oil.

6.2.4 - Acidity

Figure 6.4 shows the TAN trends for the three exhaust aged oils with each value being the standard deviation of 3 measurements, with the error being less than ±1.5% at each measured point. The three test fluids all exhibit a steady decrease with age and have a very similar overall drop in TAN, with slight fluctuations and several periods of overlapping. Comparing the TAN data with the results of Figure 5.8 in chapter 5, the trends shift inversely to the change in fuel content shown in Figure 6.3. For example the RME content is now greater than in chapter 5, and the measured TAN is now lower. Likewise there is now a lower ULSD content resulting in a higher TAN than before. This shows the extent of the difference

in property due to the changing fuel dilution; however this has not shown the effects of sooting.

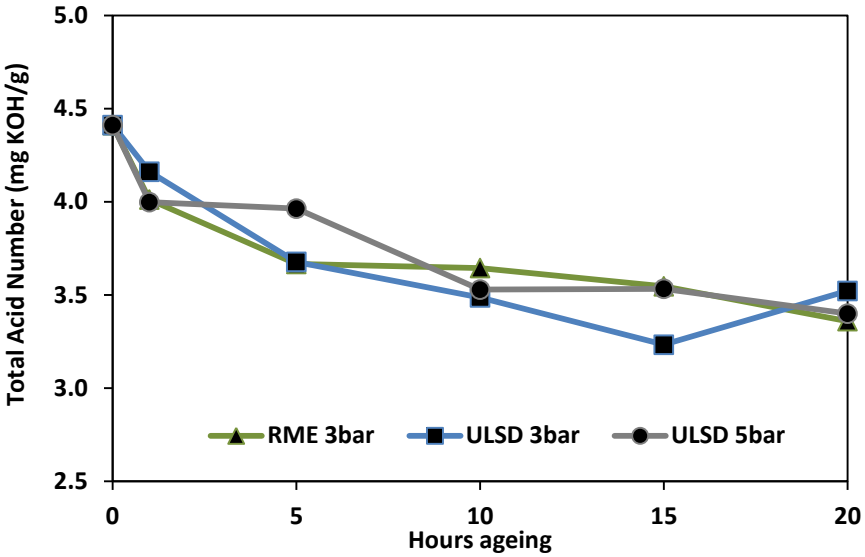

Figure 6.4 - TAN of sooted exhaust aged oils

There are several factors thought to account for these changes, each competing with one another to influence the overall TAN. The oil therefore has to balance the effects of each factor, with the resultant TAN seen in Figure 6.4. Table 6.4 is a summary of the TAN contributing factors and their relative influence on the oil.

Table 6.4 - Overall combustion influence on TAN

	Test Condition	RME 3 bar	ULSD 3 bar	ULSD 5 bar
Fuel	Fuel is comparatively neutral; therefore any fuel dilution will reduce TAN.			
	Fuel content	High	Low	Lowest
	Actual effect	↓ but slight +	Neutral ↓	Neutral ↓
Exhaust	Exhaust gas heats and oxidises the oil creating weak acids, increasing TAN			
	Exhaust condition	Low	Low	High
	Actual Effect	Small ↑	Small ↑	High ↑
Soot	Soot is amphoteric with a slightly acidic surface, but has a low overall TAN			
	Soot content	Lowest	Low	High
	Actual Effect	0 to slight ↑	Slight ↑	Slight ↑
TAN Rank High-Low		**2**	**3**	**1**

Notes about Table 6.4; firstly the ULSD and RME have a far lower TAN than the oil, so any contamination of the oil with one of these fuels will cause a diluted TAN as mentioned in both chapter 4 and chapter 5. Likewise the RME is faintly acidic so it will contribute to the overall TAN slightly whereas the ULSD will not. High engine loads will cause the oil to experience greater temperatures, which may accelerate any oxidative processes. This in turn has a knock on effect with the addition of weak organic acid formation. Soot particles have both acidic and basic elements upon its surface, interfering with oil additives and buffers (Nagai et al. 1983; Kornbrekke et al. 1998; Birch 2004). It is thought that although soot may have some acidic elements, its overall influence on TAN is minimal unless entrained in significant quantities.

What has not been included in the influencing factors is the effect of fuel and oil reacting to form oxidised and acidic compounds, which thus far have not been detected using the GC-MS. Neither has the effects of other combustion by-products been seen, and so have also been neglected. It was stated in chapter 5 that although the effects of other exhaust compounds were not seen, this may be due to the short sample time of only 20 hours not being long enough to observe these changes. Any acidic exhaust contaminants may therefore be influencing the results of Figure 6.4, but have so far not been great enough to be measurable.

The development of the test rig was intended to behave as an engine sump that would accelerate ageing. The rig therefore may not be an adequate representation of the sump, which does successfully accelerate the differing ageing factors, except unequally. Each

ageing factor has been seen in some form, but time is a significant constraint which may be the rig's downfall. This may explain why the fuel content seems to be the most dominant, as it is the most accelerated factor of them all.

6.2.5 - Viscosity

All fluids aged within the rig were tested for high shear dynamic viscosity using the USV, with the results shown in section 6.2.5.1. These measurements were then repeated using a low shear rate rheometer described in section 3.4.2 for exhaust aged fluids and artificially soot dosed oil samples, shown in section 6.2.5.2.

6.2.5.1 - Ultra Shear Viscometry

Figure 6.5 illustrates the change in dynamic viscosity for three test fluids measured at four different USV parameters: the lower (A) and upper (C) temperature bounds; and the lower (A-C) and upper (D) shear rates. The trends are similar across test parameters A-D, irrelevant of USV conditions. But again graph C which is run following ASTM D4741 shows the greatest level of deviation between measured points at ±0.97%, whereas graph A, B and D are as low as ±0.23%; ±0.64%; and ±0.19% respectively. The above trends are also similar to those found in Figure 5.1 of chapter 5, with fuel dilution being the most significant factor, with the viscosity trends mirroring the fuel content of Figure 6.3.

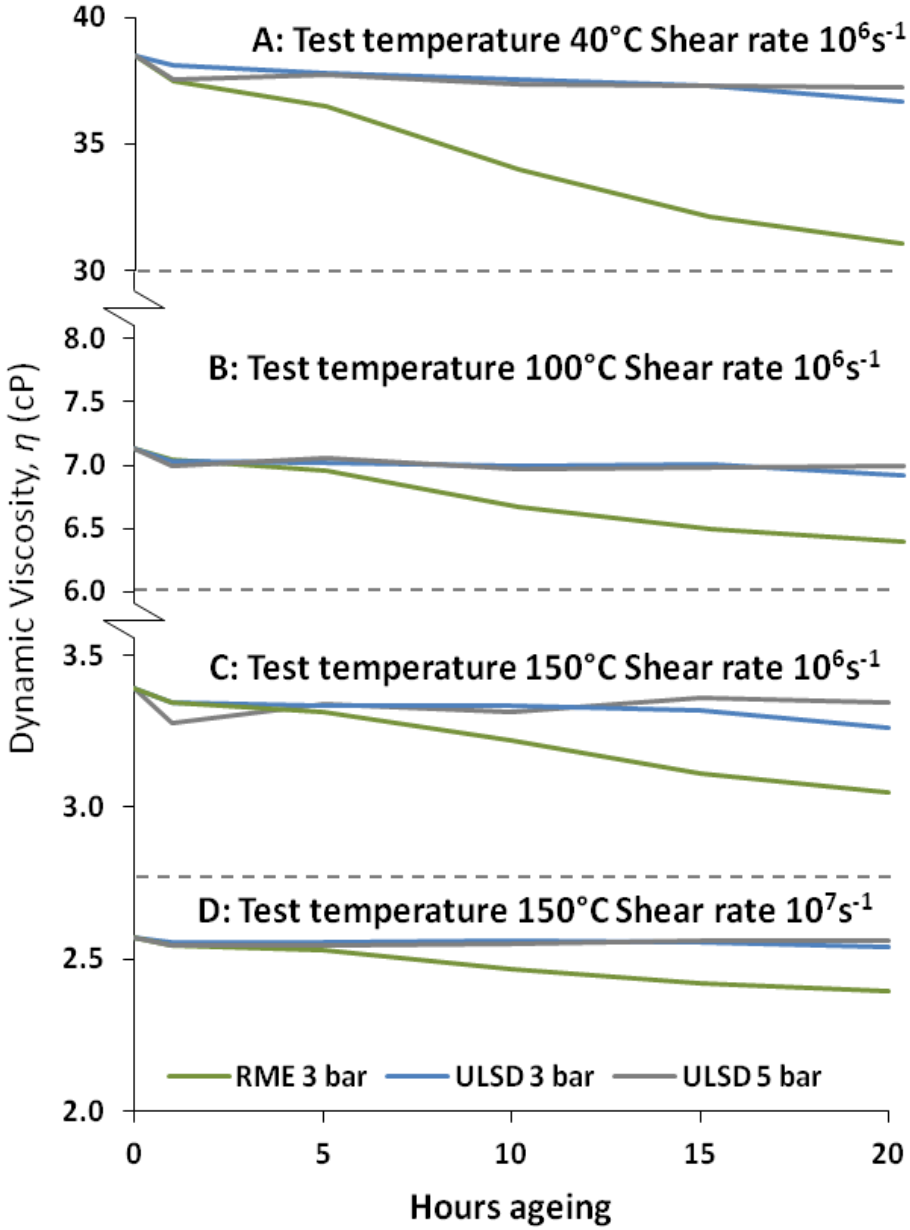

Figure 6.5 - Dynamic Viscosity of engine oil aged from sooted exhaust emissions

Table 6.5 takes into consideration the total viscosity change (%$\Delta\eta$) at each measured USV parameter, and compares them for the three test fluids. Two data sets are shown here, the first is the overall change between 0-20 hours, the total ageing during each test run. The second data set shows the same measured viscosity change, but measured between

2-20 hours, as some of the test fluids showed significant changes within the first 1-2 hours that later were not seen.

Table 6.5 - Viscosity change with sooted exhaust ageing (%$\Delta\eta$)

USV Parameters			%$\Delta\eta$:- 0–20hrs			%$\Delta\eta$:- 2–20hrs		
Graph	Temp (°C)	Shear rate (s^{-1})	RME 3 bar	ULSD 3 bar	ULSD 5 bar	RME 3 bar	ULSD 3 bar	ULSD 5 bar
A	40	10^6	-23.85%	-4.86%	-3.27%	-21.24%	-3.72%	-1.39%
B	100	10^6	-11.59%	-3.07%	-2.03%	-10.85%	-1.73%	-0.27%
C	150	10^6	-11.16%	-3.91%	-1.26%	-8.10%	-2.95%	0.99%
D	150	10^7	-7.27%	-1.26%	-0.42%	-6.55%	-0.69%	0.58%

As stated earlier, the expected factors here are the influence of fuel dilution, the exhaust conditions, and the soot content. The effects of the exhaust gases are thought to increase the viscosity (Johnson & Korcek 1991; Trujllo 2004), but are only slight and the overall effects are small within the 20 hour timeframe. Therefore the two main factors are fuel dilution, which has been shown to decrease the viscosity (Gatto et al. 2008; Andreae et al. 2007), and soot content which is expected to increase the viscosity (Selby 1998; Kornbrekke et al. 1998). The oil aged by the exhaust of RME entrains high levels of fuel, and low levels of soot, therefore as expected the overall viscosity is seen to continually decrease with age.

The viscosity of the oil aged from ULSD exhaust at 3 bar is also shown to decrease with age. This is expected as the soot loading effects are still not high enough to significantly thicken the oil. Even though the effects of sooting are higher than the RME, the fuel contamination is high enough to significantly thin the oil. That being said, the overall viscosity change is still a continual decrease, however it is only slight and is visibly lowest in graphs B and D. At these

USV parameters the viscosity looks at points as though there is no change and that there is a balance between factors. The trade-off between the soot and fuel entrainment under these engine conditions seems to favour the fuel content as the more influential factor.

The oil aged from ULSD exhaust at 5 bar differs from the 3 bar results in that the effects of soot loading is higher, and the entrained fuel is less. Therefore it would be expected that there would be an eventual increase in oil viscosity. This was not seen in any of the viscosity graphs of Figure 6.5 even though the net change was very low. However looking at the viscosity change between 2-20 hours, there is an increase in viscosity under test conditions C and D. This is the first sign that soot loading can increase the overall viscosity of engine oils whilst balanced with increasing fuel content.

6.2.5.2 - Rheometry

The lack of measurable visco-thickening of the oil under heavy engine loads was surprising as the oil was observably more viscous. It was felt that the USV was not adequately suited to measure the effects of soot-thickened oil. However ASTM standard D6895 was developed precisely to measure this, however it required the use of a low shear rate rheometer. The AR2000 Rheometer made by TA instruments was used for further viscosity measurements as it is ideal for measuring the viscosity of suspensions and flocculated fluids. Test samples also do not require filtering which the USV needed, which was later believed to be eliminating much of the larger agglomerated soot content, reducing the envisaged soot-thickening effect.

Following ASTM D6895, the three exhaust aged oils viscosity measurements were repeated using the rheometer for low shear rates as shown on the left of Figure 6.6. The second rheometer graph on the right measures soot induced oil thickening with artificially soot dosed oils. Soot was collected from the exhaust stream of both the ULSD and RME at 3 bar, and blended with fresh oil at 0.5, 1 and 2% w/w.

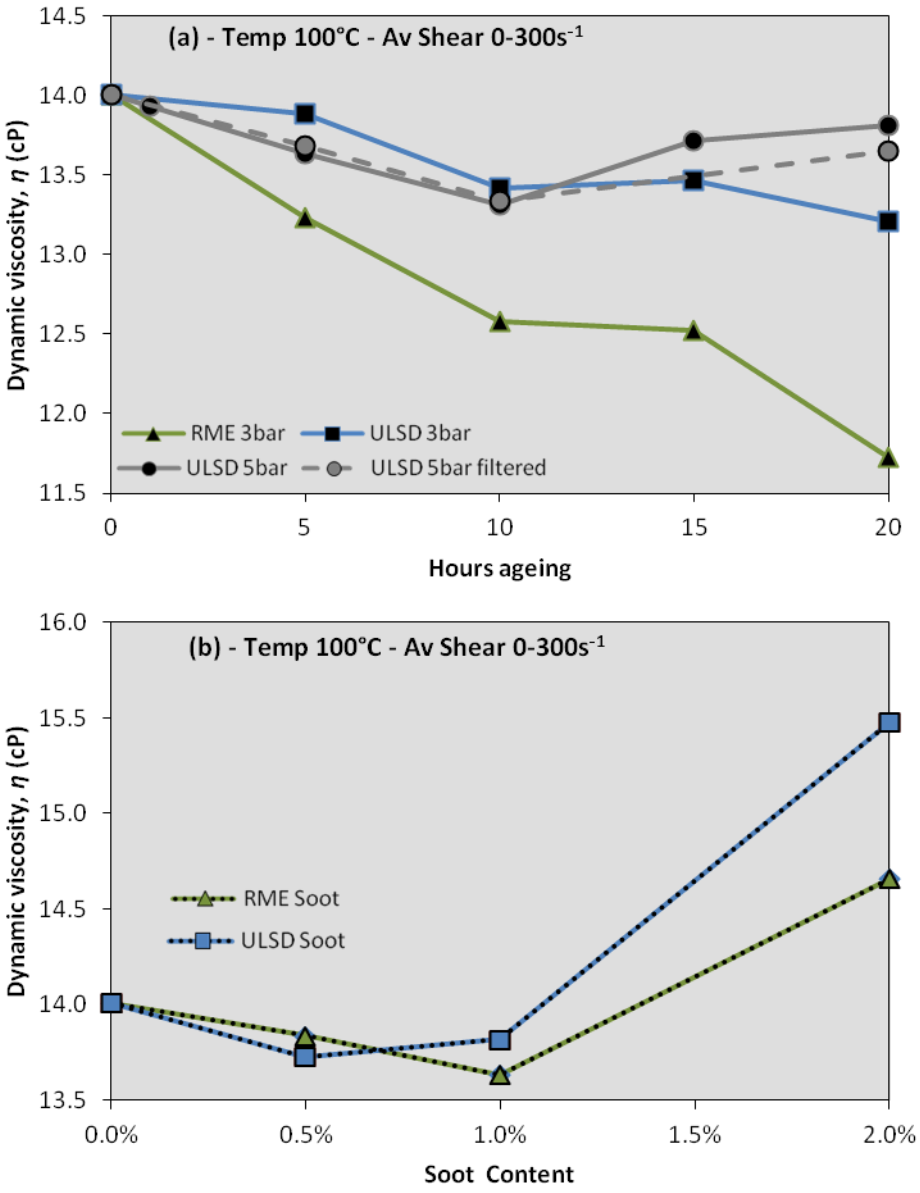

Figure 6.6 - Low shear rate Rheometry for sooted Exhaust aged (a) and Soot dosed (b) oils

Figure 6.6a shares an almost identical resemblance to the trends seen in Figure 6.5. Here four fluids were tested, the same three as before with the fourth (*grey dashed line*) being the ULSD exhaust aged oil at 5 bar filtered through a 0.8µm Millipore filter, as done previously for the USV. Within the first 10 hours, the filtered and non-filtered samples both exhibit identical viscosity trends; only between the 10-20 hours do the two fluids differ. This shows two things, firstly that the filtering does remove some of the soot, reducing the visco-thickening of the oil. Secondly the effects of sooting is not truly seen under heavy engine loads until after 10 hours, hence the decreasing viscosity trend, most likely from the continued fuel entrainment.

Figure 6.6b shows the impact of soot content from the two fuels on oil viscosity. The soot from ULSD is shown in blue and the soot from RME in green. Between 0-1% content, there is little to distinguish between the two fuel derived soots, with both lowering the viscosity of the oil. This may be due to the slight presence of soot disrupting the inter-boundary layers of the oil during the test, or the point that Selby (1998) makes about highly flocculated oils having less reliability whilst measuring viscosity. Although the rheometer is used at low shear rates, the coned rotor pressed against the oil has the ability to shear larger agglomerates, adding to reliability issues. As each test was repeated, and taken through a ramped shearing regime, it is thought that this effect is suitably minimised during testing, but is an issue that should be kept in mind.

The trend between 0-1% soot content for the ULSD soot dosed oil is very similar to the ULSD exhaust aged oil at 5 bar between 0-20 hours. Both fluids show a decrease in viscosity before

increasing, and have the same measured viscosity at 1% and 20 hours respectively. It would be unsurprising therefore if the total soot content of the exhaust aged oil was greater than 1% w/w after 20 hours, even with the highest soot load. This would also correspond well with the almost negligible sooting effects seen for the low load exhaust aged oils. Below 0.5% soot content, the increased soot level seems to lower viscosity, not increase it. Also, neither of the low load exhaust aged oils show any increase in viscosity, as their profiles relate more with fuel contamination.

A final observed trend from the soot content graphs of Figure 6.6 are the differences in viscosity at 2% w/w for the two fuel derived soots. At this soot concentration, the ULSD derived soot increases the oil viscosity by 1.5cP, whereas the RME derived soot only causes a 0.6cP increase. The assumption as to why the ULSD soot causes the greater increase is thought to be due to the increase in average particle size (Mueller et al. 2003; Rounce et al. 2012; Selby 1998; Kornbrekke et al. 1998). The ULSD has a higher proportion of larger sized soot particles, which occupy a greater phase volume causing the viscosity to increase. Up until now, the main reason for the differences in viscosity between the two fuels was due to the RME producing less soot and having an increased level of fuel contamination. Now, by dosing the oil with an equal mass of soot derived from the two fuels, it can be seen that RME soot may actually have less influence on the thickening of engine oils as ULSD soot. Again the point made by Selby (1998) should be adhered to, but so far this finding may have some truth but requires further examination.

6.2.6 - Lubricity

The HFRR tests were split into two groups; oil samples that were aged in the rig (section 6.2.6.1), and artificially soot dosed oil samples (section 6.2.6.2).

6.2.6.1 - Rig aged sooted oil

Table 6.6 - Summary of lubricity properties of sooted exhaust aged oils

Sooted Oil Lubricating Properties		Film thickness (%)				Coefficient of Friction, μ			
		60°C		120°C		60°C		120°C	
Fluid	Age	Ave	Min Max	Ave	Min Max	Ave	Min Max	Ave	Min Max
Oil	Fresh	81.4	2% 100%	27.4	2% 100%	0.129	0.124 0.135	0.145	0.126 0.151
RME exhaust 3 bar	5 Hours	49.8	6% 100%	79.0	19% 100%	0.126	0.121 0.138	0.136	0.120 0.150
	10 Hours	90.5	6% 100%	93.0	12% 100%	0.129	0.125 0.143	0.131	0.117 0.154
	15 Hours	87.6	6% 100%	80.7	9% 100%	0.128	0.125 0.141	0.132	0.122 0.147
	20 Hours	87.9	6% 100%	78.7	8% 100%	0.127	0.120 0.136	0.130	0.120 0.139
ULSD exhaust 3 bar	5 Hours	33.0	6% 100%	72.5	15% 100%	0.136	0.127 0.148	0.148	0.125 0.156
	10 Hours	30.4	10% 100%	70.9	38% 100%	0.136	0.123 0.145	0.142	0.124 0.154
	15 Hours	38.5	10% 100%	64.5	36% 100%	0.133	0.123 0.145	0.144	0.126 0.159
	20 Hours	37.0	8% 100%	69.0	18% 100%	0.139	0.117 0.153	0.139	0.125 0.155
ULSD exhaust 5 bar	5 Hours	40.9	6% 100%	64.0	15% 100%	0.129	0.122 0.142	0.146	0.125 0.155
	10 Hours	32.7	7% 100%	76.2	21% 100%	0.134	0.123 0.141	0.146	0.126 0.155
	15 Hours	28.0	8% 100%	53.3	23% 100%	0.135	0.121 0.145	0.144	0.128 0.160
	20 Hours	31.4	7% 100%	66.2	22% 100%	0.130	0.121 0.145	0.140	0.124 0.152

Table 6.6 is a summary of the lubricity which is also graphically shown in Figure 6.7. Within the six graphs, it can be seen that the two ULSD exhaust aged oils behave similarly whereas the RME aged oil behaves independently. Considering first, Figure 6.7a for the average film thickness at 60°C, the trends show the clearest difference between the two fuelled exhaust streams. Similarly to Figure 5.4 of chapter 5, the effects of exhaust ageing causes all three fluids to decrease rapidly before the RME exhaust diverges and increases. As stated in

chapter 5, this is due to the improved lubricity from the diluted RME, which is more prevalent now as dilution levels are higher as shown in Figure 6.3. The two ULSD aged oils further decrease the film thickness due to the entrained fuel content thinning the oil, disrupting the film formation. At 120°C (Figure 6.7b), all three fluids increase in film thickness with age, however the two ULSD exhaust fluids do not drop away as per the results of chapter 5. This may be the influence of the increased soot content, or the improved additive functionality at higher temperatures (Chiñas-Castillo & Spikes 2004; Aldajah et al. 2007).

Looking at Figure 6.7d for the COF at 120°C, the fluids have their most visible trend with all fluids reducing in COF with age and increasing fuel content, with the trend almost mirroring that of fuel content in Figure 6.3. This again is unlike the results of chapter 5 which increases with the age for the ULSD, with all of the results following their respective film thickness trends.

Finally, looking at Figure 6.7e for AWSD, the results at 120°C mirror the film thickness results at 60°C (Figure 6.7a). All three fluids increase the AWSD between 0-5 hours at an identical rate. The RME exhaust reaches a critical level between 5-10 hours, where the contamination levels no longer detract from the oil properties but instead enhances them. This is not observed for either of the ULSD exhaust aged oils which both show a continued increase in wear with age and fuel content. At 60°C the trends for the two fuels at 3 bar both show identical fluctuating points in wear. Whether this is to do with similar ageing conditions or repeatability error from the HFRR remains an unknown.

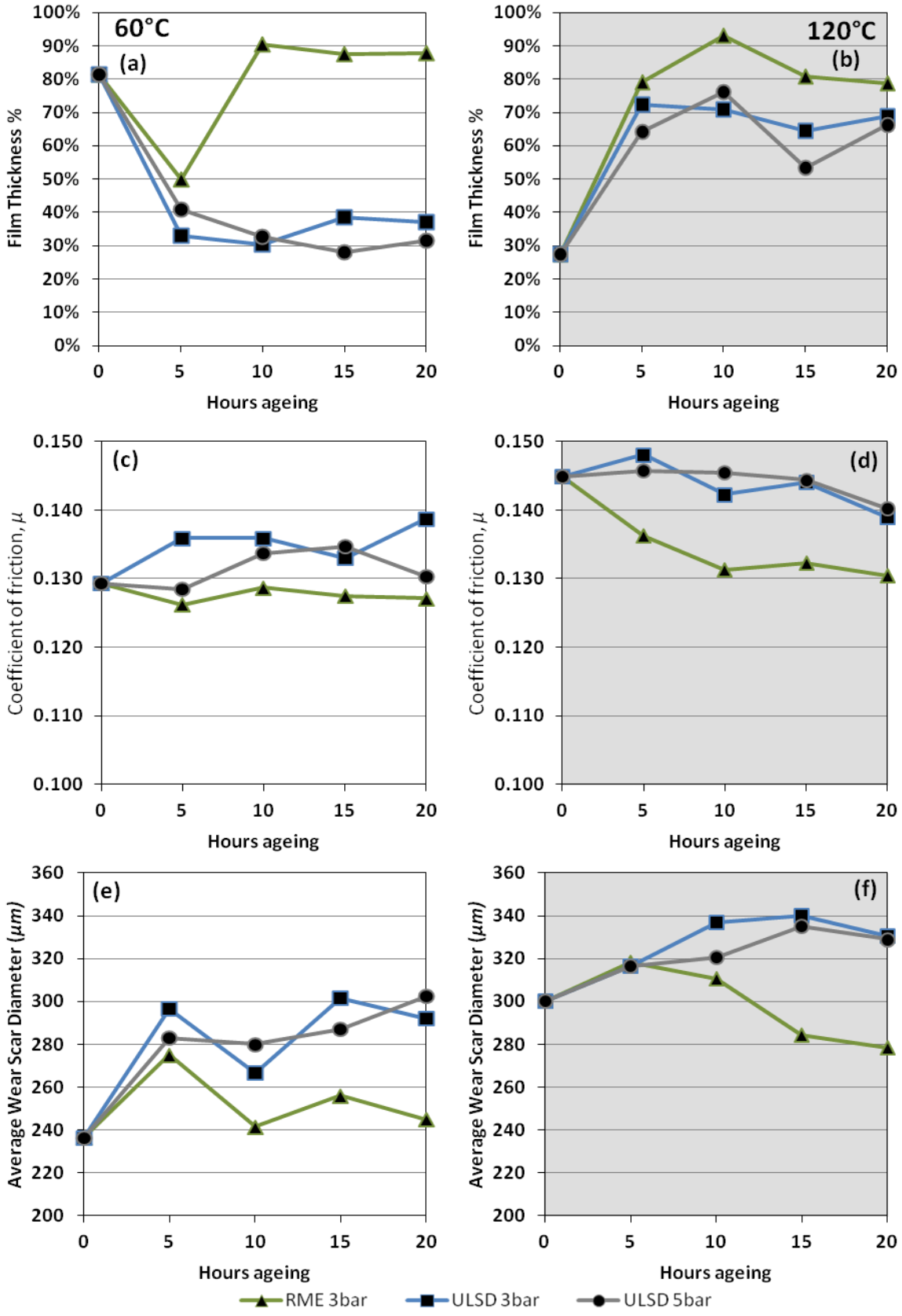

Figure 6.7 - Oil Lubricity properties with ageing; Film thickness (a & b); Coefficient of Friction (c & d); and average wear scar diameter (e & f) at 60°C (L) and 120°C (R)

Table 6.7 shows the upper specimen wear scars for the three aged test fluids when tested using the HFRR at 60°C.The first visible difference in wear scars is that of the RME exhaust aged oil which not only decreases with fluid age, but becomes less intense. This is due to the increased RME content that behaves as lubricity enhancer, reducing both the levels of friction and wear whilst increasing the film strength. The wear scars for the two ULSD exhaust aged oils are very similar throughout testing, exhibiting similar shapes and sizes, however they do differ slightly. The measured AWSD is only an average measurement of the upper test specimen between the x-axis (perpendicular to the specimen's motion path), and the y-axis (parallel to the motion path). Some fluids will have a wider wear scar at the expense of being shorter and still have the same AWSD.

At 20 hours it can be seen that the AWSD for the ULSD exhaust aged oil at 5 bar is larger than at 3 bar, but by looking at the x and y scar dimensions, this may not always be the case. At 3 bar, the wear scar in the x-axis is greater, and at 5 bar the wear is greater along the y-axis. The differences are due to the influence of the two contaminants at work, one being the increased dilution of the oil with fuel, producing a weaker oil film thus generating a wider wear scar (x-axis). The second is the direct influence of the soot which causes a more abrasive looking wear scar along the specimen's path length (y-axis). At this stage, the difference may seem minimal as both ULSD exhaust aged oils have similar looking wear scars at each time frame, but this may be more evident with heavier sooted oils.

Table 6.7 - HFRR wear scar dimensions at 60°C of sooted exhaust aged oil

Age	RME 3 bar			ULSD 3 bar			ULSD 5 bar		
0 hours				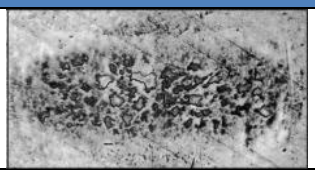					
	x-axis			y-axis			AWSD		
	308			165			236.5		
5 hours	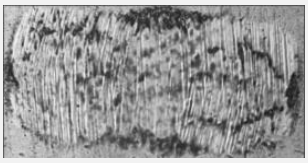			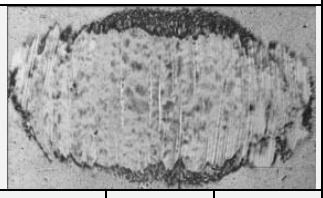			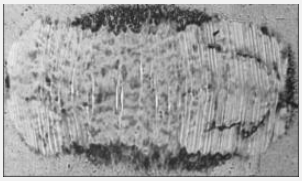		
	x-axis	y-axis	AWSD	x-axis	y-axis	AWSD	x-axis	y-axis	AWSD
	363	187	275	373	220	296.5	356	210	283
10 hours				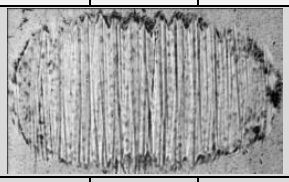			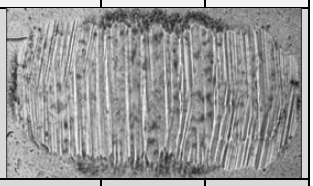		
	x-axis	y-axis	AWSD	x-axis	y-axis	AWSD	x-axis	y-axis	AWSD
	323	160	241.5	334	199	266.5	356	204	280
15 hours	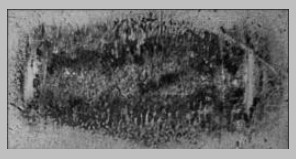			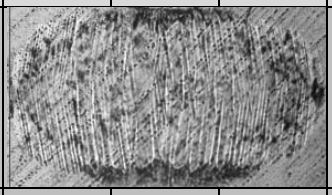			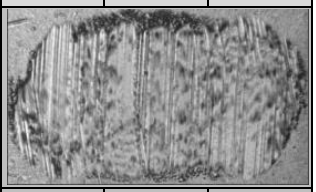		
	x-axis	y-axis	AWSD	x-axis	y-axis	AWSD	x-axis	y-axis	AWSD
	341	171	256	383	220	301.5	362	212	287
20 hours	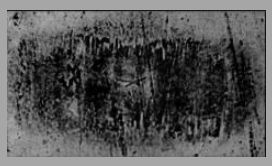			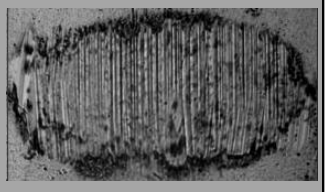			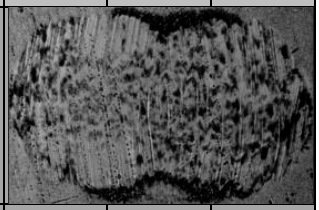		
	x-axis	y-axis	AWSD	x-axis	y-axis	AWSD	x-axis	y-axis	AWSD
	315	175	245	374	210	292	367	238	302.5

6.2.6.2 - Artificially soot dosed oil

To further investigate the influence of soot on the oil's performance, the HFRR tests were repeated with oil that had been artificially dosed with soot. An additional sample group

was also pre-dosed with ULSD soot and unblended oil aged for 100 hours from chapter 4. This amounted to nine samples in total plus the two non-dosed samples (fresh and aged oil) with the results shown in Table 6.8 which is a repeated format of Table 6.6 from earlier.

Table 6.8 - Summary of lubricity properties of soot dosed oils

Soot dosed Oil Lubricating Properties		Film thickness (%)				Coefficient of Friction, μ			
		60°C		120°C		60°C		120°C	
Fluid	Soot content	Ave	Min Max	Ave	Min Max	Ave	Min Max	Ave	Min Max
Fresh Oil	0%	81.4	2% 100%	27.4	2% 100%	0.129	0.124 0.135	0.145	0.126 0.151
Fresh Oil + RME Soot	0.5%	81.9	6% 100%	62.6	10% 100%	0.138	0.104 0.145	0.144	0.126 0.150
	1%	39.6	6% 100%	50.2	8% 100%	0.140	0.116 0.150	0.142	0.125 0.151
	2%	11.8	6% 100%	20.5	9% 100%	0.139	0.107 0.151	0.137	0.120 0.142
Fresh Oil + ULSD Soot	0.5%	81.5	6% 100%	64.8	9% 100%	0.136	0.121 0.140	0.144	0.126 0.151
	1%	43.4	6% 100%	59.5	9% 100%	0.145	0.110 0.154	0.147	0.126 0.157
	2%	13.3	6% 100%	26.8	8% 100%	0.135	0.110 0.145	0.137	0.124 0.142
Aged Oil + ULSD Soot	0%	59.2	1% 100%	25.2	2% 100%	0.130	0.123 0.140	0.142	0.123 0.149
	0.5%	13.9	6% 100%	24.0	8% 100%	0.137	0.110 0.143	0.122	0.114 0.137
	1%	8.8	6% 100%	7.4	6% 100%	0.142	0.098 0.151	0.143	0.110 0.151
	2%	7.0	6% 100%	8.5	7% 100%	0.144	0.110 0.151	0.132	0.106 0.140

Noticeable within the six graphs in Figure 6.8, is that the two fuel derived soots in fresh oil follow very similar trends across all HFRR parameters, with the aged oil performing independently. Considering the average film thickness (Figure 6.8a & b), the trends are very clear for both temperatures as all three fluids decrease in film thickness with increasing soot content. However the aged oil drops immediately to a thickness slightly greater than 10%, dropping slightly further with a doubling in soot concentration.

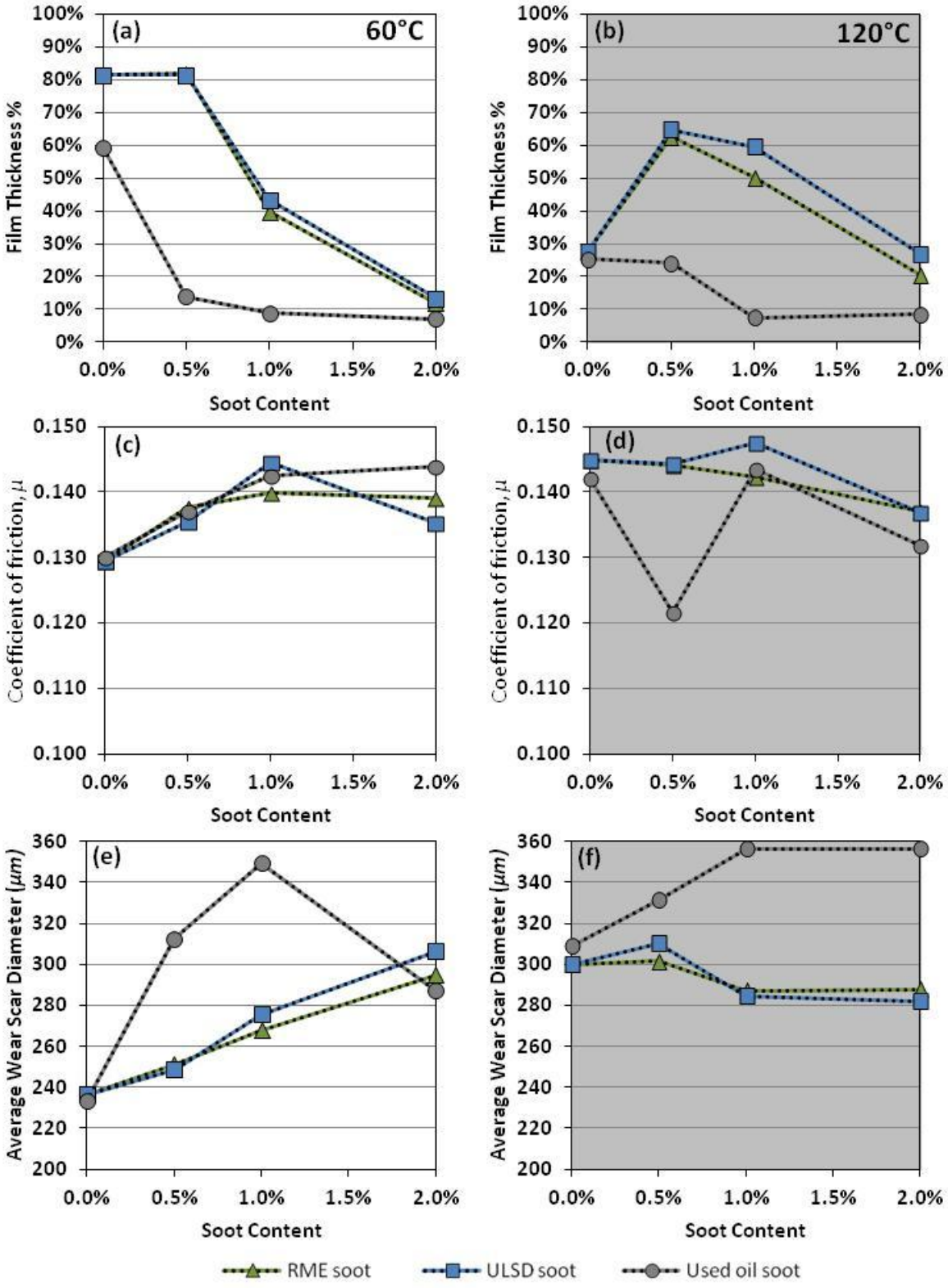

Figure 6.8 - Oil Lubricity properties with soot; Film thickness (a & b), Coefficient of Friction (c & d) and average wear scar diameter (e & f) at 60°C (L) and 120°C (R)

At 60°C (Figure 6.8a), the two fresh oil samples have negligible change between 0-0.5% soot content, before steadily falling away. However at 120°C (Figure 6.8b), the film thickness increases before decreasing which is unusual as the film thickness would be expected to be lower at higher fluid temperatures due to the reduced viscosity. This may be explained by the measurement of film thickness through Electrical Contact Resistance (ECR) between the specimen pairs.

The oil forms an EHD film between specimens due to their relative movement. Under heating, the oil film becomes less viscous and thins, allowing the soot to penetrate the EHD film more easily. With a thinner film, the ratio of primary particle size to EHD film thickness increases, which not only affects the overall fluid viscosity, but can also increase film formation (Chiñas-Castillo & Spikes 2004). It would therefore be possible to form thicker films at higher temperatures with the same soot content, but only up to certain concentration levels. This is seen at both 1% and 2% soot concentrations, which exhibit slightly greater film thicknesses when measured at 120°C than at 60°C. ULSD soot is also seen to have a higher film thickness throughout, which may be due to having larger average primary particles as shown in Figure 6.1, further increasing the particle size to film thickness ratio.

However the interaction of the soot colloids with the oil film will both contribute to its thickening and destruction. Soot can interfere with the laminar film layers, interact with the additives, saturate dispersants and reduce the available surface for the oil to adsorb to (Devlin et al. 2008; Sato et al. 1999). This gain in film thickness at 120°C is not seen in the

soot dosed aged oil, however it does maintain the same low film thickness between 0-0.5%, before further dropping with soot concentrations greater than 1%. This would indicate that the effects of sooting on the film thickness may have more to do with additive or dispersant functionality which depletes with age.

Looking at the COF in Figure 6.8c at 60°C, all fluids increase in friction with increasing soot concentration. This correlates well with the film thickness, as one decreases, the other should increase. However at 120°C (Figure 6.8d), the COF decreases with increasing soot content, similar to the film thickness. This is again due in part to the thinner oil film increasing the likelihood of soot particles penetrating the EHD contact between specimens, sharing load between the soot and the oil. The soot being graphitic in nature and under high loads could deform or be pressed into the surface asperities, and behave as a solid lubricant (Aldajah et al. 2007).

Finally, looking at Figure 6.8e for AWSD at 60°C, the results show that the two fresh oils increase almost proportionally in wear with increasing soot content. This is only at the lower temperature which seems to increase the wear scar along the y-axis with increasing soot content, but is not affected at 120°C. This is also noticeable in Table 6.9 which is a summary of the HFRR upper specimen wear scars for all of the soot dosed oil samples. Here the two fresh oil samples show similar wear patterns which increase in abrasive nature as the soot content increases. The levels of wear at 120°C (Figure 6.8f), are seen to follow the previous trends of film thickness and COF, decreasing in size with increasing soot content and show little to no signs of abrasive wear from the soot.

Table 6.9 - HFRR wear scars for soot dosed oil

w/w	RME Soot			ULSD Soot			Used oil		
0%	x-axis	y-axis	AWSD	x-axis	y-axis	AWSD	x-axis	y-axis	AWSD
	308	165	236.5	304	162	233	400	218	309
0.5%	x-axis	y-axis	AWSD	x-axis	y-axis	AWSD	x-axis	y-axis	AWSD
	350	152	251	340	157	248.5	291	334	312.5
1%	x-axis	y-axis	AWSD	x-axis	y-axis	AWSD	x-axis	y-axis	AWSD
	286	250	268	318	233	275.5	271	428	349.5
2%	x-axis	y-axis	AWSD	x-axis	y-axis	AWSD	x-axis	y-axis	AWSD
	299	291	295	306	307	306.5	281	293	287

w/w	RME Soot			ULSD Soot			Used oil		
0%	x-axis	y-axis	AWSD	x-axis	y-axis	AWSD	x-axis	y-axis	AWSD
	401	401	401	401	401	401	400	218	309
0.5%	x-axis	y-axis	AWSD	x-axis	y-axis	AWSD	x-axis	y-axis	AWSD
	408	212	310	401	202	301.5	434	229	331.5
1%	x-axis	y-axis	AWSD	x-axis	y-axis	AWSD	x-axis	y-axis	AWSD
	372	197	284.5	358	216	287	383	330	356.5
2%	x-axis	y-axis	AWSD	x-axis	y-axis	AWSD	x-axis	y-axis	AWSD
	358	206	282	370	205	287.5	395	318	356.5

Also noticeable between Figure 6.8 and Table 6.9 is the effects of increasing soot content on aged engine oil which increases wear. Visually the wear scars are more prevalent becoming larger with deeper and sharper gauges scored into the specimen surface. This is thought to be due to the antiwear additive depleting as the oil ages, allowing the soot to have more influence over the lubricity properties, and thus increasing the levels of abrasive wear. This would overall suggest that the influence of soot on the oil is more influenced by the age and state of the base fluid than by the overall soot content as seen by the consistent worsening of the oil lubricity and the very different nature of the wear scars that are formed.

6.2.7 - Microscopy

Soot particles were sampled from the exhaust stream and collected onto copper mesh gilding grids to be examined using a TEM. The TEM was used to answer several queries surrounding the sampling method, firstly if the grids were actually collecting soot, which Figure 6.9 attests to. Secondly, the TEM was used to tune the sampling time to prevent clogging of the grids with agglomerated structures, seen in the lower pictures of Figure 6.9. The copper grids coated with a Formvar film acts as a photo still of the exhaust stream, requiring a caption time of only 1 second to achieve an adequate level of sampling.

The TEM was also used to establish whether soot can only be collected thermophoretically, or whether a diluent such as ethanol can be used simply to wash the soot onto the grid. This was shown also to be possible but some level of clarity is lost as the soot colloids naturally flocculate within the diluent, forming larger and less naturally agglomerated structures. Lastly the TEM was used to establish if there were any noticeable differences between the

two fuelled soot morphologies and structures. Unfortunately this went beyond the capability of the current TEM for the primary particles; however the secondary particles showed little difference in soot size and distribution, but require further statistical analysis to definitively answer this question. Once confirmed that soot was being collected on the gilding grids, the samples were then analysed using the AFM as shown in Figure 6.10.

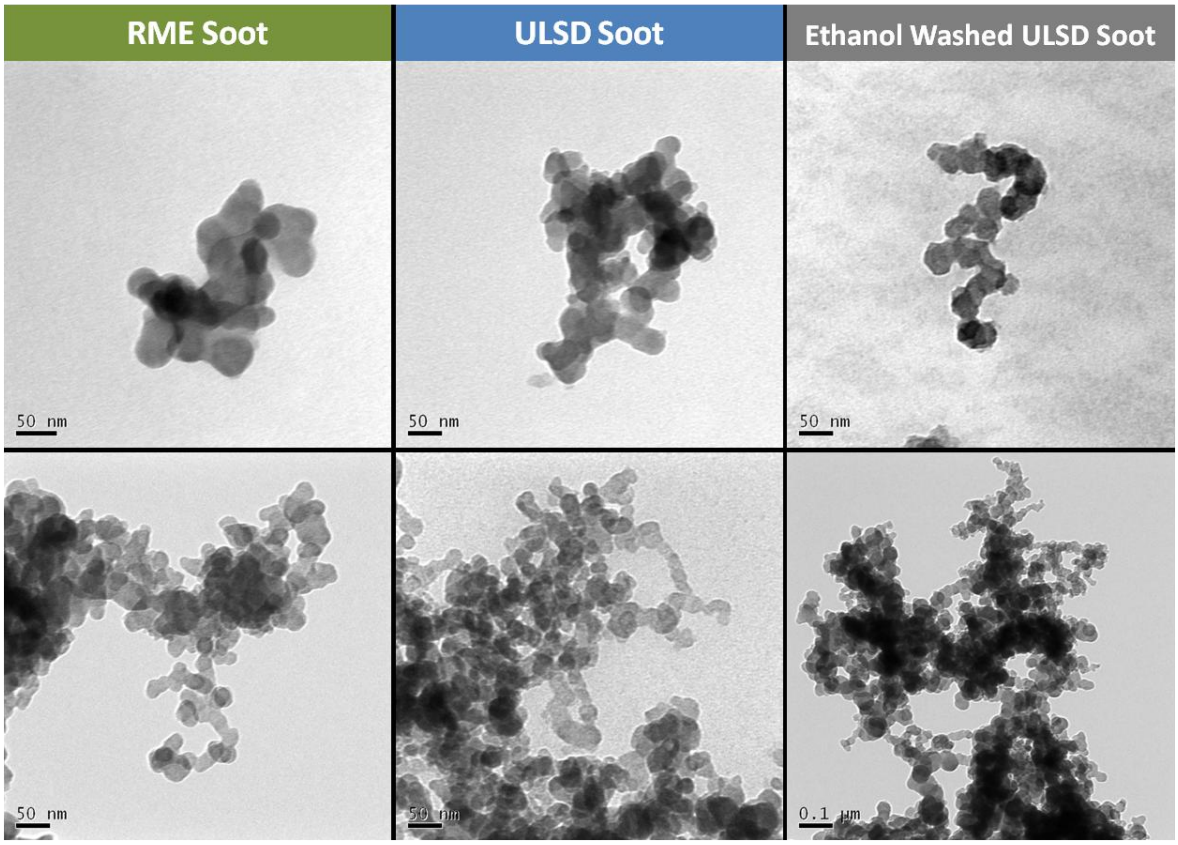

Figure 6.9 - TEM imaged soot agglomerates

Using the AFM in 'contact mode', a 3D map was produced of the grid surface to locate sufficiently sized soot particles as shown on the left of Figure 6.10. Once located, the particle was probed at nine equidistant sites using the AFM's stylus tip as a nano-indenter. The graph on the right of Figure 6.10 shows the Young's modulus for six soot particles at their relative

sites. The three blue charts depict the three probed soot particles formed from the combustion of ULSD. Here the young's modulus is typically high with two of the three particles averaging 2.0GPa, and one averaging 1.2GPa. The three green charts represent the three probed soot particles formed from the combustion of RME. Here the young's modulus is more consistent for all three particles averaging between 0.8-1.0GPa.

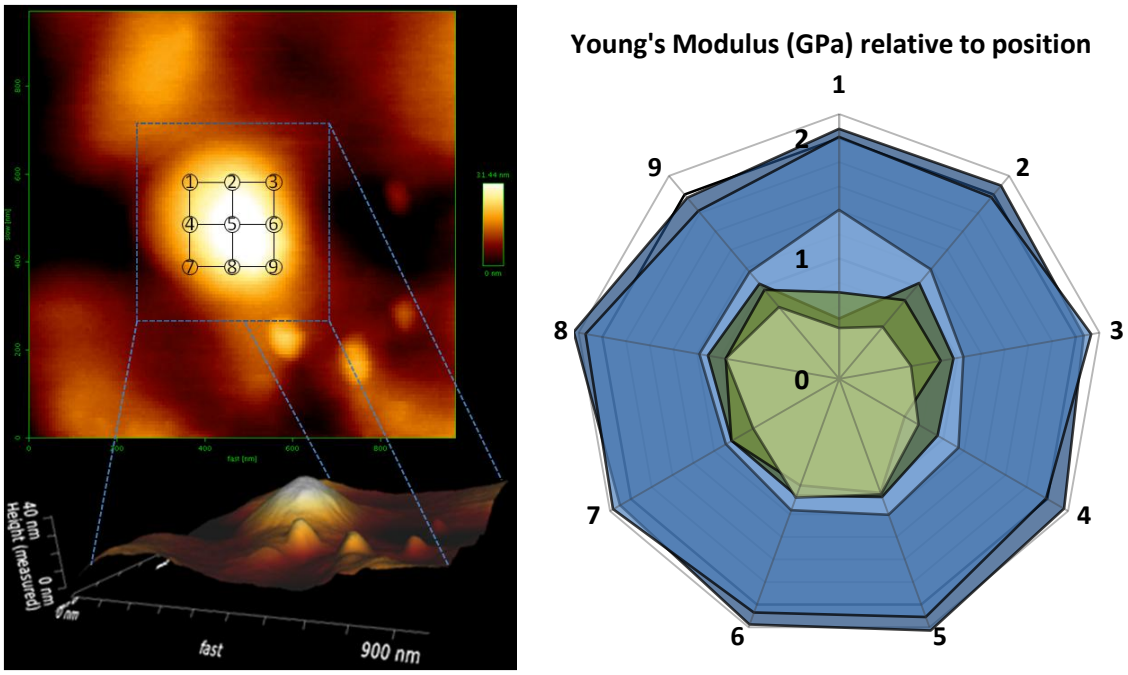

Figure 6.10 - AFM soot stiffness measurements (R) relative to location (L)

From the above data, it would appear that soot from RME is less stiff than soot from ULSD. However, with only a very small sampling group, the level of certainty of these measurements is very low. Fluctuations in the measured stiffness may be as a result of the orientation of the particles when probed due to the polygranular anisotropic soot structure. It is also uncertain how this data relates to other soot properties as the stiffness is a nanoscale measurement, and is comparable to the young's modulus of bulk materials such

as Nylon or Polyethylene. These are only early attempts to look at the individual soot's properties separate to the oil, but require further study to prove whether there are physical differences between the two fuelled soots.

6.3 - Conclusions

The aim of this chapter was to measure the influence of exhaust gases and PM from two diesel fuels on the measureable properties of engine oil. This was achieved by entraining soot within the oil by using an ageing rig, and also by artificially dosing the oil with known soot concentrations.

RME was seen to produce less PM overall than ULSD, with a higher proportion of nano-sized particles. At high engine loads, the ULSD produces more PM mass but with a lower PM number due to there being a higher proportion of large diameter particles. This is visually observed with all engine oils losing their clarity and becoming a thick black colour at different ageing times, however this does not necessarily indicate a drop in property.

This chapter differs from the previous one in that there was no DPF fitted in the exhaust stream, allowing all of the PM to enter the ageing rig. This also caused an undesired affect of changing the fuel content collected by oil from the results seen in chapter 5 with the DPF present. In a similar fashion to chapter 4 and chapter 5, the fuel content was seen to dilute all properties such as density, acidity, viscosity and lubricity.

The influence of soot was barely observed at low engine loads due to the increased fuel dilution and the low soot entrainment by the rig oil. The effects of sooting were only just present from the ULSD at high engine loads, but required a second viscometer to confirm the visco-thickening effect. The dosing of the oil with soot showed that beyond a critical limit, the oil does begin to thicken with the effects being slightly greater for ULSD soot than RME. This was thought to be due to the larger soot particles attributed to the combustion of ULSD, which when entrained in the oil occupy a larger phase volume.

Lubricity trends were mixed due to fuel contamination, but the influence of soot was observed to increase wear. This was more noticeable with the dosed samples, specifically at lower test temperatures when the increasing soot content exhibited a more abrasive wear scar. At higher test temperatures, the increasing soot content showed improved lubricity, thought to be due to a combination of the soot behaving as a solid lubricant, and improved additive functionality at higher temperatures. Oil age was also shown to be more significant than fuel choice as the lubricity drastically worsened with increasing soot content in comparison to the fresh oil. Both fuel soots showed little difference in lubricity; however results from the AFM may suggest that ULSD produced soot that is potentially stiffer than soot from RME.

CHAPTER 7 - CONCLUSIONS

7.1 - Concluding remarks

This chapter is a summary of the findings and conclusions for each of the analytical chapters, drawing them all together to answer the initial questions posed by this thesis. The aim of each chapter was to analyse a different factor of engine oil ageing that is influenced by fuel and its combustion. To summarise the outcomes, each factor has been plotted depicting a 'performance' rating with age. The 'performance' is formed from a culmination of the tested properties from each chapter, and although cannot be quantitatively assessed against actual in-engine performance, they highlight the changes and trends observed within this research. This enables each ageing factor to be individually assessed on what its overall influence on engine oil ageing is, with each factor benchmarked against unblended oil, aged under thermal degradation within chapter 4.

7.1.1 - Fuel Dilution

The purpose of this chapter was to investigate the ageing of engine oils whilst operated under similar conditions to IC engines, without the influence of engine emissions or PM. The question intended to be answered here was:

- **How influential is fuel dilution upon the thermo-oxidative degradation of oil, and how does this differ between fuels?**

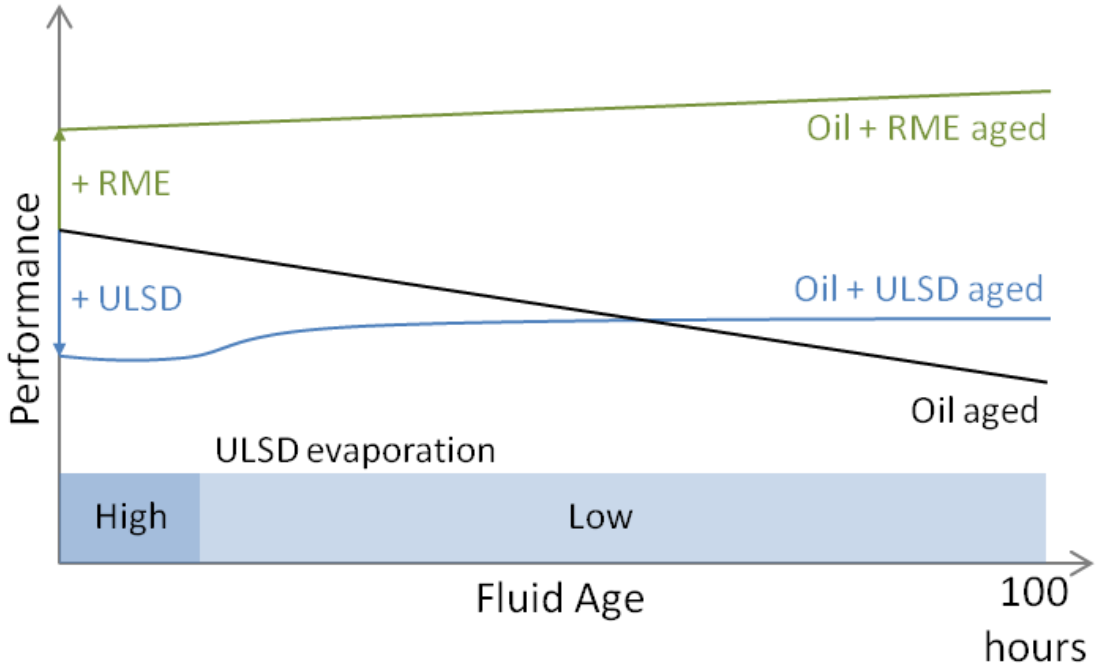

Figure 7.1 - Performance rating of thermally degraded oil and fuel blends

Figure 7.1 depicts the loss in performance of unblended oil (*black*) as it is thermally degraded in the presence of air. What occurs is a natural loss to both the base oil content as well as the additives which has an effect of increasing the oil's viscosity, density and diminishes its lubricity, all of which are undesirable and reduces performance. On the whole, this loss in performance is nearly constant, with the oil eventually falling out of specification after a predetermined time, when it will require replacing.

Figure 7.1 also depicts the loss in performance of the oil when pre-blended with 11% w/w ULSD (*blue*), which affects performance both in the long and short term. Initially, the ULSD behaves by 'diluting' all of the oil's properties, by transforming the overall blend's performance away from the oil and towards that of the fuel, resulting in a reduction in viscosity, density and acidity. However as the ULSD is quickly lost through evaporation,

heavier fuel constituents remain in the oil causing the performance to dramatically change, almost by deteriorating further before improving again. Over time these effects settle as the oil finds a natural balance of fuel content, with the density and viscosity returning to more normalised levels. At comparable aged states, the lubricity is improved over unblended oil and the viscosity is much lower. The volatile fuel fraction which was more detrimental to performance continues to evaporate, leaving behind heavier fuel fractions and additives. Both of which have benefits to overall oil performance, indicating that the effects of ULSD dilution are not as detrimental as previously thought.

Similar results are seen in Figure 7.1, when the oil is diluted by 13% w/w RME (*green*), which also shows a 'diluting' of measured properties away from the oil towards that of the fuel. Overall the gains in performance far outweigh its drawbacks, which include a lower viscosity but greatly improved lubricity. The benefits of RME dilution have also been seen to be greater at higher temperatures and are further improved with age. The negative effects include increased interaction with oil additives, and the low volatility causing dilution levels to become dangerously high over time. This could eventually lead to the oil losing functionality as the proportion of RME within the sump dominates over the oil. This is a potential risk for future engines developed with extended drainage intervals.

Overall the effects of fuel dilution has not been as detrimental as was once feared, as ULSD dilution is almost self-governed due to its high evaporation rate, and the biodiesel diluent behaves as a natural lubricity aid. If the risks of heavy dilution from biodiesel were not so high, and the fuel more volatile to behave like ULSD's self-governed dilution levels, B100

fuelling could become a more attractive option. Likewise, utilising the self-governed dilution levels of ULSD could be a way to maintain the performance of engine oils, as a means of replenishing naturally depleted additives within the sump oil, reducing the number of drainage intervals required.

7.1.2 - Exhaust Blowby

The purpose of this chapter examines the effects of diesel fuel combustion and its by-products on the ageing of sump oil by establishing the influence of exhaust-borne contaminants from the combustion of ULSD and RME. This included by-products such as water, unburnt hydrocarbons and nitrous oxides, but excluded the influence of PM and soot. The question intended to be answered here was:

- What effects do combustion blowby gases have on oil functionality and age, and how does this differ between fuels?

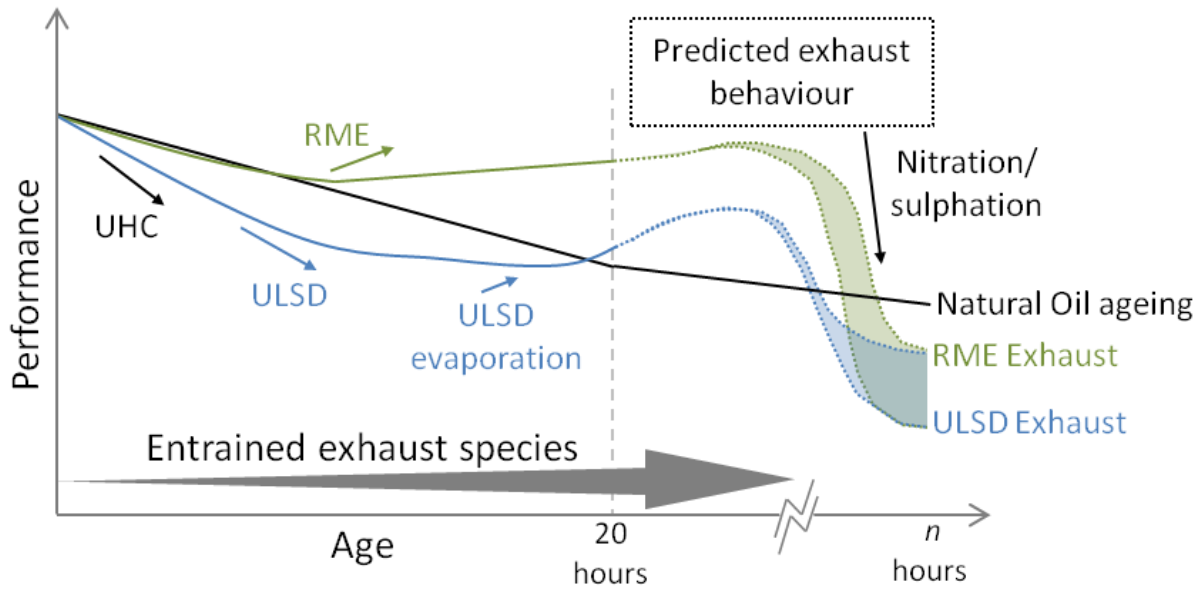

Figure 7.2 - Performance rating of exhaust aged oil from the combustion of ULSD and RME

Slight differences in exhaust composition were measured between fuels with total HC and CO content being lower for RME at the expense of increased NOx emissions. However chemical analysis using the GC-MS showed the predominant entrained exhaust-borne contaminant within the oil was Unburnt Hydrocarbons (UHC) and fuel entrainment for both ULSD and RME.

The main effect from the UHCs was a 'diluting' of properties and an overall reduction in performance shown in Figure 7.2 as an initial drop for the ULSD exhaust (*blue*) and RME exhaust (*green*). In the case of the ULSD exhaust, the additional entrainment of fuel further reduced performance; however this became less influential with age as the fuel evaporated. The RME exhaust as with the previous chapter again showed an improved performance with increasing contamination levels, particularly from unburnt fuel, but will eventually saturate the oil detracting from performance after a prolonged period of time.

With a shorter timeframe than the previous experiment, the effects of contamination of UHCs and fuel dilution were heightened and more evident earlier on, masking the effects from other exhaust contaminants. However, these effects curtailed with time indicating that other factors such as oxidation and nitration could be contributing to the performance change as the oil aged, but have a slower response. It is thought that with a longer experimental time, some of these secondary influences from the exhaust may become more influential. As such, the fuel saturates most of the measured oil properties, even in small quantities, making the detection of other exhaust contaminants challenging.

7.1.3 - Particulate Matter

The purpose of this chapter was to further investigate the effects of exhaust emissions on sump oil, specifically focussing on PM and soot. This chapter looks at the soot formed from different diesel fuels such as ULSD and RME and its interaction with engine oil. The question intended to be answered here was:

- What are the true effects of Particulate Matter entrainment on oil performance, and how does this differ between fuels?

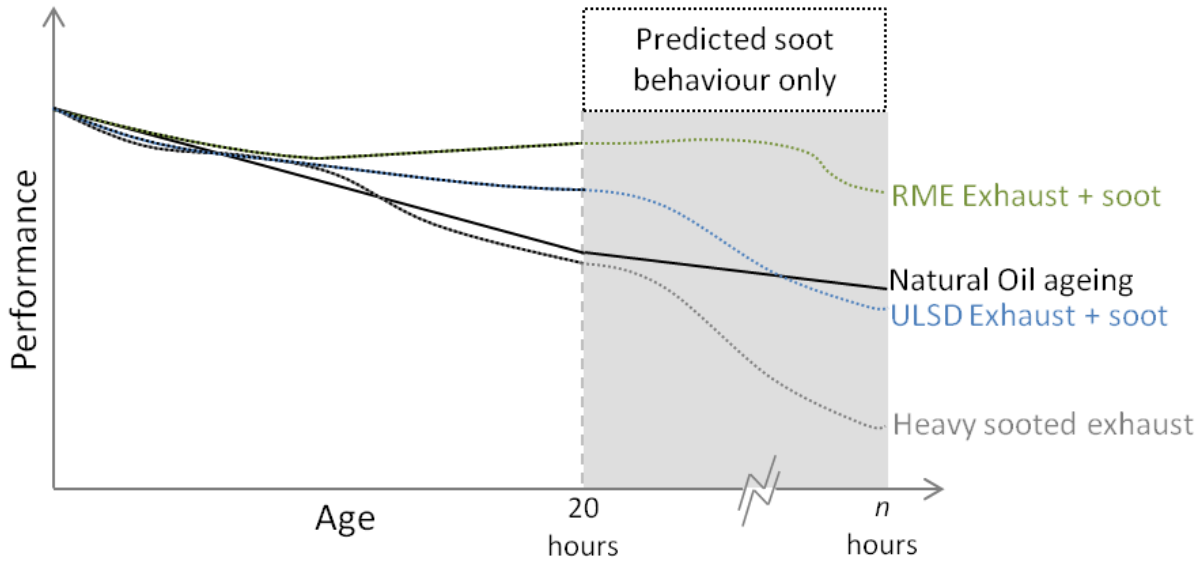

Figure 7.3 - Performance rating of aged oil from sooted exhaust

RME was seen to produce less PM overall than ULSD, with a higher proportion of nano-sized particles (< 50nm). At high engine loads, ULSD produces more PM mass than at low engine loads, but with a lower particle number due to a higher proportion of large sized particles. Figure 7.3 illustrates that the influence of soot on oil performance was barely observed at low engine loads (*both blue and green dashed lines*) due to the increased levels of fuel and UHC dilution and the low soot entrainment efficiency of the ageing rig. The effects of sooting

were only just observed from the ULSD operated at high engine loads (*black and grey dash*) requiring a second viscometer to confirm the visco-thickening effect experienced by the oil.

When artificially dosed with increasing soot masses up to 2% w/w, beyond a critical limit the oil rapidly thickened with the viscosity being slightly greater for ULSD soot than RME. This was thought to be due to the larger soot particles attributed to the combustion of ULSD, which when entrained in the oil, occupy a larger phase volume than dispersed particles, causing the viscosity to increase

Lubricity trends were mixed due to fuel contamination, but the influence of soot was observed to increase wear. This was more noticeable with the dosed oil samples, specifically at lower test temperatures when the increased soot content exhibited more abrasive wear scars. However, at higher test temperatures, the soot content showed an improved lubricity, thought to be due to a combination of the soot behaving as a solid lubricant, and improved additive functionality with temperature.

Pre-dosed soot samples from both fuels exhibited little difference in lubricity, with oil condition and age shown to be more significant as lubricity drastically worsened with pre-aged oil. However, results from the Atomic Force Microscope suggest that ULSD produces stiffer soot particles than RME, which could influence the overall impact on the oil.

7.2 - Thesis outcomes

Fuel dilution has been shown to have the greatest influence on oil performance, both in terms of impact and time. Impact because fuel dilution causes the largest change in any single measured property, and time because the effects could be seen throughout the duration of each experiment. Effects are seen with an instant 'diluting' of properties away from the fresh unblended oil, towards that of the fuel resulting in an amalgamation in performance of the oil with the entrained fuel. This has been observed to be both a positive and a negative effect, depending on which property is being measured.

The influence of ULSD as a diluent can be seen from as low as 1% w/w, but in quantities of more than 5% can be detrimental to oil performance. ULSD significantly reduces fluid viscosity leading to a thinner and less stable oil film which in turn increases wear. But due to the volatile nature of ULSD, the lighter mass fractions quickly evaporate, leaving additives and heavier fuel constituents that increase the viscosity, returning lubricity performance back to that of the unblended oil, and in some circumstances with a measured improvement.

The effects of biodiesel dilution of oil likewise can be seen in quantities as low as 1% w/w. However, at both low and high dilution concentrations (> 10%), the effects are positive with a reduced viscosity that decreases viscous drag within oil lubricated components, and improves lubricating effects. This includes producing a thicker and more stable oil film, reduced coefficient of friction, and lower wear, irrelevant of fluid age and exerting a greater influence at higher temperatures.

From the exhaust emissions, there is little influence from the majority of combustion pollutants, except for the entrainment of UHC's, which is very high for both fuels. The influence of unburnt fuel on the oil is again significant; with drastic differences in volatility as the RME accumulates at a faster rate. However, the entrainment of other significant combustion by-products such as water, nitrates and sulphates is either negligible, or a lot less than fuel entrainment, or a lot slower for it to not be measured or detected within the experimental timeframe.

The influence of particulate matter and soot on engine oil performance seems to be in balance with the respective fuel content. I.e. RME contamination has a positive influence which far outweighs its negligible soot production, whereas ULSD detracts from oil performance, whilst also producing more soot. Therefore the natural influence of RME-borne soot will be less than ULSD soot during an equivalent operating window.

However, for an equivalent soot mass, there may not be much difference between the two fuels. Beyond a critical level, there is an exponential increase in viscosity and a loss in lubricity. However, there may be some differences between the two fuelled soots in their physical properties, with ULSD soot seen to be stiffer than RME soot, and thus their overall influence on oil lubricity may be different; however this requires further investigating.

7.3 - Further work

The research conducted within chapter 4 studied the influence of thermal degradation, but was limited to an average sump temperature of only 90-100°C. This work could be extended to higher temperatures such as 120°C using the rig, and possibly even 150°C with additional insulation, to further study the influence of temperature on oil degradation rates.

The method to measure Total Acid Number (TAN) showed many weaknesses in its approach, leading to greater levels of error than expected. This could be improved by using a Potentiometric method, and complement this with Total Base Number (TBN) measurements. By improving these methods, the study of the interplay between fuels, additives and acid levels, especially at various operating temperatures could be conducted. By using known and referenced additives relevant to the additive package in the oil, this study could be enhanced with further use of Mass Spectrometry and Infra-red Spectroscopy.

A relationship that was stated earlier within the literature and reinforced within this research was the huge benefits gained in lubricity from the use of biodiesels. However it also showed a very peculiar relationship in that its influence increased with both age and temperature. With more time, an independent study into the causes and limits of these effects could be conducted to determine whether this occurs over a specific temperature interval, or after specific ageing of either fluid. This would also be useful in the study of future bio-sourced additives and lubricants.

Within chapter 5, the expected effects of from exhaust pollutants were not visible enough or perhaps sufficiently explored, specifically from nitrates and sulphates. To further this research, the current exhaust studies could be extended beyond 20 hours to determine whether there is truly any significant influence from these exhaust species. Alternatively, this could be achieved by synthetically exposing the oil or selectively filtering exhaust elements to test the individual effects of CO, CO_2, SO_X and NO_X, as done similarly by Uy et al. (2010) using the Ford Oil Aging Test (FOAT). Any changes would then be observed and measured using Infra-red Spectroscopy, and/or Flame Ionisation Detection (FID).

It was felt that the initial work conducted on the characterisation of individual soot particles chapter 6 was too brief, and that further studies are required to truly analyse soot morphology and measure its micro-hardness. This work could then be expanded further to look at these properties when soot is formed under different engine conditions and from different fuels. This would require a deeper study using the Atomic Force Microscope (AFM), Transmission and Scanning Electron Microscopy (TEM) and (SEM), and Energy Dispersive Spectroscopy (EDS).

Within the findings of Aldajah et al. (2007) it was stated that soot goes from being an abrasive, to a solid lubricant. This relationship was not fully seen within this research, but would interesting to examine further to see whether this happens after a temperature threshold, or when a specific soot mass content is reached, or if it only occurs with specific engine oils. This could be investigated with the aid of Thermo gravimetric Analysis (TGA), Extreme Pressure (EP) Tribology equipment, and SEM.

Within this research, the effects of only two diesel fuels, a high grade commercial diesel (ULSD), and a current biodiesel (RME) were studied. This work should be extended to other fuels such as the next generation of biodiesels, synthetic Fischer-Tropsch fuels, and perhaps even low quality fuels commonly used in developing markets.

Other tests which were originally proposed but were incomplete and would further enhance the current work include:

- More in-depth HC speciation using the GC-MS or GC-FID.
- Thermo gravimetric Analysis (TGA) to measure volatile content, Noack volatility, soot content and ash.
- Infrared Spectroscopy (FTIR) to measure changes in chemical functional groups for the base oil, additives, and the measuring of entrained exhaust species.
- Potentiometric acidity measurement and alkalinity tests (TAN and TBN).
- Pentane insolubles for oxidative stability tests.
- Further morphology testing of soot and ash using Electron Microscopy (SEM and TEM) and Energy Dispersive Spectroscopy (EDS).

REFERENCES

ACEA, 2010. *EUROPEAN OIL SEQUENCES - Service Fill Oils For Gasoline Engines, Light Duty Diesel Engines, Engines With After Treatment Devices and Heavy Duty Diesel Engines*, European Automobile Manufacturers Association.

Adams, Carole, Kruchinin, Dennis, Paddon, Chris and Seiler, Oliver, 2009. Quantification of Biofuel Components in Automotive Lubricants. *SAE*, (2009-24-0159).

Adhvaryu, A., Erhan, SZ and Sahoo, SK, 2002. Thermo-oxidative stability studies on some new generation API group II and III base oils. *Fuel*, 81, pp.785–791.

Agarwal, A.K., Bijwe, J. and Das, L.M., 2003. Effect of Biodiesel Utilization of Wear of Vital Parts in Compression Ignition Engine. *Journal of Engineering for Gas Turbines and Power*, pp.604–611.

Agarwal, A.K. and Das, L.M., 2001. Biodiesel Development and Characterization for Use as a Fuel in Compression Ignition Engines. *Journal of Engineering for Gas Turbines and Power*, 123(2), pp.440–447.

Agarwal, Avinash Kumar, 2007. Biofuels (alcohols and biodiesel) applications as fuels for internal combustion engines. *Progress in Energy and Combustion Science*, 33, pp.233–271.

Aldajah, S., Ajayi, O.O., Fenske, G.R. and Goldblatt, I.L., 2007. Effect of exhaust gas recirculation (EGR) contamination of diesel engine oil on wear. *Wear*, 263(1-6), pp.93–98.

Alleman, Teresa L. and Mccormick, Robert L., 2003. Fischer-Tropsch Diesel Fuels – Properties and Exhaust Emissions : A Literature Review. *SAE*, (2003-01-0763).

Andreae, Morgan, Fang, Howard L. and Bhandary, Kirtan, 2007. Biodiesel and fuel dilution of engine oil. *SAE*, (2007-01-4036).

Antusch, Steffen, Dienwiebel, Martin, Nold, Eberhard, Albers, Peter, Spicher, Ulrich and Scherge, Matthias, 2010. On the tribochemical action of engine soot. *Wear*, 269(1-2), pp.1–12.

Argachoy, C. and Pimenta, A.P., 2005. Phenomenological Model of Particulate Matter Emission from Direct Injection Diesel Engines. , XXVII(3), pp.266–273.

ASTM D1298, 2012. *Standard Test Method for Density , Relative Density , or API Gravity of Crude Petroleum and Liquid Petroleum Products by Hydrometer Method*,

ASTM D2270, 2010. *Standard Practice for Calculating Viscosity Index from Kinematic Viscosity at 40 and 100°C*,

ASTM D3524, 2004. *Standard Test Method for Diesel Fuel Diluent in Used Diesel Engine Oils by Gas Chromatography*,

ASTM D4683, 2010. *Standard Test Method for Measuring Viscosity of New and Used Engine Oils at High Shear Rate and High Temperature by Tapered Bearing Simulator Viscometer at 150°C*,

ASTM D6895, 2006. *Standard Test Method for Rotational Viscosity of Heavy Duty Diesel Drain Oils at 100°C*,

ASTM D974, 2008. *Standard Test Method for Acid and Base Number by Color-Indicator Titration*,

Bardasz, Ewa A., Cowling, Susan, Ebeling, Vikki L., George, Herman F., Graf, Michelle M., Kornbrekke, Ralph E. and Ripple, David E., 1995. Understanding Soot Mediated Oil Thickening Through Designed Experimentation Part 1 : Mack EM6-287, GM6.2L. *SAE*, (952527).

Barman, B.N., 2002. Behavioral differences between group I and group II base oils during thermo-oxidative degradation. *Tribology international*, 35(1), pp.15–26.

Barnes, Mark, 2004. What Is Oxidation In Lubricating Oil ? *LubeTrak*.

Berbezier, I., Martin, J.M. and Kapsa, Ph., 1986. The role of carbon in lubricated mild wear. *Tribology International*, 19(3), pp.115–122.

Berbezier, I. and Martin, JM, 1988. The adverse effect of carbon in mild wear with ZDDP lubricant additive. *Tribology international*, pp.89–96.

Bijwe, Jayashree, Sharma, Atul and Agarwal, Avinash Kumar, 2004. Assessment of lubricity of biodiesel blends in reciprocating wear mode. *SAE*, (2004-01-3068).

Birch, BL, 2004. Soot & Acid Control in Diesel Lubricating Systems. *SAE*, (2004-01-3014).

Bovington, C., Korcek, S. and Sorab, J., 1999. The importance of the Stribeck curve in the minimisation of engine friction. *Tribology Series*, pp.205–214.

Bowman, Craig T., 1975. Kinetics of pollutant formation and destruction in combustion. *Progress in energy and combustion science*, 1(3).

BS EN ISO 12156-1:, 2006. *Diesel fuel — Assessment of lubricity using the reciprocating rig (HFRR)*,

Chen, Chun-I. and Hsu, Stephen M., 2003. A chemical kinetics model to predict lubricant performance in a diesel engine. Part I: Simulation methodology. *Tribology Letters*, 14(2), pp.83–90.

Chiñas-Castillo, F. and Spikes, H.A., 2004. The behavior of diluted sooted oils in lubricated contacts. *Tribology Letters*, 16(4).

Clague, ADH, Donnet, JB, Wang, TK and Peng, JCM, 1999. A comparison of diesel engine soot with carbon black. *Carbon*, 37(10), pp.1553–1565.

Cracknell, R.F. and Stark, M.S., 2007. Influence of Fuel Properties on Lubricant Oxidative Stability : Part 2 – Chemical Kinetics Modelling Fuels & Emissions Conference. *SAE*, (2007-01-0003).

Daido, Shigeki, Kodama, Yoshitada, Inohara, Takayuki, Ohyama, Naohisa and Sugiyama, Toshihisa, 2000. Analysis of soot accumulation inside diesel engines. *JSAE Review*, 21.

Dec, John E., 1997. A Conceptual Model of DI Diesel Combustion Based on Laser-Sheet Imaging. *SAE*, (970873).

Dennis, AJ, Garner, C.P. and Taylor, D.H.C., 1999. The effect of EGR on diesel engine wear. *SAE transactions*, 108(3), pp.1185–1197.

Devlin, Cathy C., Passut, C.A., Campbell, R.L. and Jao, Tze-Chi, 2008. Biodiesel fuel effect on Diesel engine lubrication. *SAE*, (2008-01-2375).

Diaby, M., Sablier, M., Le Negrate, A., El Fassi, M. and Bocquet, J., 2009. Understanding carbonaceous deposit formation resulting from engine oil degradation. *Carbon*, 47(2), pp.355–366.

Diaby, Moussa, Sablier, Michel, Le Negrate, Anthony and El Fassi, Mehdi, 2010. Kinetic Study of the Thermo-Oxidative Degradation of Squalane (C30H62) Modeling the Base Oil of Engine Lubricants. *Journal of Engineering for Gas Turbines and Power*, 132(3), pp.1 – 9.

Fang, Howard L., Alleman, Teresa L. and McCormick, Robert L., 2006. Quantification of biodiesel content in fuels and lubricants by FTIR and NMR spectroscopy. *SAE*, (2006-01-3301).

Fang, Howard L., Whitacre, Shawn D., Yamaguchi, Elaine S. and Boons, Maarten, 2007. Biodiesel impact on wear protection of engine oils. *SAE*, (2007-01-4141).

Flynn, Patrick F., Durrett, Russell P., Hunter, Gary L., zur Loye, Axel O., Akinyemi, O.C., Dec, John E. and Westbrook, Charles K., 1999. Diesel Combustion : An Integrated View Combining Laser Diagnostics , Chemical Kinetics , And Empirical Validation. *SAE*, (1999-01-0509).

Fraer, Richard, Dinh, Han, Proc, Kenneth, McCormick, Robert L., Chandler, Kevin and Buchholz, Bruce, 2005. Operating Experience and Teardown Analysis for Engines Operated on Biodiesel Blends (B20). *SAE*, (2005-01-3641).

Fritz, A. and Pitchon, V., 1997. The current state of research on automotive lean NOx catalysis. *Applied Catalysis B: Environmental*, 13(1), pp.1–25.

Froelund, Kent and Ross, Michael G., 2005. Laboratory Benchmarking of Seven Model Year 2003-2004 Heavy-Duty Diesel Engines Using a CI-4 Lubricant. *SAE*, (2005-01-3715).

Gatto, Vincent, Moehle, William, Schneller, Emily, Burris, Thalan, Cobb, Tyler and Featherstone, Mark, 2008. *A Review of Engine Oil Oxidation Bench Tests and Their Application in the Screening of New Antioxidant Systems for Low Phosphorus Engine Oils*, ASTM International.

Gautam, Mridul, Chitoor, Karthik, Durbha, Murali and Summers, Jerry C., 1999. Effect of diesel soot contaminated oil on engine wear — investigation of novel oil formulations. *Tribology international*, 32(12), pp.687–699.

George, Sam, Balla, Santhosh, Gautam, Vishaal and Gautam, Mridul, 2007. Effect of diesel soot on lubricant oil viscosity. *Tribology International*, 40(5), pp.809–818.

Giakoumis, Evangelos G., Rakopoulos, Constantine D., Dimaratos, Athanasios M. and Rakopoulos, Dimitrios C., 2012. Exhaust emissions of diesel engines operating under transient conditions with biodiesel fuel blends. *Progress in Energy and Combustion Science*, 38(5), pp.691–715.

Gill, S.S., Turner, D., Tsolakis, A. and York, A.P.E., 2012. Controlling soot formation with filtered EGR for diesel and biodiesel fuelled engines. *Environmental science & technology*, 46(7), pp.4215–22.

Gómez-Rico, María F., Martín-Gullón, Ignacio, Fullana, Andrés, Conesa, Juan a and Font, Rafael, 2003. Pyrolysis and combustion kinetics and emissions of waste lube oils. *Journal of Analytical and Applied Pyrolysis*, 68-69, pp.527–546.

Graboski, Michael S. and McCormick, Robert L., 1998. COMBUSTION OF FAT AND VEGETABLE OIL DERIVED FUELS IN DIESEL ENGINES. *Progress in Energy and Combustion*, 24(97), pp.125–164.

Graham, Jocelyn and Spikes, Hugh, 1999. The behaviour of molybdenum dialkyldithiocarbamate friction modifier additives. *Tribology Series*, 36(11), pp.759–766.

Green, D... and Lewis, R., 2008. The effects of soot-contaminated engine oil on wear and friction: a review. *Proceedings of the Institution of Mechanical Engineers, Part D: Journal of Automobile Engineering*, 222(9), pp.1669–1689.

Green, D..., Lewis, R. and Dwyer-Joyce, R.S., 2006a. Wear effects and mechanisms of soot-contaminated automotive lubricants. *Proceedings of the Institution of Mechanical Engineers, Part J: Journal of Engineering Tribology*, 220(3), pp.159–169.

Green, D..., Lewis, R. and Dwyer-Joyce, R.S., 2006b. Wear of Valve-Train Components Due to Soot Contaminated Lubricant. *SAE*, (2006-01-1098).

Haycock, Roger F. and Hillier, John E., 2004. *Automotive lubricants reference book*, Society of Automotive Engineers, Inc.

He, Xin, Williams, Aaron, Christensen, Earl, Burton, Jonathan and McCormick, Robert L., 2011. Biodiesel Impact on Engine Lubricant Dilution During Active Regeneration of Aftertreatment Systems. *SAE*, (2011-01-2396).

Henderson, H. Ernest and LeBarge, Tony, 2013. Natural Gas Engine Oils. In Leslie R. Rudnick, ed. *Synthetics, Mineral Oils, and Bio-Based Lubricants: Chemistry and Technology*. pp. 747–762.

Heywood, J.B., 1988. *Internal combustion engine fundamentals*, Mc-Graw Hill.

Inderwildi, Oliver R. and King, David A., 2009. Quo vadis biofuels? *Energy & Environmental Science*, 2(4), p.343.

Ishiguro, Tomoji, Takatori, Yoshiki and Akihama, Kazuhiro, 1997. Microstructure of diesel soot particles probed by electron microscopy: first observation of inner core and outer shell. *Combustion and Flame*, 2180(96), pp.231–234.

Jao, Tze-chi, Li, Shoutian, Yatsunami, K., Chen, S.J., Csontos, Aladar A. and Howe, James M., 2000. Soot characterisation and diesel engine wear. In *Proceedings of International Tribology Conference*. Nagasaki.

Johnson, M.D. and Korcek, S., 1991. Effects of NOx on liquid phase oxidation and inhibition at elevated temperatures. *Lubrication Science*, 3(2), pp.95–118.

Jost, H.P., 1966. *Lubrication (Tribology)*, Report to Education and Science Ministry, UK, HMSO, London.

Jost, H.P., 1990. Tribology–Origin and future. *Wear*, 136(1), pp.1–17.

Kapoor, Ajay, Tung, Simon C., Schwartz, Shirley E., Priest, Martin and Dwyer-Joyce, Rob S., 2001. Automotive Tribology. In *Modern Tribology Handbook*. London: CRC Press.

Kegl, Breda, 2006. Numerical analysis of injection characteristics using biodiesel fuel. *Fuel*, 85(17-18), pp.2377–2387.

Kennedy, I.M., 1997. Models of soot formation and oxidation. *Progress in Energy and Combustion Science*, 23(2), pp.95–132.

Kim, Hak-Joo, Kang, Bo-Seung, Kim, Min-Ju, Park, Young Moo, Kim, Deog-Keun, Lee, Jin-Suk and Lee, Kwan-Young, 2004. Transesterification of vegetable oil to biodiesel using heterogeneous base catalyst. *Catalysis Today*, 93-95, pp.315–320.

Kittelson, David B., 1998. Engines and nanoparticles: a review. *Journal of Aerosol Science*, 29(5), pp.575–588.

Knothe, Gerhard and Steidley, KR, 2005. Lubricity of components of biodiesel and petrodiesel. The origin of biodiesel lubricity. *Energy & fuels*, pp.1192–1200.

Korcek, S., Jensen, R.K. and Johnson, M.D., 2000. Interactions Leading to Formation of Low Friction Films in Systems Containing Molybdenum Dialkyldithiocarbamate and Zinc Dialkyldithiophosphate Additives. *Tribology Series*, pp.399–407.

Korcek, Stefan, Jensen, Ronald K., Johnson, Milton D. and Sorab, Jagadish, 1999. Fuel efficient engine oils, additive interactions, boundary friction, and wear. *Tribology Series*, pp.13–24.

Kornbrekke, Ralph E., Patrzyk-Semanik, Pamela, Kirchner-Jean, Tara, Galic Raguz, Mary and Bardasz, Ewa A., 1998. Understanding Soot Mediated Oil Thickening Part 6 : Base Oil Effects. *SAE*, (982665).

Kuo, Cheng C., Passut, Charles A., Jao, Tze-chi, Csontos, Aladar A. and Howe, James M., 1998. Wear Mechanism in Cummins M-11 High-Soot Diesel Test Engines. *SAE*, (981372).

Ladommatos, Nicos, Balian, Razmik, Horrocks, Roy and Cooper, Laurence, 1996. The effect of exhaust gas recirculation on soot formation in a high-speed direct-injection diesel engine. *SAE*, (960841).

Lakkireddy, Venkata R., Mohammed, Hasan and Johnson, John H., 2006. The Effect of a Diesel Oxidation Catalyst and a Catalyzed Particulate Filter on Particle Size Distribution from a Heavy Duty Diesel Engine Reprinted From : Diesel Exhaust. *SAE*, (2006-01-0877).

Lam, Su Shiung, Russell, Alan D. and Chase, Howard A., 2010. Microwave pyrolysis, a novel process for recycling waste automotive engine oil. *Energy*, 35(7), pp.2985–2991.

Lapuerta, Magín, Armas, Octavio and Gómez, Arántzazu, 2003. Diesel Particle Size Distribution Estimation from Digital Image Analysis. *Aerosol Science and Technology*, 37(4), pp.369–381.

Lapuerta, Magín, Armas, Octavio and Rodríguez-Fernández, José, 2008. Effect of biodiesel fuels on diesel engine emissions. *Progress in Energy and Combustion Science*, 34(2), pp.198–223.

Lavoie, George A., Heywood, John B. and Keck, James C., 1970. Experimental and theoretical study of nitric oxide formation in internal combustion engines. *Combustion Science and …*, 1(1935), pp.313–326.

Lee, Kyeong Ook, Zhu, Jinyu, Ciatti, Stephen, Yozgatligil, Ahmet and Choi, Mun Young, 2003. Sizes, graphitic structures and fractal geometry of light-duty diesel engine particulates. *SAE*, (2003-01-3169).

Lee, P.M., Priest, M., Stark, M.S., Wilkinson, J.J., Lindsay Smith, J.R., Taylor, R.I. and Chung, S., 2006. Extraction and tribological investigation of top piston ring zone oil from a gasoline engine. *Proceedings of the Institution of Mechanical Engineers, Part J: Journal of Engineering Tribology*, 220(3), pp.171–180.

Lee, P.M., Stark, M.S., Wilkinson, J.J., Priest, M., Lindsay Smith, J.R., Taylor, R.I. and Chung, S., 2005. The degradation of lubricants in gasoline engines: Development of a test procedure to evaluate engine oil degradation and its consequences for rheology. *Tribology and Interface*, pp.593–602.

Levendis, Yiannis A., Pavlatos, Iraklis and Abrams, Richard F., 1994. Control of Diesel Soot , Hydrocarbon and NO x Emissions with a Particulate Trap and EGR. *SAE*, (940460).

Lewis, Ralph E., 2009. *Safety and Integrity of Marine Fuel Pumps Operating on 0.1% Sulfur Marine Gas Oil*, Houston, Texas.

Li, Shoutian, Csontos, Aladar A., Gable, Brian M., Passut, Charles A. and Jao, Tze-chi, 2002. Wear in cummins M-11/EGR test engines. *SAE*, (2002-01-1672).

Llamas, Alberto, Lapuerta, Magín, Al-Lal, Ana-María and Canoira, Laureano, 2013. Oxygen Extended Sooting Index of FAME Blends with Aviation Kerosene. *Energy & Fuels*, 27(11), pp.6815–6822.

Martyr, A.J. and Plint, M.A., 2007. Tribology, fuel and lubrication testing. In *Engine Testing*. Elsevier Ltd.

McQueen, J.S., Gao, H., Black, E.D., Gangopadhyay, A.K. and Jensen, R.K., 2005. Friction and wear of tribofilms formed by zinc dialkyl dithiophosphate antiwear additive in low viscosity engine oils. *Tribology International*, 38(3), pp.289–297.

Monyem, Abdul and Van Gerpen, Jon H., 2001. The effect of biodiesel oxidation on engine performance and emissions. *Biomass and Bioenergy*, 20, pp.317–325.

Mueller, Charles J., Pickett, Lyle M., Siebers, Dennis L., Pitz, William J., Westbrook, Charles K. and Martin, Glen C., 2003. Effects of Oxygenates on Soot Processes in DI Diesel Engines : Experiments and Numerical Simulations. *JSAE*, (2003-01-1791).

Muller, Michael, Fan, Jingyan and Spikes, Hugh, 2008. Design of functionalized PAMA viscosity modifiers to reduce friction and wear in lubricating oils. *ASTM International*, 4(10), pp.1–10.

Murakami, Yasuhiro, 1995. Analysis of corrosive wear of diesel engines: relationship to sulfate ion concentrations in blowby and crankcase oil. *JSAE Review*, 16, pp.43–48.

Musculus, Mark P., Dec, John E. and Tree, Dale R., 2002. Effects of Fuel Parameters and Diffusion Flame Lift-Off on Soot Formation in a Heavy-Duty DI Diesel Engine In-Cylinder Diesel Particulates and NOx Control. *SAE*, (2002-01-0889).

Nagai, Isamu, Endo, Hiroyasu, Nakamura, Hideo and Yano, Hisashi, 1983. Soot and valve train wear in passenger car diesel engines. *SAE*, (831757).

Nakasa, M., 1995. Engine Friction Overview. In *International Tribology Conference*. Japan: Yokohama.

Naylor, Malcolm G., Kodali, Padma and Wang, Jerry C., 2001. Diesel Engine Tribology. In *Modern Tribology Handbook*. CRC Press.

Ofunne, GC, Maduako, AU and Ojinnaka, C.M., 1989. Studies on the ageing characteristics of automotive crankcase oils. *Tribology International*, 50, pp.401–404.

Olomolehin, Yewande, Kapadia, Rita and Spikes, Hugh, 2009. Antagonistic Interaction of Antiwear Additives and Carbon Black. *Tribology Letters*, 37(1), pp.49–58.

Parker, Tom, Girnary, Sofia and O'Connor, Keith, 2009. *Evaluating the opportunities for high blend liquid and gaseous biofuel penetration in the UK*,

Parsons, Gary M., 2007. Biodiesel and Engine Lubrication Part 1. *Lubrication*, (October 2007).

PCS Instruments, 2009a. HFRR Installation & Test Preparation Manual.

PCS Instruments, 2009b. USV System Operation Manual.

Perez, Joseph M., 2000. Oxidative properties of lubricants using thermal analysis. *Thermochimica acta*, (June 1999), pp.47–56.

Perkin Elmer, 2009. Clarus 600 GC / MS Brochure.

Pinzi, Sara, Rounce, Paul, Herreros, José M., Tsolakis, Athanasios and Pilar Dorado, M., 2013. The effect of biodiesel fatty acid composition on combustion and diesel engine exhaust emissions. *Fuel*, 104, pp.170–182.

Priest, M., Dowson, D. and Taylor, C.M., 1999. Predictive wear modelling of lubricated piston rings in a diesel engine. *Wear*, 231(1), pp.89–101.

Priest, M. and Taylor, C.M., 2000. Automobile engine tribology –approaching the surface. *Wear*, 241, pp.193–203.

Richter, H. and Howard, J..., 2000. Formation of polycyclic aromatic hydrocarbons and their growth to soot—a review of chemical reaction pathways. *Progress in Energy and Combustion Science*, 26(4-6), pp.565–608.

Rizvi, Syed Q.A., 2009. Dispersants. In L. R. Rudnick, ed. *Lubricant Additives: Chemistry and Applications*. CRC Press, pp. 143–170.

Rounce, P., Tsolakis, A. and York, A.P.E., 2012. Speciation of particulate matter and hydrocarbon emissions from biodiesel combustion and its reduction by aftertreatment. *Fuel*, 96, pp.90–99.

Rounds, Fred G., 1977. Carbon: Cause of Diesel Engine Wear? *SAE*, (770829).

Rounds, Fred G., 1981. Soots from used diesel-engine oils: their effects on wear as measured in 4-ball wear tests. *SAE*, (810499).

Ryason, P.R., Chan, I.Y. and Gilmore, J.T., 1990. Polishing wear by soot. *Wear*, 137(1), pp.15–24.

Ryason, P.R. and Hansen, T.P., 1991. Voluminosity of soot aggregates: a means of characterizing soot-laden oils. *SAE*, (912343).

SAE J300, 2009. *Engine Oil Viscosity Classification*, SAE International.

Sappok, Alexander G. and Wong, Victor W., 2008. Impact of Biodiesel on Ash Emissions and Lubricant Properties Affecting Fuel Economy and Engine Wear : Comparison with Conventional Diesel Fuel. *SAE*, (2008-01-1395).

Sato, Hiromitsu, Tokuoka, Naochika, Yamamoto, Hidetsugu and Sasaki, Miki, 1999. Study on Wear Mechanism by Soot Contaminated in Engine Oil (First Report: Relation Between Characteristics of Used Oil and Wear). *SAE*, (1999-01-3573).

Schmidt, R., Klingenberg, G. and Woydt, M., 2006. Thermophysical and viscosimetric properties of environmentally acceptable lubricants. *Industrial Lubrication and Tribology*, 58(4), pp.210–224.

Selby, K., 1998. Rheology of soot thickened diesel engine oils. *SAE*, (981369).

Shahid, Ejaz M. and Jamal, Younis, 2008. A review of biodiesel as vehicular fuel. *Renewable and Sustainable Energy Reviews*, 12(9), pp.2484–2494.

Shimokoji, Daichi and Okuyama, Yosuke, 2009. Analysis of Engine Oil Deterioration under Bio Diesel Fuel Use. *SAE*, (2009-01-1872).

Singh, S.P. and Singh, Dipti, 2010. Biodiesel production through the use of different sources and characterization of oils and their esters as the substitute of diesel: A review. *Renewable and Sustainable Energy Reviews*, 14(1), pp.200–216.

Sinha, Shailendra and Agarwal, Avinash Kumar, 2008. Experimental Investigations of the Tribological Properties of Lubricating Oil from Biodiesel Fuelled Medium Duty Transportation CIDI Engine. *SAE*, (2008-01-1385).

Smith, G.C., Hopwood, A.B. and Titchener, K.J., 2002. Microcharacterization of heavy-duty diesel engine piston deposits. *Surface and Interface Analysis*, 33(3), pp.259–268.

Spikes, Hugh, 2006. Origins of the friction and wear properties of antiwear additives. *Lubrication Science*, (18), pp.223–230.

Stachowiak, G.W. and Batchelor, A.W., 2005. *Engineering tribology* 3rd ed., Butterworth-Heinemann.

Stark, M.S., Wilkinson, J.J. and Lee, P.M., 2005. The degradation of lubricants in gasoline engines: Lubricant flow and degradation in the piston assembly. *Tribology and Interface*, pp.779–786.

Sukjit, E. and Dearn, K.D., 2011. Enhancing the lubricity of an environmentally friendly Swedish diesel fuel MK1. *Wear*, 271(9-10), pp.1772–1777.

Tan, Pi-Qiang, Hu, Zhi-Yuan and Lou, Di-Ming, 2009. Regulated and unregulated emissions from a light-duty diesel engine with different sulfur content fuels. *Fuel*, 88(6), pp.1086–1091.

Taylor, C.M., 1998. Automobile engine tribology--design considerations for efficiency and durability. *Wear*, pp.1–8.

Terry, B., 2006. *Impact of biodiesel blends on fuel system component durability*,

Thornton, Matthew J., Alleman, Teresa L., Luecke, Jon and McCormick, Robert L., 2009. Impacts of Biodiesel Fuel Blends Oil Dilution on Light-Duty Diesel Engine Operation. *SAE*, 2(2009-01-1790), pp.781–788.

Thornton, Matthew, Webb, Cynthia C., Weber, Phillip A., Orban, John and Slone, Elizabeth, 2006. Fuel Sulfur Effects on a Medium-Duty Diesel Pick-Up with a NOx Adsorber, Diesel Particle Filter Emissions Control System : 2000-Hour Aging Results. *SAE*, (2006-01-0425).

Tokura, Naomi, Terasaka, Katsunori and Yasuhara, Seishi, 1982. Process through which soot intermixes into lubricating oil of a diesel engine with exhaust gas recirculation. *SAE*, (820082).

Trujllo, G., 2004. Resetting oil analysis parameters for changing diesel engines. *Practicing Oil Analysis*.

Tsolakis, A., 2006. Effects on particle size distribution from the diesel engine operating on RME-biodiesel with EGR. *Energy & Fuels*, (20), pp.1418–1424.

Tsolakis, A., Megaritis, A., Wyszynski, M.L. and Theinnoi, K., 2007. Engine performance and emissions of a diesel engine operating on diesel-RME (rapeseed methyl ester) blends with EGR (exhaust gas recirculation). *Energy*, 32(11), pp.2072–2080.

Uy, Dairene, Anderson, James and Gangopadhyay, Arup, 2010. Effect of Different B20 Fuels on Laboratory-Aged Engine Oil Properties. *SAE*, (2010-01-2102), pp.569–578.

Uy, Dairene, Simko, Steven J., Carter III, R.O., Jensen, Ron K. and Gangopadhyay, Arup, 2007. Characterization of anti-wear films formed from fresh and aged engine oils. *Wear*, 263(7-12), pp.1165–1174.

Uy, Dairene, Simko, Steven J., O'Neill, Ann E., Jensen, Ronald K., Gangopadhyay, Arup and Carter III, Roscoe O., 2006. Raman Characterization of Anti-Wear Films Formed from Fresh and Aged Engine Oils. *SAE*, (2006-01-1099).

Wang, Zhendi and Stout, Scott A., 2007. Chemical fingerprinting of spilled or discharged petroleum–methods and factors affecting petroleum fingerprints in the environment. *… Spill Environmental Forensics–Fingerprinting …*, pp.1–53.

Waynick, J. Andrew, 2005. *Characterization of Biodiesel Oxidation and Oxidation Products*,

Xu, Xiaoyin, Brandon, Nigel and Spikes, Hugh, 2002. Study of zinc dialkyldithiophosphate using electrochemical techniques. *Tribology Series*, 40(1), pp.175–181.

Zdrodowski, Rob, Gangopadhyay, Arup, Anderson, James, Ruona, William C., Uy, Dairene and Simko, Steven J., 2010. Effect of Biodiesel (B20) on Vehicle-Aged Engine Oil Properties. *SAE*, (2010-01-2103), pp.579–597.